Chromium Stabilization in Ferrochromium Slag for its Utilization as Aggregate Material

by

Tahmeed Bin Tasnim

B.Sc., Bangladesh University of Engineering and Technology, 2016

A THESIS SUBMITTED IN PARTIAL FULFILLMENT OF

THE REQUIREMENTS FOR THE DEGREE OF

MASTER OF SCIENCE

in

THE FACULTY OF GRADUATE AND POSTDOCTORAL STUDIES

(Materials Engineering)

THE UNIVERSITY OF BRITISH COLUMBIA

(Vancouver)

July 2021

The following individuals certify that they have read, and recommend to the Faculty of Graduate and Postdoctoral Studies for acceptance, a thesis entitled:

Chromium Stabilization in Ferrochrome Slag for its Utilization as Aggregate Material

submitted by Tahmeed Bin Tasnim in partial fulfillment of the requirements for

the degree of Master of Science

in Materials Engineering

Examining Committee:

Leili Tafaghodi Khajavi, Associate Professor, Materials Science and Engineering, McMaster
Supervisor

Dogan Paktunc, Research Scientist, CanmetMINING
Supervisory Committee Member

Edouard Asselin, Professor, Materials Engineering, UBC
Supervisory Committee Member

Wenying Liu, Associate Professor, Materials Engineering, UBC
Supervisory Committee Member

Abstract

Ferrochromium slag is a byproduct of ferrochromium production via the smelting of chromite ores. Every year 12-16 million tonnes of ferrochromium slag are produced, a majority of which is dumped in landfills. The mechanical properties of this slag make it a potential material to be used as an inexpensive construction material, the utilization of which can reduce the use of natural resources. Despite its potential use, ferrochromium slag is treated as a waste due to environmental and health concerns regarding the leaching of its heavy metal content, the most concerning of which is carcinogenic chromium (VI). Research has shown that the spinel phase in ferrochromium slag stabilizes chromium by trapping it in the spinel structure and preventing its leaching to the environment. This study investigates the effect of heat treatment and composition change on spinel formation in ferrochromium slag and subsequently on the stabilization of chromium.

Slag samples of the MgO-Al_2O_3-SiO_2-CaO-FeO-Cr_2O_3 system were synthesized at 1650°C for 10 h in a vertical tube furnace. Samples were heat treated after synthesis by holding them at 1400, 1475, 1550°C for 12 h before quenching. Leaching tests on heat treated slag samples reveal that samples held at 1400°C have the lowest chromium leachability. With a holding temperature of 1400°C, slag samples were prepared with variations in Al_2O_3 content in the range of 0-20%. Higher Cr leaching is observed from samples as the Al_2O_3 content increases. Similar heat-treated samples were prepared with constant Al_2O_3 content and basicity (CaO/SiO_2) varying from 0.3 to 0.7. An increase in basicity increases the amount of Cr released from the samples during leaching experiments.

Lay Summary

Ferrochromium which is composed of iron and chromium is an essential alloy for the production of stainless steel. Ferrochromium is commonly produced by smelting chromite ores in submerged arc furnaces. A by-product of this smelting process is ferrochromium slag which contains various metal oxides including chromium oxide. The slag has excellent properties that make it a viable replacement for construction material. However, the utilization of this slag is halted due to environmental concerns regarding the release of harmful heavy metals to the environment. Chromium is the most notable of these heavy metals due to its carcinogenic nature. The current study aims to stabilize chromium in the slag structure and prevent its release into the environment.

Preface

The original idea of this research was proposed by Dr. Leili Tafaghodi in collaboration with Dr. Dogan Paktunc. The objectives were identified by the supervisor in discussion with the author, Tahmeed Bin Tasnim. The author was responsible for designing and performing the lab experiments, preparing and analyzing the results, and writing the thesis. Dr. Tafaghodi supervised all aspects of the research work.

Table of Contents

List of Tables

List of Figures

List of Symbols

η	Viscosity
I	Nucleation Rate
µm	Micron/Micrometer
P_{O_2}	Oxygen Partial Pressure
r	Crystallization Rate
T_{liq}	Liquidus Temperature
U	Growth Rate
wt%	Weight Percentage
X	Mole Fraction

List of Abbreviations

AOD	Argon Oxygen Decarburization
AAS	Atomic Absorption Spectrometer
AES	Atomic Emission Spectroscopy
BOF	Basic Oxygen Furnace
DCF	Direct Current Arc Furnace
EAF	Electric Arc Furnace
EDS	Energy Dispersive X-Ray Spectroscopy
EDTA	Ethylenediamine Tetra Acetic Acid
ICP	Inductively Coupled Plasma
MAC	Maximum Acceptable Concentration
ppm	Parts Per Million
SEM	Scanning Electron Microscopy
SAF	Submerged Arc Furnace
TCLP	Toxicity Characteristic Leaching Procedure
USEPA	United States Environmental Protection Agency
VOD	Vacuum Oxygen Decarburization
WDS	Wavelength Dispersive X-Ray Spectroscopy
XRD	X-Ray Diffraction
XRF	X-Ray Fluorescence

Acknowledgements

I would like to express my deepest gratitude to my supervisor Dr. Leili Tafaghodi, whose continuous guidance, encouragement and support has helped me throughout every step of my research and thesis writing. I am thankful for your dedication and understanding over the past few years. Furthermore, I am thankful to NRCan for providing the financial support necessary for the project.

Besides my supervisor, I would like to thank my co-supervisor, Dr. Dogan Paktunc as well as Dr. Eleanor J. Berryman from NRCan for providing their valuable insight for the research.

I am grateful to my fellow researchers, Muhammad Haziq Uddin, Rishu Kumar, Golam Ismot Ara Taposhe and Sahand Sarbishei for listening to, and at times, having to tolerate me throughout the years.

Most importantly, I am forever indebted to my family, without whom, none of this would be possible. My mother, who provided emotional strength through countless calls, during the many ups and downs in my life. My father, who taught me perseverance and the importance of pursuing my dreams. My wife, who pushed me forward every time I was ready to give up. This dissertation stands as a testament to your unconditional love and support.

1. Introduction

Ferrochromium (FeCr) is a crude alloy obtained from chromite ore and is regularly used in stainless steel production. Due to the strategic importance of stainless steel production in North America, the discovery of the so-called Ring of Fire chromite reserves in Northern Ontario has presented a remarkable opportunity for the Canadian mining industry. Chromite ore is applied mostly in metallurgical processes after being converted to ferrochromium, with over 90% of all ores being used for steelmaking [1]. Chromite mineral is found in spinel form with the general formula of $(Fe^{2+}, Mg^{+2})O.(AI^{3+}, Cr^{3+}, Fe^{3+})_2O_3$ [2]. The spinels are minerals with general formula of AB_2X, where the X anions (typically oxygen and sulfur) are arranged in a cubic close-packed lattice and the cations A and B occupy some or all of the octahedral and tetrahedral sites.

The composition of the chromite ore can significantly vary depending on its origin. The average composition for the chromite ore from the Ring of Fire area in Northern Ontario can be represented as $(Mg_{0.5}Fe_{0.5})$ $(Cr_{1.4}Fe_{0.1}Al_{0.5})O_4$ [3]. Ferrochromium is produced by carbothermic reduction of chromite ore in an electric arc furnace (EAF). Ferrochromium slag which is the by-product of the extraction process is produced at a rate of 1.1 to 1.5 times of the ferrochromium metal itself, resulting in a global ferrochromium slag production of 12 to 16 million tonnes annually [4]. The majority of the slag is discarded in landfills with the possibility of creating environmental impacts in the future. These slags have excellent properties that make them an attractive choice for cheap construction materials in road building and as an aggregate substitute in concrete. If properly utilized, ferrochromium slag can help save natural resources while removing the cost of its transportation and disposal in landfills. Slag reutilization is a common practice in developed countries; however, it is generally applicable to low alloy slags with negligible or no heavy metal content. In 2010, over 80% of all low-alloy EAF slag produced in Sweden was used as construction material, while less than 10% of high-alloyed EAF slag was utilized [5]. Ferrochromium slag is generally treated as a waste material since concerns have been raised regarding the leachability of heavy metals from the slag, the most concerning of which is chromium [6].

Amongst the different oxidation states of chromium, three are the most common. Metallic chromium Cr(0) is produced by human interventions while trivalent chromium Cr(III) and hexavalent chromium Cr(VI) are naturally found near the earth's surface [7][8]. Cr(III) causes no

health concerns, is necessary for a balanced nutritional diet, and is specified in dietary supplements in some circumstances [9]. However, Cr(VI) compounds are known as carcinogens and cause several human respiratory ailments including lung tumors, fibrosis, perforation of the nasal septum, lung fibrosarcoma, adenocarcinomas, and nasal polyp development [10][11][12]. If not stabilized, chromium in slag can oxidize to its hexavalent form and leach out when exposed to an acidic and oxygen rich environment [13]. Chromium present in some ferrochromium slag components such as wustite (FeO), spinel, and glass, can resist dissolution in water. In other phases like periclase (MgO), merwinite ($Ca_3MgSi_2O_8$), dicalcium silicate (Ca_2SiO_4), and lime (CaO), chromium is easily released in water [14]. Trapping chromium in a spinel phase stabilizes it and prevents the leaching of harmful Cr(VI) from the slag. It is believed that the formation of the spinel phase depends on the melting temperature, chemical composition, and cooling cycle of the slag [14].

This study aims to examine the chemical composition of a synthetic ferrochromium slag for its utilization as a replacement for construction materials. The slag was synthesized to mimic the possible composition of the Ring of Fire's ferrochromium slag. The main concern with the utilization of ferrochromium slag as a construction material is the leachability of carcinogenic and environmentally hazardous chromium (VI). Canadian and Ontario criteria requires a maximum 2.77 mg/L of total chromium in aqueous waste leachate using TCLP (Toxicity Characteristic Leaching Procedure) method [15]. This limit is lower than the US environmental protection agency (US EPA) standard of 5 mg/L [7] but significantly more than the German limit of 0.5 mg/L [16]. In addition, many other countries have set specific limits for Cr(VI) which range from 0.02 to 1.5 mg/L [17].

This work investigates the effect of the slag chemical composition and the phases formed after solidification on the leaching of Cr(VI) from the slag. Critical slag composition factors influencing the stability of Cr(VI) are the MgO content and the CaO/SiO_2 ratio responsible for the formation of the spinel phase that traps Cr in its structure. The volume fraction of the spinel phase also benefits from the increase in Al_2O_3 content in the slag, but its effect on Cr stability is debatable due to Al taking up Cr space in the spinel structure. While the effect of MgO in promoting spinel formation has been widely accepted, the effect of other factors is studied in the present investigation to obtain a better understanding of their influence on the leachability of Cr(VI).

2. Literature Review

The literature study includes an introduction to the Ring of Fire deposits, an overview of ferrochromium (FeCr) production, FeCr slag properties crucial to its synthesis, slag chemical composition and other factors such as heat treatment and the furnace environment that influence Cr leaching behaviour of the slag.

2.1. Ring of Fire Deposit

While Cr can occur in several types of ores, chromite is the only commercially significant ore for stainless steel production. Chromite is largely available from deposits in South Africa and Zimbabwe (90% of the world reserves), and partly from several other countries including India and Kazakhstan [18]. Out of the 24 million tons of chromite ore produced globally in 2008, 70% was obtained from South Africa, India and Kazakhstan [19]. In 2012, only 0.13% of the global 24.5 million ton chromite production was produced in North America [18]. In 2008, a very large chromite reserve was discovered in the Ring of Fire area in northern Ontario. The deposit can potentially meet North America's needs for several centuries [20]. It contains billions worth of chromite and is considered the most significant mineral discovery in Canada since the Timmins gold camp in 1909.

The Ring of Fire area is located far north of Ontario in the remote James Bay Lowlands. This 5000 km^2 area is located about 1000 km from Toronto and near 500 km from Thunder Bay. Despite the large surface area most of the mineral deposits are located within a 20 km strip of land [20]. The area is also within the Hudson Bay Lowlands which is part of the world's largest peatland (wetland). The peatland act as an important carbon store and careful planning will be required to manage the tailings and waste rock in the naturally saturated environment. This poses environmental and logistical challenges in developing mining operations and infrastructure in the area. In addition, the Ring of Fire area is located within the traditional territories of Matawa First Nation communities. The developments are expected to influence their lives significantly, and the stakeholders are required to negotiate and implement an Impact Benefit Agreement with these communities.

The typical composition of ferrochromium slag consists of 19-33% Al_2O_3, 13-25% MgO, 15-30% SiO_2, 1-5% CaO, 1-18% Cr and 1-12% Fe [2]. Cr and Fe are present as unreduced CrO/Cr_2O_3 and

FeO respectively or entrapped as ferrochromium alloy. For the sake of comparison, the composition of typical chromite ores from different countries and the ore obtained from the Ring of Fire area are shown in Table 2.1.

Table 2.1: Chemical composition of chromite ore in mass%.

Country/Region	Cr_2O_3	Al_2O_3	MgO	CaO	SiO_2	FeO*	Others
Ring of Fire [3]	44.36	10.84	14.07	0.08	4.54	19.71	6.40
South Africa [21]	44.50	15.00	10.00	0.31	3.90	12.23	14.06
Kazakhstan [22]	61.90	8.60	14.70	-	-	14.20	0.60
India [23]	36.49	11.40	15.35	-	7.39	21.35	8.02

*FeO is calculated from total Fe or from Cr/Fe ratio

2.2. Ferrochromium Production

Chromium alloys and compounds are essential to meet the growing demand for stainless steel production worldwide. The source of this Cr is usually ferrochromium alloys obtained from carbothermic reduction of chromite ores. During the production of ferrochromium, a large amount of slag (1.1 to 1.5 times the alloy) is produced [4]. Ferrochromium slag is generated while reducing chromite ore using carbonaceous material with the addition of silica and lime/dolomite to adjust the chemistry.

Four different grades of ferrochromium are produced commercially with compositions shown in Table 2.2 [18]. Since the high carbon and charge grade FeCr have similar composition, they are commonly referred together as high carbon charge grade FeCr. Development of processes like argon oxygen decarburization (AOD) and vacuum oxygen decarburization (VOD) that allow easier carbon removal from stainless steel, have significantly decreased the demand for low and medium carbon grade FeCr. We will thus focus on the more relevant high carbon charge grade FeCr production.

Mined chromite ore generally goes through a beneficiation and pelletizing process before FeCr extraction (Figure 2.1). Common beneficiation processes include primary and secondary crushing, screening, milling, dense media separation and gravity separation methods [19]. The only

beneficiation step that has been proven to generate Cr(VI) is milling, specifically dry milling [24][25].

Table 2.2: Cr and C content (in Wt%) of different grades of FeCr [18].

Grade	Chromium	Carbon
High carbon	>60	6-9
Charge grade	50-60	6-9
Medium carbon	56-70	1-4
Low carbon	56-70	0.015-1.0

Extreme pressure applied on Cr(III) contained in the ores can produce enough heat to oxidize Cr(III) to Cr(VI). Wet milling on the other hand has shown no tendencies for Cr(VI) formation since the ore is not in contact with oxygen in the air. Dissolved oxygen in the wet milling would allow oxidation of Cr(III) species via the following reaction.

$$2Cr^{3+}(aq) + 7H_2O(l) \rightarrow Cr_2O_7^{2-}(aq) + 14H^+(aq) + 6e^-$$

Milling is a necessary step for ore agglomeration during the subsequent pelletizing process. The product of the pelletizing stage called green pellets are then cured by sintering in a furnace to form evenly sized, hard and porous feed material for EAF [18].

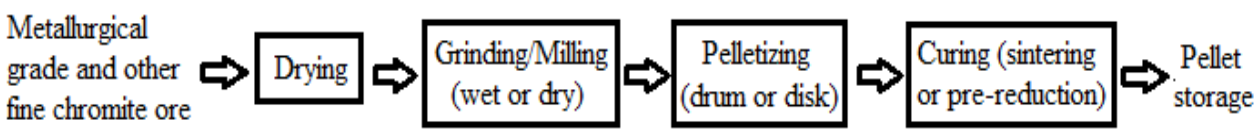

Figure 2.1: Chromite ore beneficiation and pelletizing process [18].

Coarse and fine raw ore with or without the sintered, pre-reduced or green pellets are charged to the furnace, along with carbonaceous reductants and appropriate flux materials (Figure 2.2). The type of raw ore and pellet depends on the type of furnace and subsequently the process applied using that furnace. For example, when using closed submerged arc furnaces (SAF), oxidative sintered feed pellets are used for the Outotec process, whereas pre-reduced feed pellets are used for the Premus process. On the other hand, conventional open SAF are employed using exclusively

coarse chromite feed. Higher content of the coarse ore helps the gases produced during smelting to easily permeate to the surface and prevent the top from sintering. This could be beneficial in processes where there is a risk of blowouts or bed turnovers if too many fines are present in the feed. The type of feed material (coarse/fine chromite, pre-treated/green pellet) will rely heavily on the process as different countries use feeds unique to their operation.

The production of high carbon charge FeCr is typically carried out in an EAF. The most common furnaces for FeCr production are listed below [18]:

(1) Open, Semi-closed submerged arc furnace (SAF) - Worldwide

(2) Closed submerged arc furnace - South Africa

(3) Direct current arc furnace (DCF) - Kazakhstan

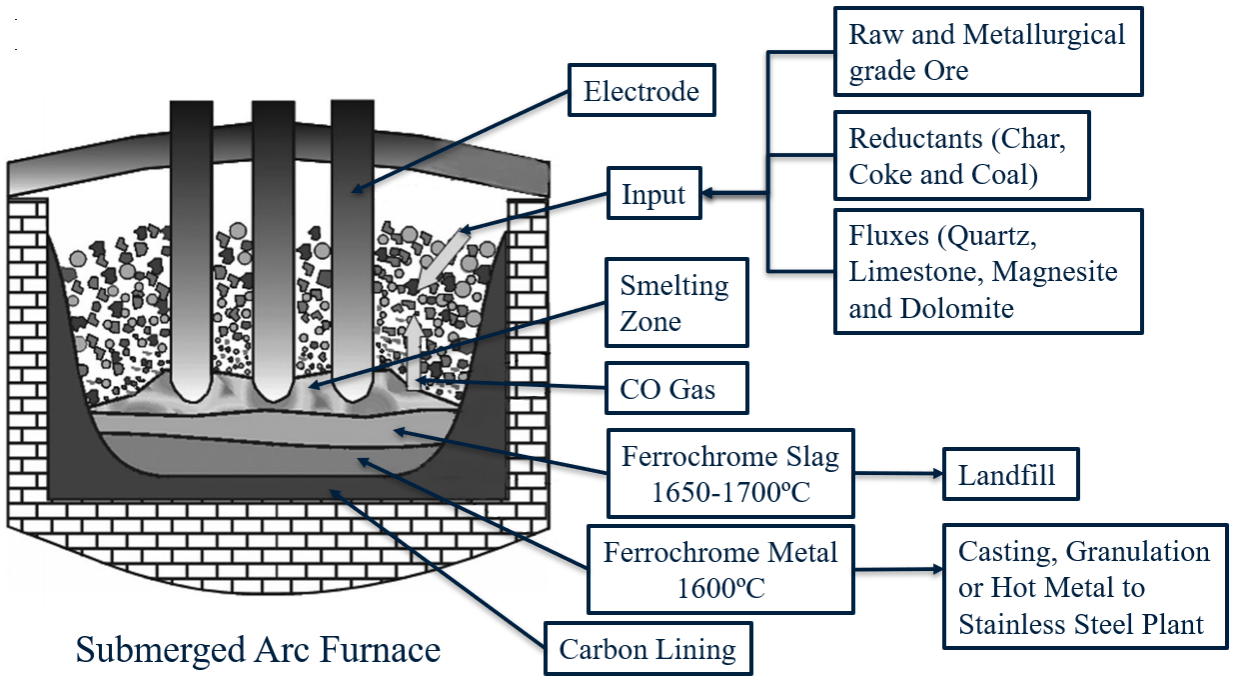

Figure 2.2: Schematic of ferrochrome production using a submerged arc furnace.

The open, semi-closed submerged arc furnace is the oldest and the most conventional furnace for FeCr production. These furnaces are not provided with a gas tight seal and as such, combustion of the process carbon monoxide (CO) rich gas occurs on top of the furnace bed. Generally, coarse chromite ore is smelted along with coarse reductants and coarse fluxes so that the processed CO gas can easily permeate to the top of the furnace and prevent the bed from sintering.

During the smelting process both FeCr alloy and the slag are produced. The alloy is heavier than the slag and settles through the slag and collects at the bottom of the furnace. Both the alloy and slag are tapped out of the same tapping hole into two ladles in series. The slag having a lower density floats at the top and overflows from the first ladle to the second one. The FeCr metal remains in the first ladle while the slag is separated into the second ladle. Inside the furnace the temperature of the alloy phase is typically around 1600ºC and the slag on top is around 1650-1700ºC. The composition of the slag and its melting point depends on the composition of the chromite ore and the fluxing agents. Generally, FeCr slag consists of SiO_2, MgO, Al_2O_3, in different proportion along with minor amounts of CaO, chromium and iron oxides. While the extracted FeCr is sent to stainless steel production plants, the FeCr slag is usually dumped in landfills and is not used as construction material due to concerns regarding Cr(VI) leaching from the slag.

The current study will examine the stability of Cr in FeCr slag with different compositions. Since, Cr(III) can oxidize to form the more harmful Cr(VI), our goal is to reduce the total Cr leaching from the slag to an acceptable level for its utilization.

2.3. Estimation of the Slag Properties

The study will involve characterization of synthetic slag samples with various compositions including those we expect to get from smelting chromite ores from the Ring of Fire deposits [26]. The compositions were to be adjusted to maintain certain properties of the slag, such that the samples can be synthesized using the available equipment. The melting point of the slag had to be below the upper threshold of the vertical furnace (1700ºC) while maintaining low viscosity (<5 Poise) values typical in FeCr slag [27]. Turbulence in the furnace during smelting and tapping can cause droplets of metal to get physically trapped in high viscosity slags. Other operational difficulties, such as slow tapping speed can occur due to excessively viscous slag. Reaction kinetics of low viscosity slags would allow the process to reach equilibrium in a shorter time through diffusion interactions at the slag/metal interface.

2.3.1. Liquidus Temperature

To analyze the properties of a synthetic slag, it is essential to determine its liquidus temperature. While there are models for calculating the liquidus temperature for SiO_2-Al_2O_3-MgO-CaO slags

[28][29] they would not account for the presence of Cr_2O_3 and FeO in the synthetic slag. A more accurate estimate of the liquidus temperature is obtained using Eq (1) [30].

$$\begin{aligned} T_{liq}(K) = {} & 656.9X_{SiO2} + 1040.7X_{CaO} + 1343.2X_{Al2O3} + 1090.5X_{MgO} \\ & + 137X_{Na2O} - 668X_{K2O} + 408.7X_{Li2O} + 522X_{FeO} + 760.9X_{MnO} \\ & + 1022X_{CrO} + 794X_{Fe2O3} + 2198X_{Cr2O3} - 532X_{CaF2} \\ & + 844X_{TiO2} - 12.6X_{B2O3} + 1207X_{BaO} + 1768X_{SrO} \\ & + 2234X_{ZrO2} \end{aligned} \qquad \text{Eq (1)}$$

Here T_{liq} represents the liquidus temperature of the slag based on the mole fractions (represented by X) of its components. The equation was formulated from the regression analysis of 124 T_{liq} values taken from several sources [30]. The liquidus surface has several deviations at compositions corresponding to compound formations. The mean uncertainty of this estimated liquidus temperature value is estimated to be ±130K at these deviations in the database, whereas the uncertainty is < ±100K for the rest of the database.

2.3.2. Viscosity

Viscosity of the slag plays an important role in pyrometallurgical extraction of metals and alloys, since lower viscosity ensures better mixing of the slag and facilitates the formation of a homogenous slag composition. Slags with lower viscosity typically require less holding time in the furnace for melting or heat treatment. Several models have been proposed for calculating the viscosity of slags. Most prominent of these are the Riboud [31], Urbain [32], Iida [33] and KTH [34] models.

We will use the Urbain model due to its simplicity and ability to account for the chemical composition as well as the temperature of the slag. In this model, the slag components are classified into the following categories.

Glass Formers $X_G = X_{SiO2} + X_{P2O5}$

Modifiers $X_M = X_{CaO} + X_{MgO} + X_{FeO} + X_{MnO} + X_{CrO} + X_{NiO} + X_{Na2O} + X_{K2O} + X_{Li2O} + 2X_{TiO2} + 2X_{ZrO2} + 3X_{CaF2}$

Amphoterics $X_A = X_{Al2O3} + X_{Fe2O3} + X_{B2O3} + X_{Cr2O3}$

Here, X represents the mole fraction of the slag components. To calculate the viscosity, the model assumes Weymann - Frenkel Relation presented in Eq (2)

$$\text{Viscosity,} \quad \eta = \text{ATexp}\left(\frac{1000\text{B}}{T}\right) \qquad \text{Eq (2)}$$

Here A and B are compositionally dependant parameters and T is the temperature in Kelvin (K). Viscosity (μ) is calculated in Poise (P).

Urbain found out that Eq (3) represents the correlation between A and B.

$$-\ln A = 0.29B + 11.57 \qquad \text{Eq (3)}$$

B can be calculated using Eq (4)

$$B = B_o + B_1X_G + B_2(X_G)^2 + B_3(X_G)^3 \qquad \text{Eq (4)}$$

Where, $B_o = 13.8 + 39.9355a - 44.049a^2$

$B_1 = 30.481 - 117.1505a + 139.9978a^2$

$B_2 = -40.9429 + 234.0486a - 300.04a^2$

$B_3 = 60.7619 - 153.9276a + 211.1616a^2$

and $a = X_M / (X_M + X_A)$

After calculating B using Eq (4), A is calculated from Eq (3) and finally the viscosity is calculated by substituting both parameters in Eq (2). The estimated values for the viscosity of the slag compositions examined in the current investigation are presented in section 3.1.1.

2.4. Slag Composition

The composition of the slag will be integral in determining the Cr leachability of the slag. Most notably the MgO content, basicity (defined as CaO/SiO_2), Al_2O_3 and FeO content are expected to influence Cr resistance to leaching. While the effects of the MgO content and the basicity of FeCr slag on Cr stabilization have been observed in numerous studies, there is still lack of information on the effects of Al_2O_3. The previous studies on the effect of the slag composition are examined to understand the effect of each of the oxides on the Cr stability of the slag.

2.4.1. MgO Content

The presence of MgO is necessary for the formation of magnesium chromite/ Cr spinel, $MgCr_2O_4$, and subsequently, for the stabilization of chromium in ferrochromium slag. The previous studies on the effect of MgO on chromium stabilization agree on its benefits in reducing chromium leaching.

A study conducted on SiO_2-CaO-MgO-Cr_2O_3 slags observed the effects of MgO content on the stability of various mineralogical species, especially $MgCr_2O_4$ spinel in the slag [35]. $MgCr_2O_4$ spinel is a key phase in Cr stabilization in FeCr slag. The slag was prepared synthetically using laboratory reagent grade oxides with 0-12 wt% MgO , 10 wt% Cr_2O_3 and a slag basicity of 1 and 1.5. The samples were prepared at 1600°C in argon atmosphere using a horizontal electric resistance furnace.

The XRD results presented in Figure 2.3 show that low crystallization of the slag samples occurred for MgO content of 0-6 wt% and slag basicity of 1. The slag samples were amorphous and showed very few peaks of mainly Ca_2SiO_4 and $CaSiO_3$. This shows that the slag samples with low MgO and slag basicity of 1 consist of glassy phases after being cooled by argon gas. In case of high, i.e. 9-12% MgO, clear peaks are observed, mostly from calcium silicates and $MgCr_2O_4$ spinel with faint peaks of free Cr_2O_3 and CrO phases.

Figure 2.4 shows that the samples with higher basicity of 1.5 have higher degree of crystallinity and more phases that are complex. The main species are calcium silicates including Ca_2SiO_4, $CaSiO_3$ and Ca_3SiO_5, free Cr_2O_3 and the $MgCr_2O_4$ spinel. At higher MgO content the ternary compound, merwinite $Ca_3Mg(SiO_4)_2$ is also observed. For both cases, Cr_2O_3 is found to be bound to the $MgCr_2O_4$ spinel phase with increasing MgO content.

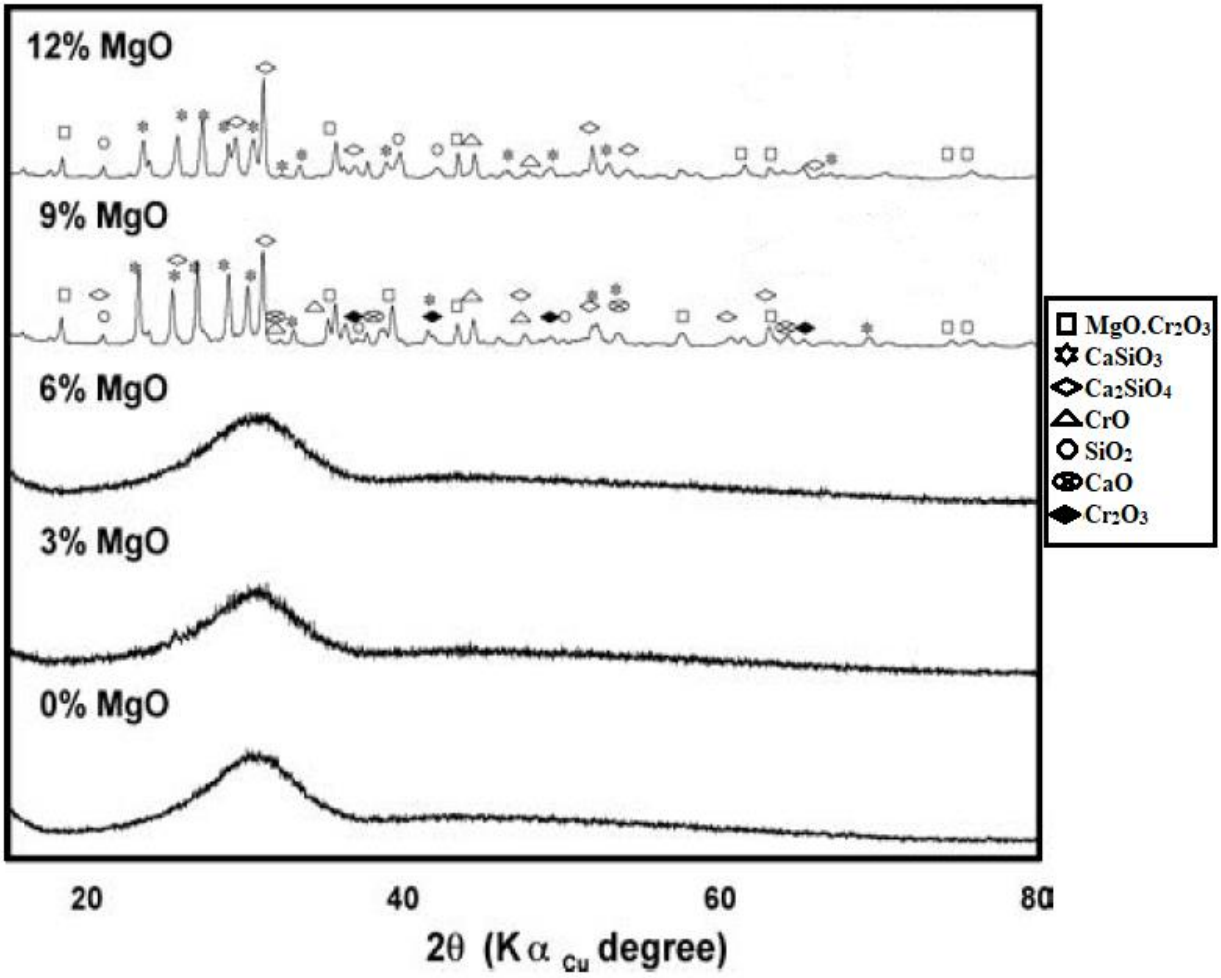

Figure 2.3: X-ray diffraction patterns for SiO_2-CaO-MgO-Cr_2O_3 slags with basicity of 1.0 [35].

In another investigation, the effect of MgO was examined using synthetic slag with 10% CaF_2, 10 and 20 % Cr_2O_3, 0-15% MgO and a slag basicity of 1 and 2 [36]. The XRD results of MgO containing slag showed the presence of cuspidine ($Ca_4Si_2O_7F_2$) and calcium silicate ($CaSi_2O_5$) along with free MgO in case of high MgO content. The only chromium containing species found was Cr spinel, even in cases with low MgO content. The presence of MgO lowered the leachability of chromium in all cases regardless of the MgO content or the slag basicity.

It is worth noting that in another study on CaO-CaF_2-SiO_2-Cr_20_3 synthetic slags, other chromium bearing phases were observed in samples with low MgO content [6] as shown in the XRD spectra presented in Figure 2.5.

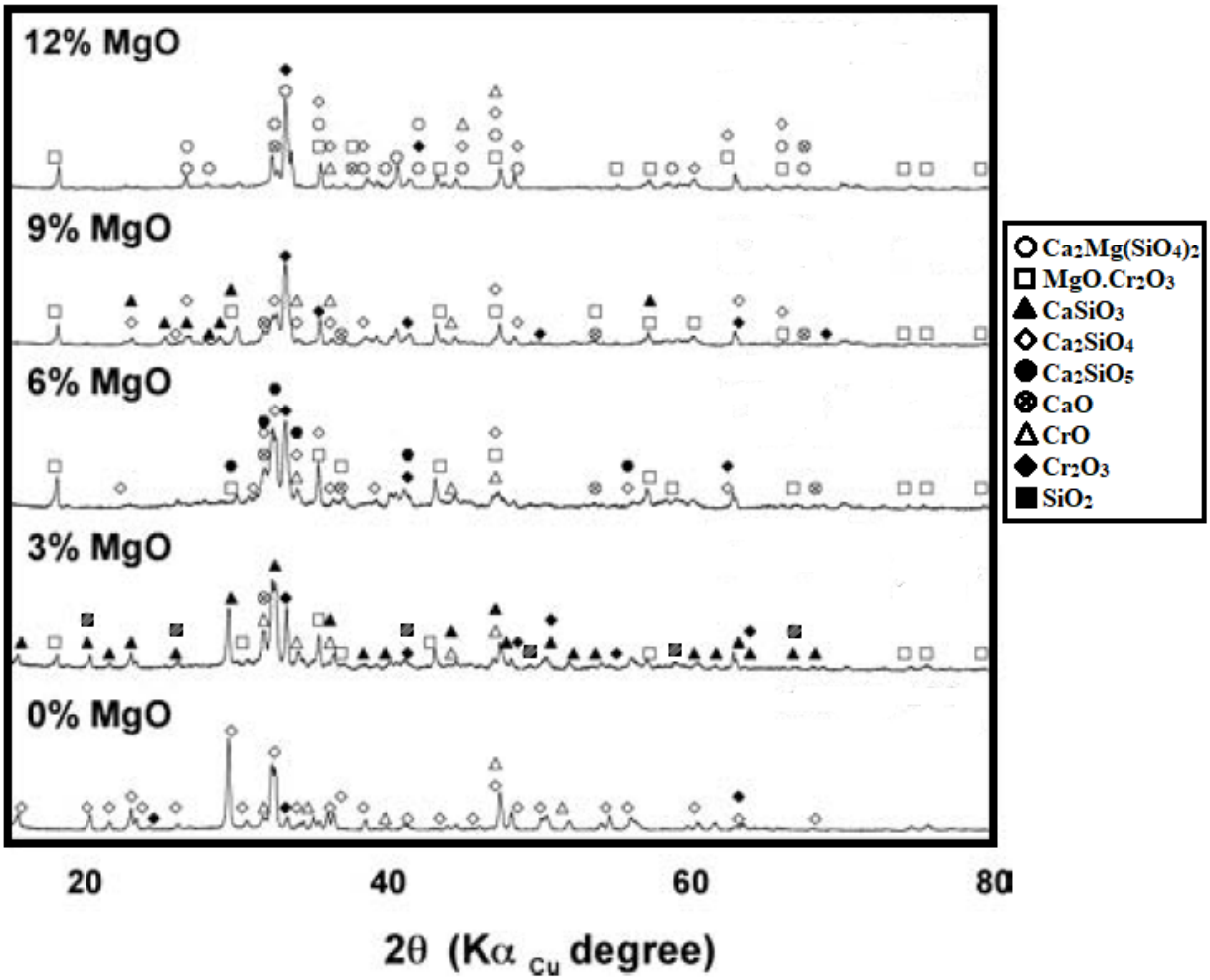

Figure 2.4: X-ray diffraction patterns for SiO_2-CaO-MgO-Cr_2O_3 slags with basicity of 1.5 [35].

The spectra confirm the presence of calcium chromite ($CaCr_2O_4$) and calcium chromate ($CaCrO_4$) in samples with 0% and 3% MgO, 10% Cr_2O_3 and 10% CaF_2 regardless of the basicity value. This is due to the presence of CaO in the slag that was not present in the previous study. When increasing the MgO content to 6% and 9%, the only Cr bearing phase is Cr spinel which is more stable than $CaCr_2O_4$ and $CaCrO_4$.

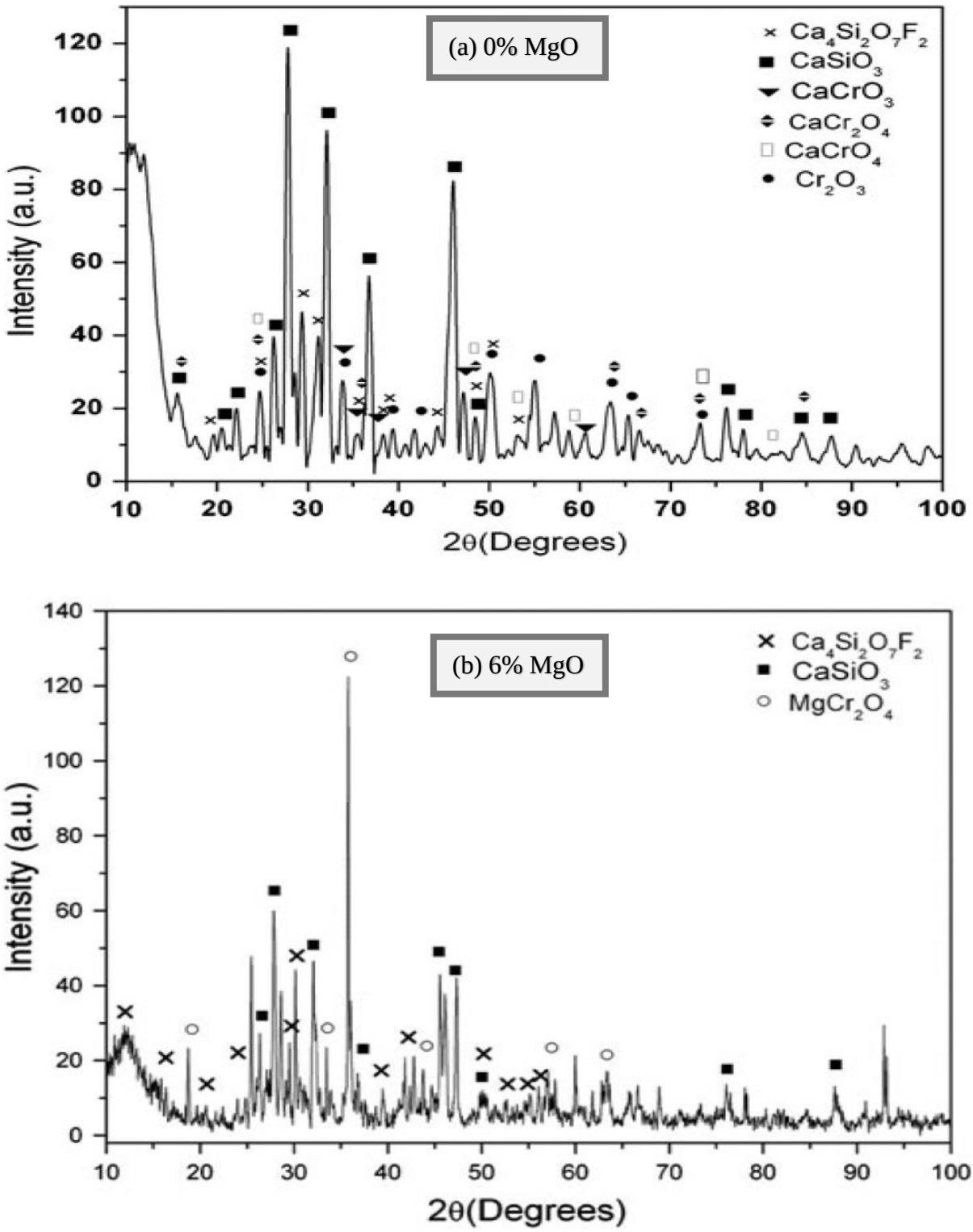

Figure 2.5: XRD patterns of $CaO-CaF_2-SiO_2-Cr_20_3$ slags at $CaO/SiO_2 = 1$ with (a) 0% MgO and (b) 6% MgO [6].

2.4.2. Slag Basicity

Slag basicity is linked to the level of networking in a slag typically caused by the 3D structure of silica. The acidic slags show high and basic slags show low networking structure respectively [37]. Quantitatively, basicity has been explained in several methods with the most common and simplest one being the ratio of the mass percentage of CaO to that of SiO_2 in the slag, which will be shown as CaO/SiO_2 hereafter.

Research work done on slag chemistry has indicated that increasing CaO/SiO_2 increases the leaching of Cr from it. An investigation on the chemical and mineralogical properties of CaO-CaF_2-SiO_2-Cr_2O_3 synthetic slags observed the effect of slag basicity and MgO content on the immobilization of chromium in the slag [6]. The slag composition consisted of 10% Cr_2O_3, 10% CaF_2, 0-9% MgO and a slag basicity of 1 and 2. To ensure that the slag was completely molten in the furnace, XRD tests were conducted on the cooled samples and the absence of free Cr_2O_3 was taken as an evidence for the system to have completely melted.

In the slag with CaO/SiO_2 of 1 and MgO content at 0% and 3%, readily leachable calcium chromite ($CaCr_2O_4$) and calcium chromate ($CaCrO_4$) phases were the only Cr bearing phases present. These phases were replaced by the more stable magnesium chromite/Cr spinel ($MgCr_2O_4$) at higher MgO content of 6% and 9% as shown previously in Figure 2.5. However, at a slag basicity of 2, $CaCr_2O_4$ content would increase along with the formation of a chromium(V) containing complex $Ca_5(CrO_4)_3F$, regardless of the MgO content (Figure 2.6). Chromium leaching behaviour was shown to be the lowest, i.e. 29-40 µg/l Cr, in case of slags with a basicity of 1 compared to those with a basicity of 2 and 68-98 µg/l Cr. The study concludes that regardless of the MgO content of the slag, high basicity can increase Cr leaching from the slag.

A comprehensive study conducted on multiple sets of slag samples consisting of CaO-MgO-SiO_2-Cr_2O_3 slag and EAF synthetic slag came to similar conclusions in terms of the effect of slag basicity on Cr leaching [5][14].

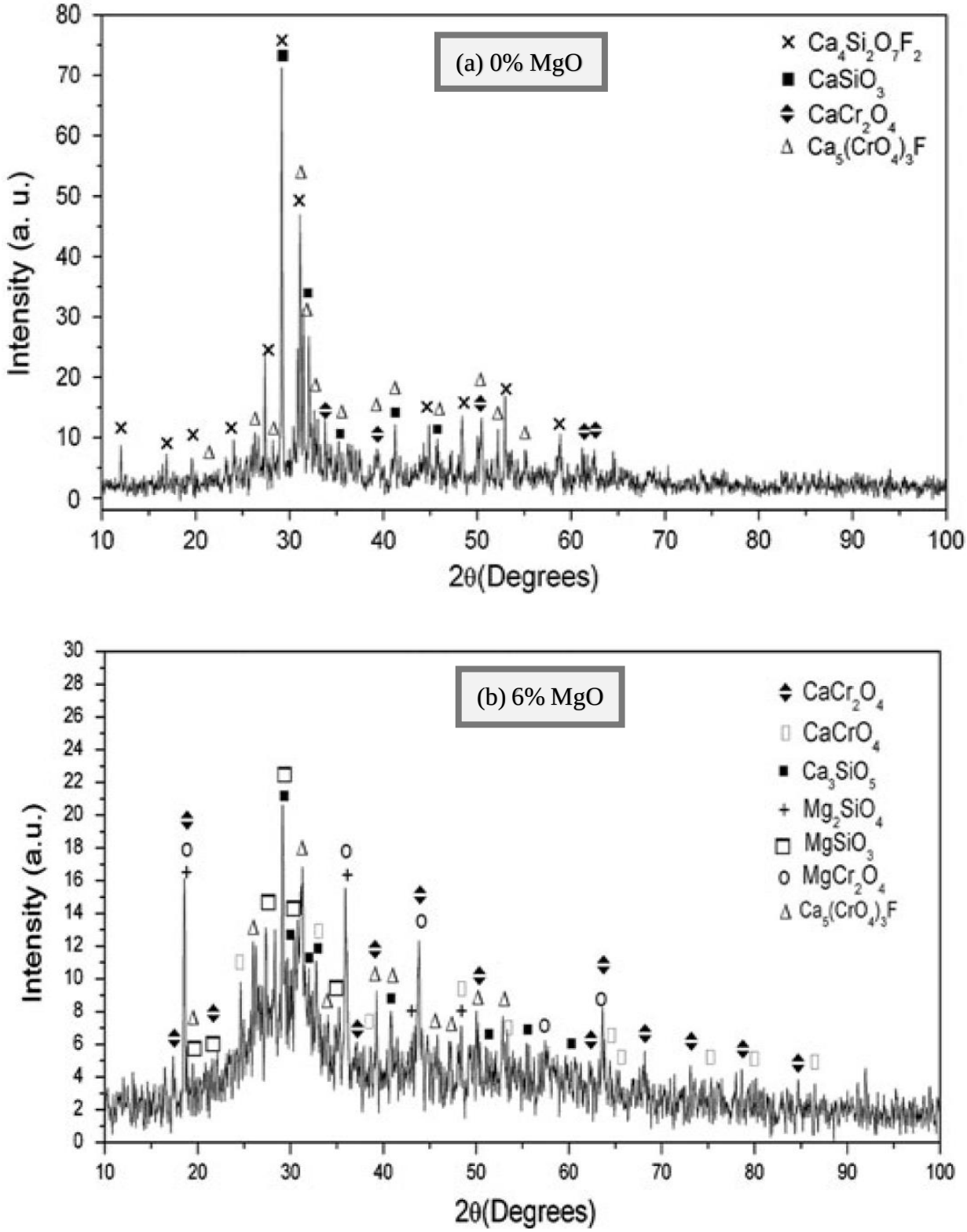

Figure 2.6: XRD patterns of $CaO-CaF_2-SiO_2-Cr_2O_3$ slags at $CaO/SiO_2 = 2$ with (a) 0% MgO and b) 6% MgO [6].

All CaO-MgO-SiO_2-Cr_2O_3 slag samples had fixed MgO (8%) and Cr_2O_3 (6%) content but varied in basicity (Table 2.3). The study focused on the distribution of Cr in spinel and the water-soluble matrix phases such as merwinite, wollastonite, periclase, and dicalcium silicate.

Table 2.3: Chemical composition of CaO-MgO-SiO_2-Cr_2O_3 slag in mass percent [14].

Sample	Basicity (CaO/SiO_2)	CaO	SiO_2	MgO	Cr_2O_3
1	1.0	43.0	43.0	8.0	6.0
2	1.2	46.9	39.1	8.0	6.0
3	1.4	50.2	35.8	8.0	6.0
4	1.6	52.9	33.1	8.0	6.0
5	1.8	55.3	30.7	8.0	6.0
6	2.0	57.3	28.7	8.0	6.0

An increase in the mean Cr content of the water-soluble matrix phase was observed due to increase in basicity. As shown in Figure 2.7 and Figure 2.8, thermodynamic calculations predict a decrease in Cr_2O_3 activity and an increase in MgO activity in the slag due to a basicity change from 1.4 to 1.6. Experimental results show that chromium was incorporated into periclase and merwinite instead of spinel. The study concluded that at CaO/SiO_2 of 1.4-1.6, the driving force for the increase in Cr partition in the slag was not spinel formation, rather Cr forming solid solutions with periclase and merwinite due to increased MgO activity at higher basicity. There was also an increased tendency to form calcium chromate ($CaCr_2O_4$) instead of magnesium chromite/Cr spinel ($MgCr_2O_4$) at higher basicity.

Basicity also seems to increase the extent of crystallization in the slag [35]. Slags with high basicity show a much more complicated array of peaks on XRD spectra compared to low basicity slags due to the formation of various mineral species (Figure 2.3 and Figure 2.4). Although crystallization in slag should increase Cr stability as the water-soluble amorphous phase decreases, the crystalline phases that are formed due to basicity increase are not Cr stable.

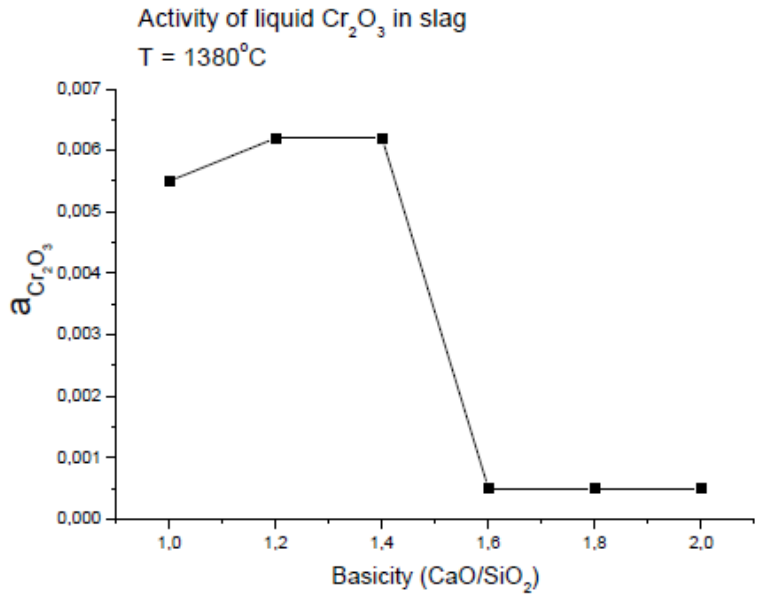

Figure 2.7: Activity of Cr_2O_3 in CaO-MgO-SiO_2-Cr_2O_3 slag system at 1653 K as a function of basicity [14].

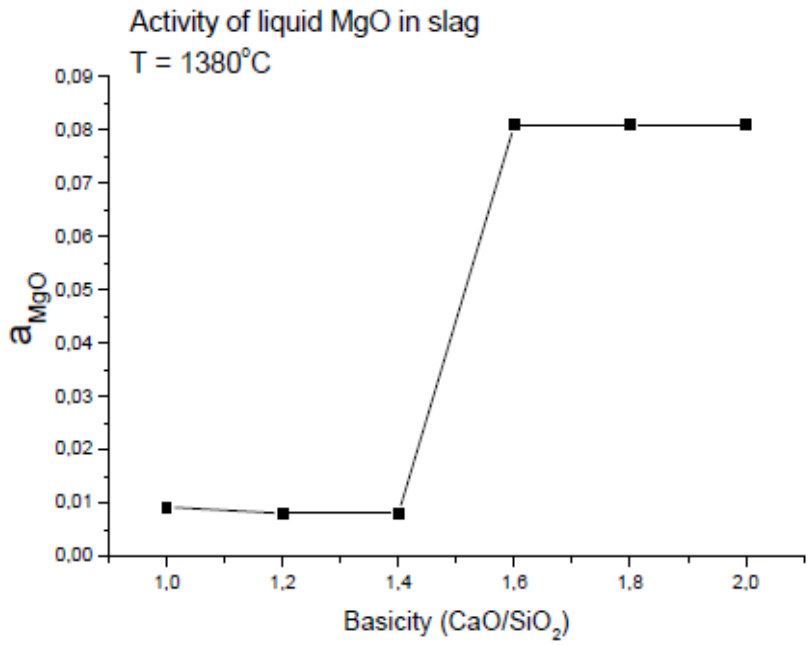

Figure 2.8: Activity of MgO in CaO-MgO-SiO_2-Cr_2O_3 slag system at 1653 K as a function of basicity [14].

2.4.3. Al_2O_3 Content

Amongst the spinel forming oxides, Al_2O_3 is expected to have a negative effect on chromium stabilization due to its tendency to replace chromium in the spinel structure. In some studies, however, increasing Al_2O_3 has decreased Cr leaching from the slag despite its expected drawback, thus demanding further investigation of its effect on chromium leaching behaviour.

A previously mentioned research on CaO-CaF_2-SiO_2-Cr_2O_3 system investigated the effects of Al_2O_3 addition on the Cr leaching behaviour of the slag [36]. The slag composed of 10% CaF_2, 10% and 20% Cr_2O_3, 0-15% Al_2O_3 with CaO/SiO_2 of 1 or 2. Each slag system was prepared using oxide reagents melted at 50°C above their melting temperature for 30 min and allowed to cool down in the furnace.

The XRD results in Figure 2.9 show that for slags with no Al_2O_3 addition and 10% Cr_2O_3, cuspidine ($Ca_4Si_2O_7F_2$), calcium chromite ($CaCr_2O_4$) and calcium silicate ($CaSi_2O_5$) formed. In case of Al_2O_3 containing slags, as shown in Figure 2.10, the main species were gehlenite ($Ca_2Al_2SiO_7$) and cuspidine ($Ca_4Si_2O_7F_2$).

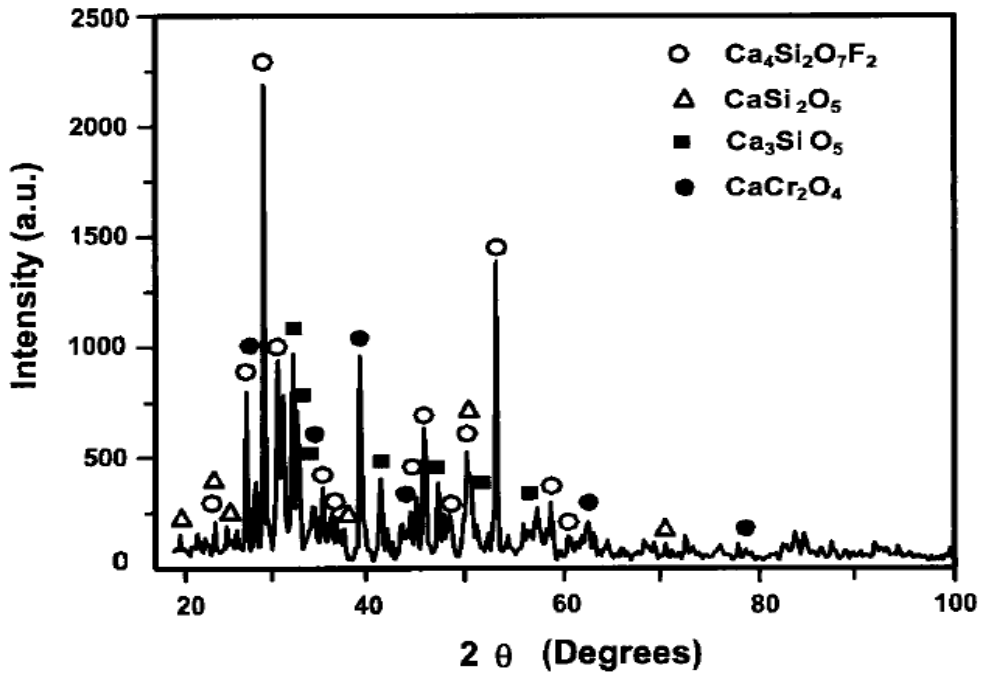

Figure 2.9: XRD patterns of CaO-CaF_2-SiO_2-Cr_2O_3 slag with 0% Al_2O_3, 10 % Cr_2O_3 and CaO/SiO_2=2 [36].

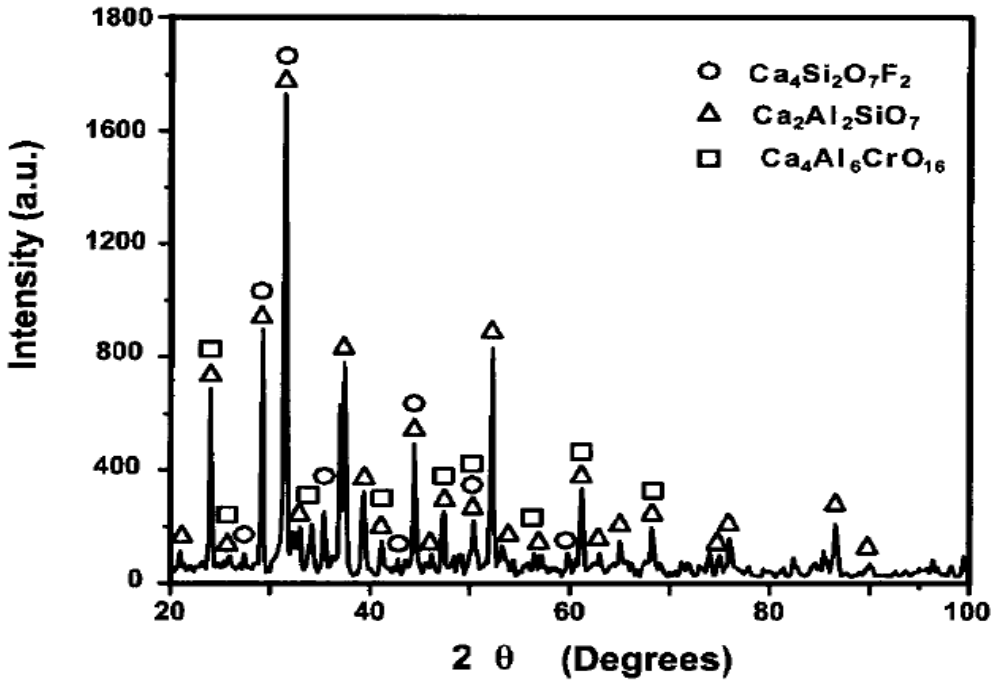

Figure 2.10: XRD patterns of $CaO-CaF_2-SiO_2-Cr_2O_3$ slag with 15% Al_2O_3, 10 % Cr_2O_3 and CaO/SiO_2=2 [36].

The presence of Al_2O_3 results in the formation of gehlenite instead of $CaCrO_4$, thus reducing the amount of leachable chromium (VI) compounds in the slag. However, at CaO/SiO_2 of 2, $Ca_4Al_6CrO_{16}$ was observed which in acidic environments could leach chromium (VI).

Figure 2.11 shows the Cr leached from the synthetic slag using acetic acid as per Mexican environmental regulations [38] with 10% Cr_2O_3 decreases with the addition of Al_2O_3. It should be noted that the above results were obtained in the absence of MgO in the slag. As presented in Figure 2.12, MgO is more effective in reducing the Cr leachability of the slag compared to Al_2O_3. Further studies are necessary to determine the effect of Al_2O_3 in slags containing MgO.

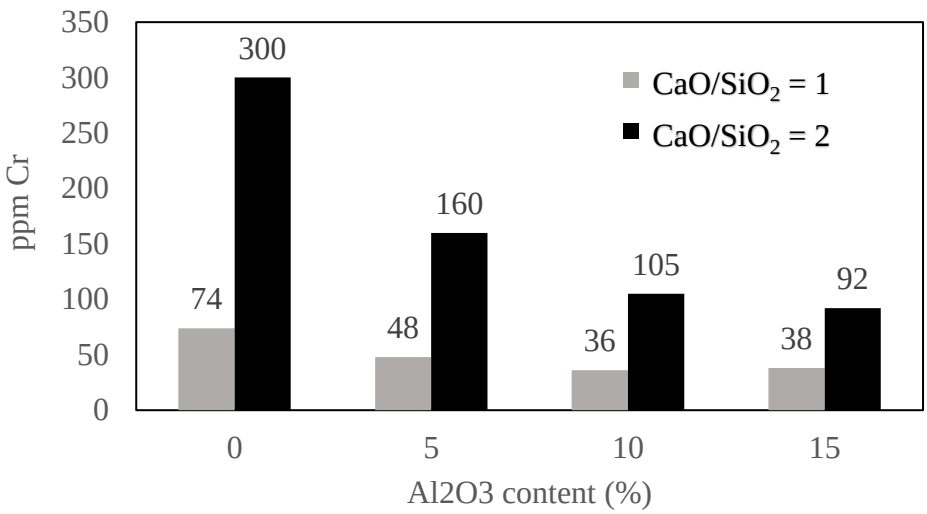

Figure 2.11: Effect of the CaO/SiO_2 and Al_2O_3 content on the Cr leaching behaviour of CaO-CaF_2-SiO_2-Cr_2O_3 slag with 10% Cr_2O_3 [36].

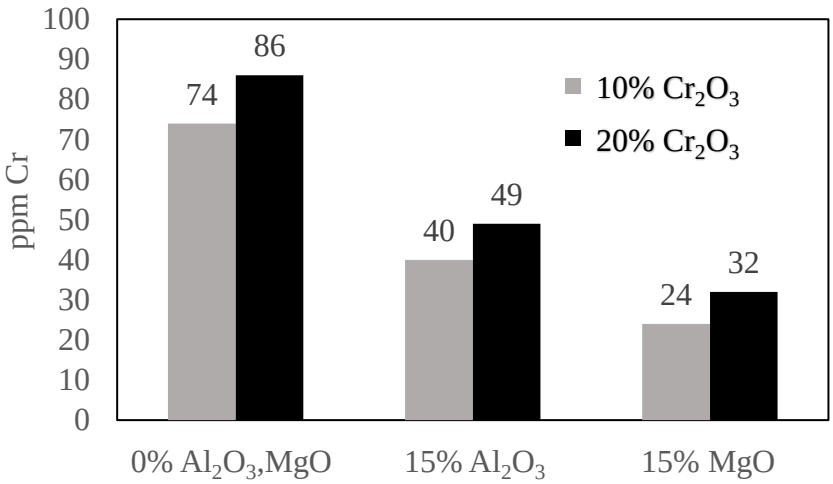

Figure 2.12: Effect of MgO, Al_2O_3 and Cr_2O_3 on the Cr leaching behaviour of CaO-CaF_2-SiO_2-Cr_2O_3 slag with CaO/SiO_2 = 1 [36].

Further clarity on the effect of Al_2O_3 addition in slags containing MgO was observed in a study on CaO-MgO-SiO_2-Cr_2O_3-Al_2O_3 synthetic slags prepared at oxygen partial pressure (P_{O_2}) of 10^{-4} Pa melted at 1600°C followed by a 1400°C holding temperature [14]. The MgO content was kept constant at 8% while the alumina content was changed from 3% to 12%. Basicity was kept constant at 1.6 but the wt% of CaO and SiO_2 was changed to compensate for the change in Al_2O_3 content. The research observed that Al_2O_3 addition increased the amount of spinel phase in the slag, as

intensities of the spinel peaks in XRD pattern was seen to increase (Figure 2.13). This was due to the formation of alumina spinel $MgAl_2O_4$ phase.

Closer inspection of the slag samples revealed that while the Cr content in the matrix phase of the slag remained constant, the Cr content in the spinel phase decreased on Al_2O_3 addition (Figure 2.14). The Al^{3+} ions replaced the Cr^{3+} ions in the spinel phase. Al_2O_3 addition was in fact reducing Cr stability provided by the MgO content by removing Cr from the spinel phase. It is worth noting that the Cr content in the present phases was analyzed by wavelength dispersive spectrometry (WDS) which is a semi quantitative technique. However, it is not clear if the researcher obtained the average Cr content from point analyses or area analysis. In addition, the number of WDS analysis for each sample is not mentioned.

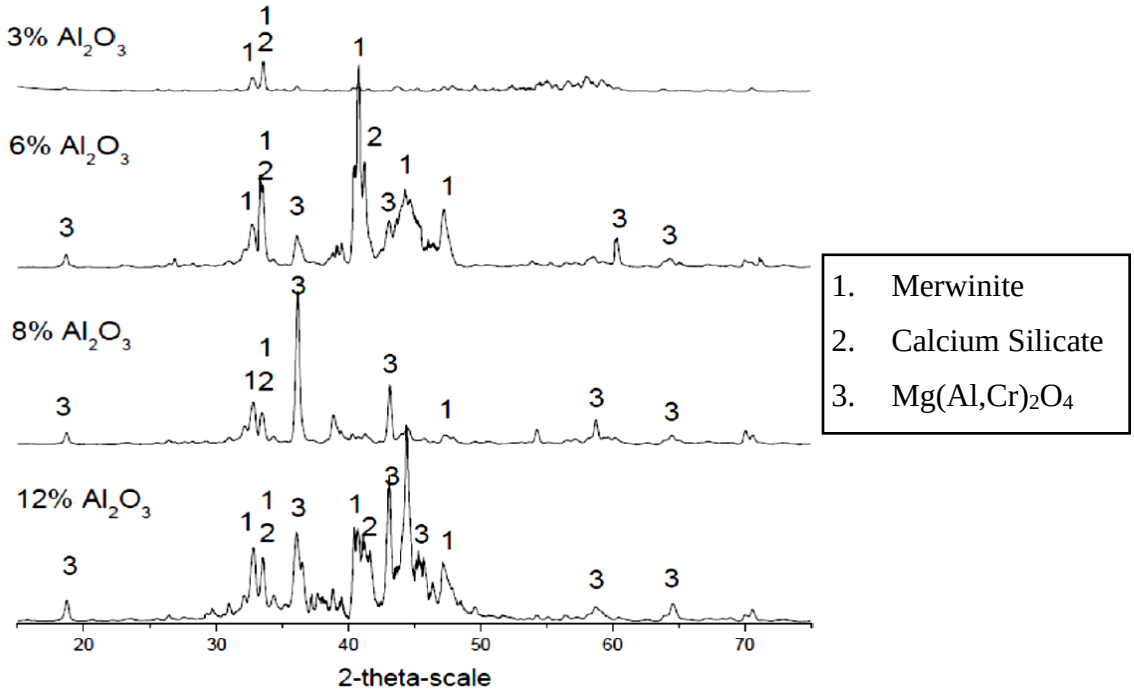

Figure 2.13: XRD analysis of $CaO-MgO-SiO_2-Cr_2O_3-Al_2O_3$ synthetic slag with varying Al_2O_3 content at $P_{O_2} = 10^{-4}$ Pa and 1400°C holding temperature [14].

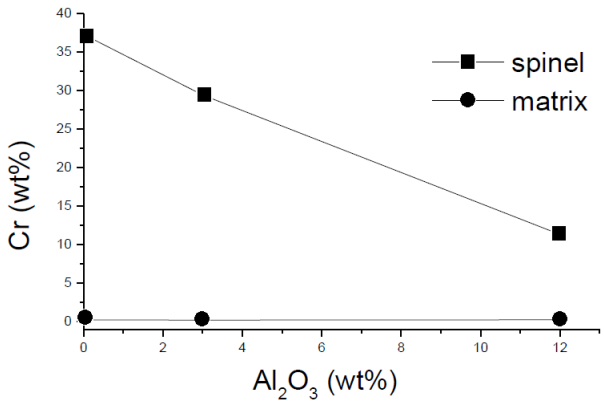

Figure 2.14: Cr partition in CaO-MgO-SiO_2-Cr_2O_3-Al_2O_3 synthetic slag at P_{O_2} =10 $^{-4}$ Pa as a function of Al_2O_3 content and 1400°C holding temperature [14].

Another investigation on CaO-SiO_2-MgO-Al_2O_3-FeO-Cr_2O_3 synthetic slags provides a theoretical basis for the effect of Al_2O_3 on the spinel enrichment and stabilization of chromium [39]. This study is particularly beneficial for us because of the presence of similar components in the slag composition, notably FeO which was missing in the previous studies. Table 2.4 shows the compositions of the CaO-SiO_2-MgO-Al_2O_3-FeO-Cr_2O_3 synthetic slags in this research. Samples were melted at 1600°C and either directly quenched or cooled to 1300°C before quenching.

Table 2.4: Chemical composition of SiO_2-MgO-Al_2O_3-FeO-Cr_2O_3 synthetic slag in Mass% [39].

No	CaO	SiO_2	MgO	FeO	Al_2O_3	Cr_2O_3	Others	Basicity
1	38.0	38.0	9.0	3.0	4.0	5.0	3.0	1.0
2	36.0	36.0	9.0	3.0	8.0	5.0	3.0	1.0
3	45.6	30.4	9.0	3.0	4.0	5.0	3.0	1.5
4	43.2	28.8	9.0	3.0	8.0	5.0	3.0	1.5
5	40.8	27.2	9.0	3.0	12.0	5.0	3.0	1.5
6	50.6	25.4	9.0	3.0	4.0	5.0	3.0	2.0
7	48.0	24.0	9.0	3.0	8.0	5.0	3.0	2.0
8	42.7	21.3	9.0	3.0	16.0	5.0	3.0	2.0

Samples 1 and 2 with a basicity of 1 show a completely glass phase when quenching from 1600°C. When quenched from 1300°C, melilite and spinel phases were also observed in the samples. Sample 2 with a higher Al_2O_3 content showed a lower chromium content in the spinel phase on EDS (Energy Dispersive X-Ray Spectroscopy) analysis compared to sample 1.

For samples with a basicity of 1.5 a significant increase in the amount of the spinel phase as well as the formation of calcium silicate was reported after quenching from 1600°C. The formation of spinel phases might have to do with the increase in solidification temperature due to increase in basicity. In the study, the calcium silicate phase was differentiated from the glass phase based on small visual differences, although the EDS analysis showed similar compositions for both. At 12% Al_2O_3 no calcium silicate is detected and only spinel precipitated. As the Al_2O_3 content increases from 4% to 12%, the chromium content in both the glass and the spinel phase decrease while it increases in the calcium silicate phase. When quenched from 1300°C, no Cr was detected in the glass phase and the Cr content in the spinel decreased with the increase in Al_2O_3. Both the amount of spinel crystals with regular polygonal shape and the grain size are increased significantly when increasing the Al_2O_3 content of the slag.

When increasing the basicity to 2, periclase along with spinel and calcium silicate forms in samples quenched from both 1600°C and 1300°C, but no periclase is observed in sample 8 with 16% Al_2O_3. At 1300°C, the presence of periclase shifts some of the chromium content to the periclase phase instead of glass with 4.31 at.% at 4% Al_2O_3 which is reduced to 0.6% at.% at 8% Al_2O_3. At 16% Al_2O_3 as the periclase phase was absent, a small amount of chromium (0.17at.%) moved to the glass.

While the chromium content of spinel decreased due to Al_2O_3 addition, a significant increase in the spinel phase was visually observed in the slag due to the formation of $MgAl_2O_4$. Increasing Al_2O_3 content also reduced the amount of water soluble periclase phase and subsequently the dissolution of Cr in periclase. Thus, Al_2O_3 addition can reduce Cr percentage in the spinel phase however it increases the total amount of Cr in spinel by increasing the spinel mass fraction while decreasing the amount of the water-soluble periclase phases.

2.4.4. FeO Content

Since the objective of chromite ore processing is to extract ferrochromium for stainless steel production, ferrochromium slag is expected to have low FeO and Cr_2O_3 contents. Our research is not focused on examining the effect of FeO content on chromium stabilization; however, it is beneficial to study the effect of FeO content on spinel formation in order to further understand the chemistry of the ferrochromium slag. Research done on the effect of FeO content on the stability of chromium in a CaO-SiO_2-MgO-Al_2O_3-Cr_2O_3 slag system can be insightful in this regard. The slag samples were synthesized with a chemical composition of 46.67% CaO, 33.33% SiO_2, 8% MgO, 6% Al_2O_3, and 6% Cr_2O_3. FeO was added as a single component to the slag at 0, 2, 5, 8, 12, 16 and 20 wt% to create 7 samples with different compositions [40].

Increasing the FeO content from 0 to 20 wt% decreases the concentration of Cr(VI) in the leachate from 0.1434 to 0.0021 mg/L which is substantially lower than the standard limits of 0.5 mg/L Cr(VI) according to the Environmental Protection Industry Standard HJ/T301-2007 of the People's Republic of China [40]. Increasing FeO content of the slag decreases the chromium content in the matrix phase. At 12 wt% FeO and higher, the chromium content is too low to be detected by EDS.

FactSage simulations for the slag with 8% FeO show that the matrix phase mainly consisted of all water-soluble phases like calcium silicate, merwinite ($Ca_3MgSi_2O_8$) and melilite (mixture of akermanite $Ca_2MgSi_2O_7$ and gehlenite ($Ca_2Al_2SiO_7$) while the spinel solid solution consists of $MgCr_2O_4$, $FeCr_2O_4$ and a small amount of $MgAl_2O_4$ as shown in Figure 2.15 and Figure 2.16.

During the initial stages of spinel precipitation, the main component in spinel is chromium. As the temperature drops, there is an increase in the content of other elements such as Fe, Mg and Al. FeO starts replacing MgO in the spinel structure. FeO also converts to Fe_3O_4 and precipitates out of the residual slag and promotes spinel solid solution precipitation by virtue of its own spinel structure.

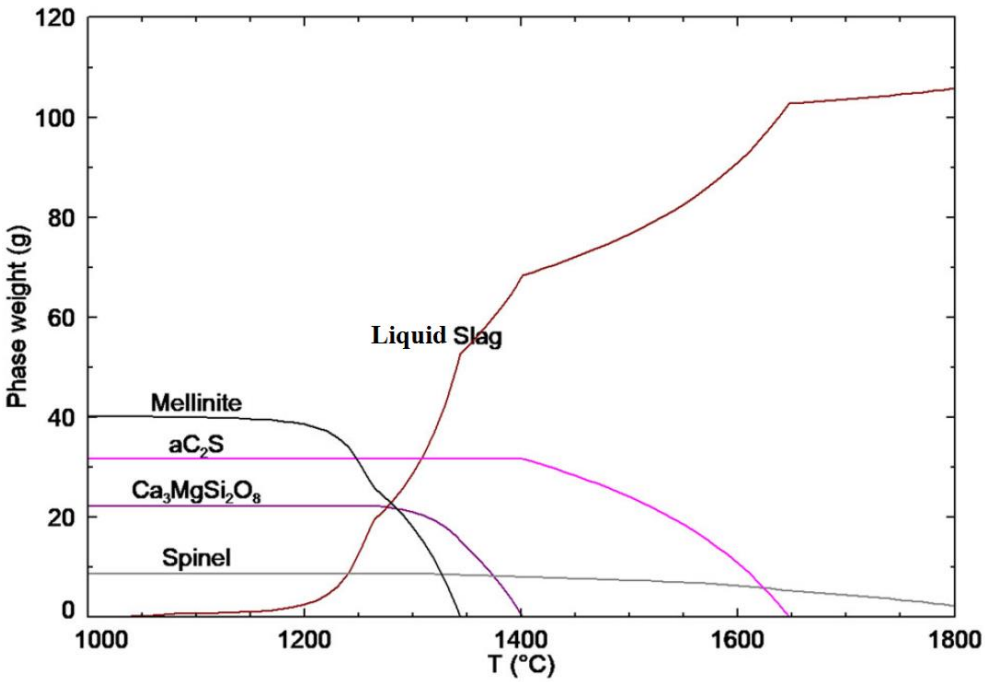

Figure 2.15: Predicted composition of the matrix phase at various temperatures for 8% FeO system calculated using Factsage 7.0 [40].

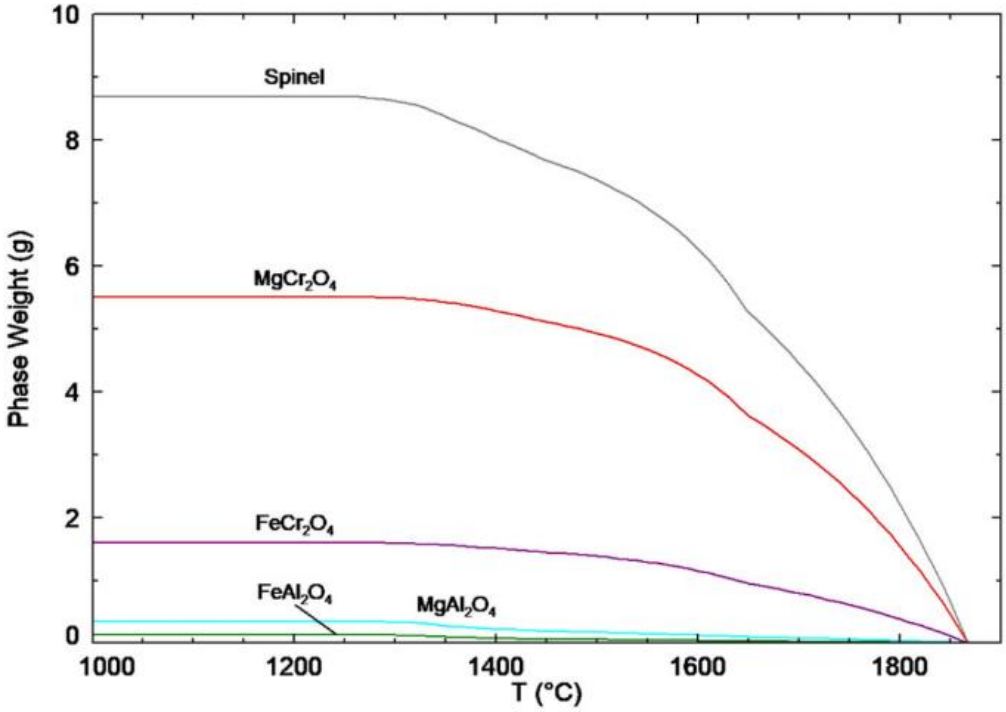

Figure 2.16: Predicted composition of the spinel phase at various temperatures for 8% FeO system calculated using Factsage 7.0 [40].

FeO promotes a three-layered structure in spinel called a core-shell heterostructure as shown in Figure 2.17, with the inner core rich in Cr and the outer layer containing Fe. The transition layer in between the core and the outer shell consists of Mg, Cr and Fe oxides. $MgCr_2O_4$ precipitates first and forms the core of the spinel phase. As the temperature decreases, $Mg_{1-x}Fe_xCr_yFe_{2-y}O_4$ transition layer is formed as Fe(II) starts to replace Mg(II) in the core. Finally, at even lower temperature, Fe replaces more of the Mg to form the $Mg_{1-x}Fe_xFe_2O_4$ outer layer.

(a) $MgCr_2O_4$ (b) $Mg_{1-x}Fe_xCr_yFe_{2-y}O_4$ (c) $Mg_{1-x}Fe_xFe_2O_4$

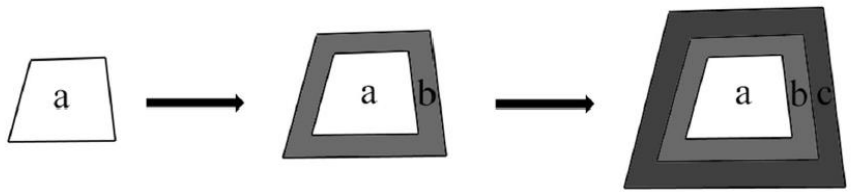

Figure 2.17: Schematic diagram of the formation of the spinel structure in the presence of FeO during cooling process [40].

Since chromium leaching is a liquid-solid interface reaction, the newly formed three-layered structure further strengthens the spinel stability by increasing the spinel size. This is observable, as increase in FeO content from 2 to 20 wt.% increases the spinel crystal size from 5.77 to 8.4 μm as FeO further replaces the MgO in spinel. As the Cr rich core is encased with more layers of spinel, it reduces the possibility of CaO from the matrix to form unstable calcium chromate. This proves that FeO in the above slag composition increases the spinel size and helps with stabilizing chromium.

2.4.5. Factor Sp

The leachability of Cr from ferrochromium slag is influenced by the slag composition; hence, it is useful to introduce a parameter that encompasses the effect of the main components of the slag. The effects of different spinel forming compounds on Cr leaching are described in a parameter called factor sp. Eq (5) which was originally developed for EAF slag shows the correlation between factor sp and the slag composition [41].

$$\text{Factor sp} = 0.2W_{MgO} + 1.0W_{Al_2O_3} + xW_{FeO_n} - 0.5W_{Cr_2O_3} \qquad \text{Eq (5)}$$

In the above equation, W represents the wt% of oxides, x is a constant that depends on the oxidation state of the EAF slag with a value between 1 and 4, and n has a value between 1 and 1.5 based on the FeO and Fe_2O_3 content [41].

The leaching of chromium depends on the value of factor sp of the slag. Low values of factor sp, i.e. < 5 wt%, indicate high leaching of chromium while high values of factor sp, i.e. > 25 wt%, indicate negligible leaching of chromium. The research was intended to recover valuable chromium from EAF slag during stainless steel production and stabilize the remaining chromium in the slag in spinel phase to make the slag suitable for use as a construction material.

Various materials listed in Table 2.5 were added to the original slag in the transfer ladle during tapping to induce spinel formation. Initial experiments on the slag conducted separately with the addition of pure oxides of Al_2O_3 and/or MgO and/or FeO_n show an increase in the amount of chromium stabilizing spinel in the slag and thus a decrease in the amount of leachable chromium. Addition of Cr_2O_3 has an opposite effect. In the following tests, rather than pure oxides, different industrial materials containing MgO, Al_2O_3 and FeO_n were used for economical purposes. The agents are divided into four categories:

- Natural Raw Materials (Bauxite)
- Residues from industrial production (Mill scale, Residue 1 and 2)
- Fluxes for secondary metallurgical slags
- Secondary metallurgical slags (S.Slag)

The results of XRD analysis of both residue materials show $MgAl_2O_4$ and Al_2O_3 as the main components. Addition of residues 1, 2 and mill scale promotes the stability of chromium in the slag. The addition of materials containing high FeO_n content such as bauxite and mill scale reduced the concentration of the leached chromium to below the equipment detection limit of <0.01 mg/l.

Failure of treatment was seen in case of secondary metallurgical slags due to their high CaO and low Al_2O_3 content. The application of the secondary metallurgical flux was unsuccessful due to its insufficient solubility in the liquid slag. In both cases, the chromium content of the leachate was unchanged.

Table 2.5: Chemical composition of the materials used for promoting spinel formation in the slag [41].

Material	Bauxite	Mill Scale	Residue 1	Residue 2	Flux	S.Slag
CaO wt%	0.37	-	3.96	3.72	51.10	23.17
SiO_2 wt%	2.85	-	22.10	10.80	1.93	3.29
MgO wt%	0.24	<0.10	7.30	11.00	11.50	6.18
Al_2O_3 wt%	54.20	0.21	62.5	70.60	35.90	60.87
FeO wt%	0.67	58.18	-	-	-	-
Fe_2O_3 wt%	25.89	37.21	-	-	-	1.04

2.5. Effect of the Cooling Rate on Cr Leaching

The cooling rate of slag during post-smelting operations in ferrochromium production has a significant effect on the crystallization of different phases in the slag. Several studies have been conducted to identify the required cooling rate for different steelmaking slags to promote a desired phase structure. While there are variations in the results obtained from these studies, their work could be used to obtain a better understanding of the phases formed due to different cooling rates and their effect on the leachability of chromium from the slag.

Modification of the structure of four different types of steelmaking slags was done by rapid cooling using water granulation and semi-rapid cooling in the crucible [42]. The formation of glassy slag under different cooling conditions and its effect on the leachability of heavy metals from the slag was investigated. It is worth noting that although the compositions of these slags are not the same as the ferrochromium slag, some of the phases such as calcium silicates and spinel are common between these slags. Therefore, examining the effect of the cooling rate on these different slags can provide insightful information on the leachability Cr from ferrochromium slag. The compositions of these slags were determined using ICP and XRF (Table 2.6).

Table 2.6: Chemical composition (in Wt%, Cr content represented in ppm.) of ladle, basic oxygen furnace, and two electric arc furnace slags [42].

Slag Sample	Fe_2O_3	FeO	Fe Met.	Al_2O_3	CaO	MgO	MnO	SiO_2	Cr(ppm)
Ladle	1.1	0.5	0.4	22.9	42.5	12.6	0.2	14.2	2700
BOF	10.9	10.7	2.3	1.9	45.0	9.6	3.1	11.1	506
EAF 1	1.0	3.3	0.1	3.7	45.5	5.2	2.0	32.2	32700
EAF 2	20.3	5.6	0.6	6.7	38.8	3.9	5.0	14.1	26800

*Negligible amounts of other heavy metals (Mo, Zn, Ni, Cu, etc.) are ignored due to their lack of relevance in the review.

All samples were re-melted at 1600°C using an induction furnace. The structure of all the slags were modified by water granulation cooling or semi-rapid cooling in the crucible except the ladle slag which was modified only by water granulation.

For granulation, as shown in Figure 2.18, each sample was poured into the granulation head where water jets hit the pouring slag to generate slag granules that were collected at the bottom of the water tank. For semi-rapid cooling, the molten slags were left to cool in the crucible from 1600°C to room temperature, which took around 5 hours. Unmodified original samples were used alongside the modified ones for comparison in the leaching tests.

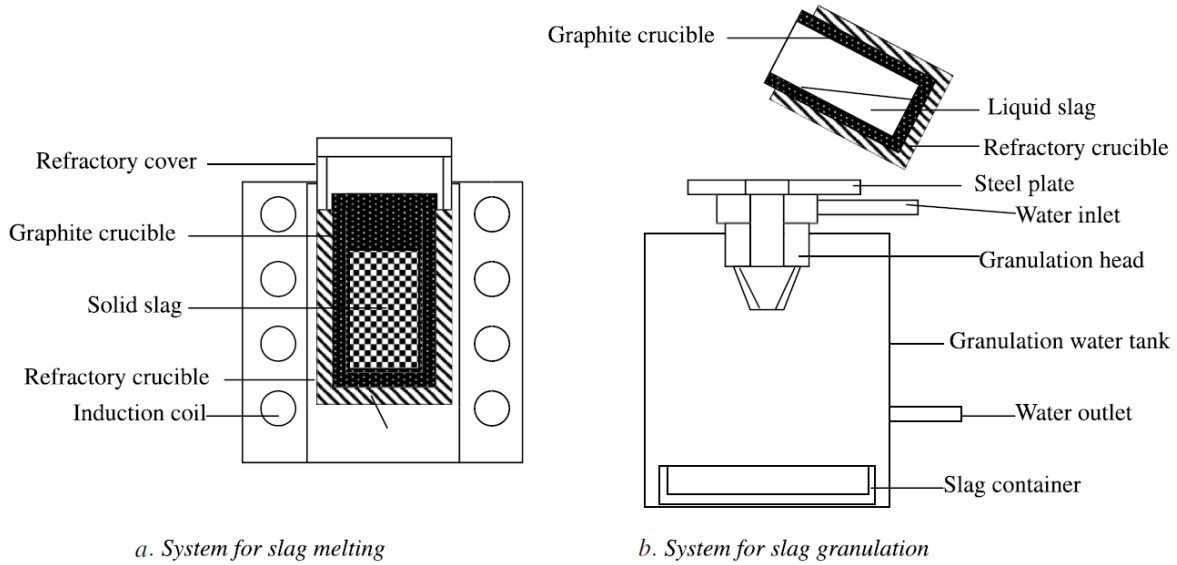

Figure 2.18: Schematic of slag melting and subsequent cooling via slag granulation [42].

Samples were crushed to <4mm before leaching. Ladle and EAF 1 slag samples were leached using two-stage batch test prEN 12457-3 [43] while BOF and EAF 2 slag samples one-stage batch test prEN 12457-2 [44].

The ladle slag is the only sample that became almost completely amorphous by granulation and showed signs of physical disintegration. The major mineral in the slag is mayenite ($Ca_{12}Al_{14}O_{33}$) along with two forms of dicalcium silicate (β-Ca_2SiO_4 and γ-Ca_2SiO_4), gehlenite ($Ca_2Al_2SiO_7$) and well distributed free MgO. The rapid cooled slag showed lower Cr content in the leachate, 0.08 ppm, compared to the unmodified slag (0.5 ppm).

Original BOF slag shows β-Ca_2SiO_4 as one of the main phases which changes to tricalcium silicate (Ca_3SiO_5) after granulation. This transformation did not occur in the original or slow cooled slag as the phase exists only at high temperature and persists due to rapid cooling. Leaching tests showed that Cr leaching decreased for the semi-rapidly cooled sample, from 0.03 ppm to 0.01 ppm.

For the EAF 1 slag, a large amount of crystalline merwinite ($Ca_3MgSi_2O_8$) is present in the original and two modified slags. γ-Ca_2SiO_4 was only found in the original and semi-rapidly cooled samples. Complex spinel phase of (Mg, Mn)(Cr, Al, Fe)$_2O_4$ was also observed in both the original and modified slag. The solubility of Cr for all 3 samples was below 1 ppm with the semi rapidly cooled sample being slightly lower (0.82 ppm) than the rapidly cooled sample (0.93 ppm).

The main compound in EAF 2 slag in all cases was β-Ca_2SiO_4 along with a wustite-type solid solution of (Fe, Mg, Mn)O, Ca_2(Al, Fe)$_2O_5$ and Fe_2O_3. The semi-rapidly cooled samples had the lowest Cr content in the leachate (0.008 ppm) compared to the unmodified (5.8 ppm) and rapidly cooled (3.8 ppm) samples.

The BOF and EAF 2 samples show lower Cr content in the leachate of the semi-rapid cooled samples while EAF 1 samples do not show a significant change. The Cr leaching from both EAF slag samples were also higher than the BOF and ladle slag. The reason behind this might have to do with the composition of the slags, since the Cr leaching behaviour of the samples appears to be influenced by their initial Cr content. The EAF slags with higher Cr content showed higher Cr leaching compared to the BOF and ladle slags. Similarly, BOF slag with lower Cr content compared to the ladle slag, had lower Cr leachability. An exception is seen when comparing the

two EAF slags, as EAF 1 slag with the higher Cr content showed significantly lower Cr leaching compared to the EAF 2 slag. This behaviour is associated with the complex $(Mg,Mn)(Cr,Al,Fe)_2O_4$ spinel phase formation in EAF 1 slag which did not form in the EAF 2 slag. The low Cr leaching (0.008 ppm) for the semi-rapidly cooled EAF 2 slag is probably an experimental error as it is significantly lower than its original or rapidly cooled counterparts.

A similar study investigated the effect of the cooling process of stainless steel EAF slag on its leaching behaviour [45]. The composition of four electric arc furnace slags from four different stainless steel grades are shown in Table 2.7. Two sets of samples were prepared for each slag composition denoted by A, B, C, and D by either slow or rapid cooling denoted by 1 and 2 respectively.

In case of slag sample B, instead of water jetting, the sample was immersed in a bucket of cold water. The slag samples were also enriched in metals like Mo, Ba and Cu which are ignored in this literature review.

Table 2.7: Total chemical composition (in Wt%) of four types of EAF slag along with their total Cr release on leaching [45].

Sample	CaO	SiO_2	Al_2O_3	MgO	Cr_2O_3	MnO	Fe	Cr (ppm)
A1	37.46	20.24	6.59	8.69	12.00	3.54	6.70	0.07
A2	35.40	19.50	6.65	9.10	12.70	3.63	7.30	0.39
B1	41.43	18.82	8.86	9.55	9.18	3.03	4.40	0.01
B2	38.20	18.52	8.08	9.59	10.61	3.58	5.30	0.30
C1	36.40	22.40	7.47	13.80	5.91	3.29	8.00	0.42
C2	37.34	22.95	7.85	13.60	5.24	3.23	6.00	0.35
D1	43.60	10.78	15.55	10.73	1.54	1.45	10.60	0.01
D2	35.40	18.83	11.13	8.70	3.04	1.76	10.50	0.03

* 1 and 2 after the symbol represent air and water cooled samples respectively.

As shown in table 6, the concentration of Cr in the leachate for all EAF slags are exceptionally low, indicating a tightly bound matrix holding Cr in place. All slag samples except C show a noticeably lower Cr content for the air-cooled samples. This observation seems to be in agreement with the previous study [42] as sample C having the highest SiO_2 content showed a minor change in the leachate Cr content while the rest showed low Cr concentration on the slower cooling rate. MgO content in these samples are higher than those in the previous tests [42], however the lack of

XRD analysis in this study leaves questions about the possibility of spinel formation. Al_2O_3 content of the samples are also high, which could reduce the stability of $MgCr_2O_4$ if they formed.

In another study, phase composition of an EAF and a BOF slag are examined under different cooling rates [46]. Similar to the study by M. Tossavainen [42], these samples were modified by re-melting followed by cooling in crucible (semi-rapid cooling) or water granulation (rapid cooling). The compositions of the slag samples are shown in Table 2.8.

Table 2.8: Chemical composition of EAF and BOF slag [46].

Sample	FeO	Fe_2O_3	Fe Met.	CaO	MgO	MnO	SiO_2	Al_2O_3	Cr_2O_3	P_2O_5
BOF	3.3	1.0	0.1	45.7	5.2	2.0	32.3	3.7	4.8	-
EAF	10.7	10.9	2.3	42.2	9.6	3.2	11.1	1.9	0.1	0.5

Figure 2.19 shows the crystalline phases in the semi-rapidly cooled BOF slag. The major phases are a wustite-type solid solution ((Mg, Fe, Mn)O), β-dicalcium silicate (β-Ca_2SiO_4), calcium ferrite ($Ca_2Fe_2O_5$) and a calcium manganese oxide ((Ca, Mn)O) phase.

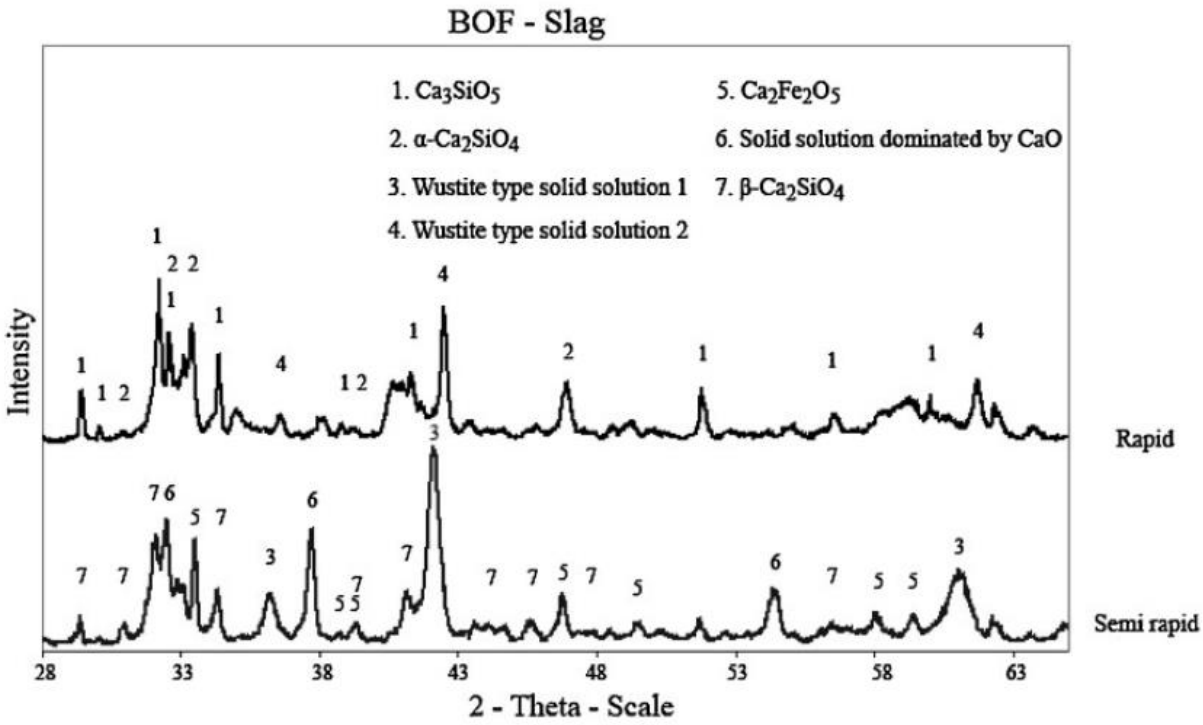

Figure 2.19: XRD analysis of the rapidly cooled and semi-rapidly cooled BOF slag [46].

The wustite like phase is enclosed in the calcium silicate phase indicating an early crystallization of wustite. The rapidly cooled BOF slag show three crystalline phases: the wustite-like phase seen before (Mg, Fe, Mn)O, tricalcium silicate (Ca_3SiO_5) and α-Ca_2SiO_4. Fast cooling is responsible for the formation of the metastable phases such as Ca_3SiO_5 and α-Ca_2SiO_4. The rapidly cooled BOF slag has much smaller crystal size compared to the semi-rapidly cooled sample as the crystals do not have enough time to grow during cooling.

The XRD pattern of the semi-rapidly cooled EAF slag in Figure 2.20 shows three crystalline phases: magnesium chromite/Cr spinel ($MgCr_2O_4$), merwinite ($Ca_3Mg(SiO_4)_2$) and γ-dicalcium silicate (γ-Ca_2SiO_4). SEM analyses show the presence of another phase consisting of Ca, Al and Si which through thermodynamic analysis using FactSage was identified to be gehlenite ($Ca_2Al_2SiO_7$). Crystal growth shows that the spinel and merwinite phase crystallized earlier than gehlenite. The rapidly cooled EAF slag show two crystalline phases: merwinite and the spinel as seen before. This was foreshadowed by the semi-rapidly cooled EAF slag as both of these phases crystallize before gehlenite, based on phase diagrams.

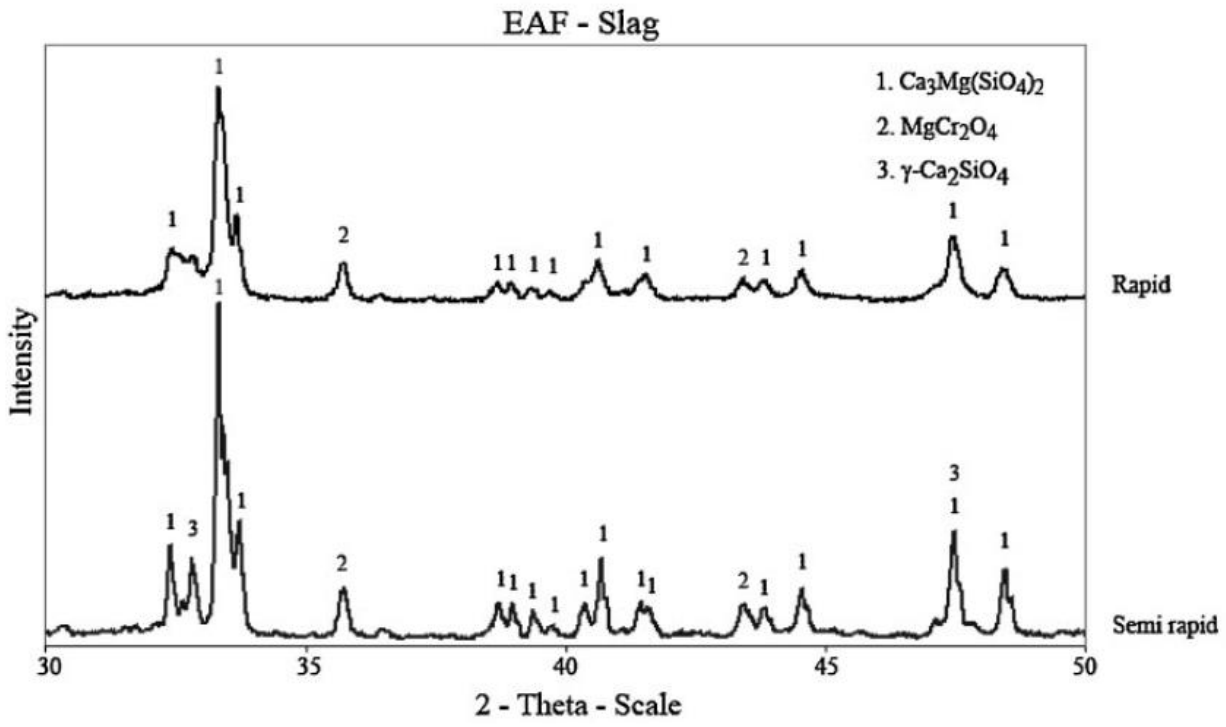

Figure 2.20: XRD analysis of rapidly cooled and semi-rapidly cooled EAF slag [46].

Rapid cooling is seen to increase the spinel formation in the EAF slag as observed from XRD analysis. SEM analysis shows that rapid cooling also promotes a smaller crystal size. The lack of leaching tests in this study makes it difficult to prove the benefit of rapid cooling as other studies with no spinel formation have favoured slow cooling to reduce Cr leaching.

We have chosen to cool down the samples rapidly by quenching the slag containing crucible in water. This was done to preserve the phase composition at the desired temperatures.

2.6. Effect of the Heat Treatment on Cr Stability

Heat treatment is expected to influence the phase transformation in the slag and hence the leachability of Cr(VI). Fast cooling (quenching) from high temperature (1300-1500°C) will prevent the crystallization of non-spinel phases, that are generally Cr unstable. On the other hand, slow cooling at these temperatures would allow more time for spinel to nucleate and grow. An appropriate heat treatment regime should encapsulate the benefits of the different cooling rates in a single cycle.

The impact of heat treatment on the stabilization of chromium involves understanding the phase distribution and chromium partition in chromium-containing slags. With the purpose of stabilizing chromium in the spinel phase, CaO-MgO-SiO_2-Cr_2O_3–(Al_2O_3) slag samples with 8% MgO, 6% Cr_3O_3, 0% Al_2O_3 and basicity of 1.8 were prepared using the heat treatment regimes shown in Figure 2.21 [5][14].

The WDS analysis of samples directly quenched from 1873K (I.a) showed a Cr content of 5.6 at% in the water soluble periclase phase. The Cr content of the periclase phase in samples that were re-annealed at 1673K after quenching (I.b) was reduced to 2.0 at%. Re-annealing released the Cr from the periclase phase, allowing it to form water insoluble spinel phase. Samples after heat treatment I.a also had higher Cr content (2.4 at%) in the silicate and merwinite matrix compared to the samples treated through I.b (1.7 at%). The slow cooling allows Cr that is dissolved in water soluble phases like periclase, merwinite, and dicalcium silicate to transfer to the dissolution resistant spinel phase. Slow cooling also increases the size of spinel phase in the slag. The effect of partial pressure of oxygen as shown with heat treatment cycles II.a and II.b is described in section 2.7.

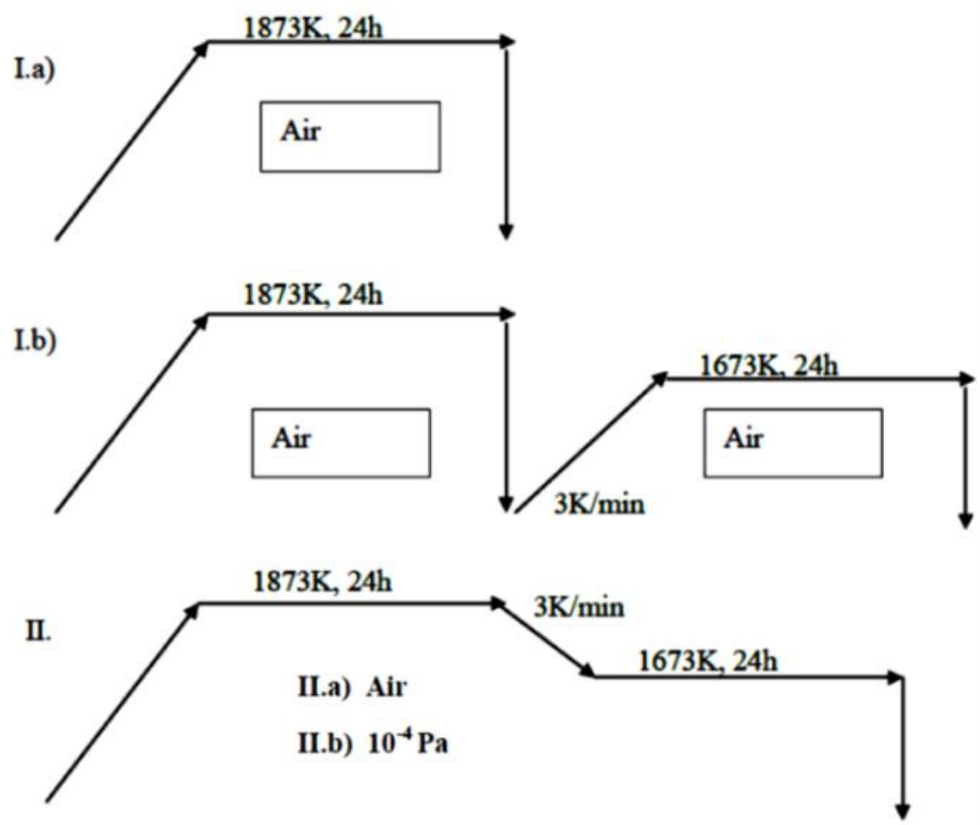

Figure 2.21: Heating sequences and oxygen partial pressures in the case of CaO-MgO-SiO_2-Cr_2O_3-(Al_2O_3) synthetic slags [14].

Based on the results obtained from various cooling regimes, it is concluded that slow cooling of the slag samples to spinel forming temperatures followed by rapid cooling (quenching) would lead to Cr stabilizing by spinel formation in slag. Quenching the samples after sufficient spinel is formed can prevent spinel transformation to other phases.

To determine the best temperature range for spinel formation, we investigated the work done on analyzing the crystallization behaviour of spinel in stainless steel slag during cooling. Previous researchers have used the crystallization kinetic model [47][48][49] to understand the relative importance of the nucleation and growth in the formation of $MgCr_2O_4$ crystals. The nucleation rate denoted by I ($m^{-3}s^{-1}$) and calculated using Eq (6).

$$I = \frac{N_0 kT}{3\pi a^3 \eta} \exp\left[\frac{-b\alpha^3\beta}{\Delta T_r^2 T_r}\right] \qquad \text{Eq (6)}$$

Here, N_0 is the number of molecules or atoms per unit volume defined by $1/a^3$; where a is the lattice parameter of crystal (denoted by m), k is the Boltzmann's constant in JK^{-1}, T is the absolute temperature, η is the viscosity of slag in Pa sec; b is a constant determined by the nucleus shape and is equal to 16π/3 for spherical nucleus, α is the crystal liquid interfacial tension in Jm^{-2}, β is the molar heat of fusion in $Jmol^{-1}$, T_r is the reduced temperature defined by T/T_m, and $\Delta T_r = 1-T_r$, T_m is the melting point of spinel,

The growth rate is denoted by U (ms^{-1}) and calculated using Eq (7).

$$U = \frac{Df}{a}(1 - exp[\frac{-\Delta H_m \Delta T_r}{RT}]) \qquad \text{Eq (7)}$$

Here, ΔH_m is the molar heat of fusion in $Jmol^{-1}$, D is the diffusion coefficient in m^2s^{-1}, R is the gas constant in $Jmol^{-1}K^{-1}$, f is the fraction of acceptor sites on the crystal surface. When $\Delta H_m<2RT_m$, f is equal to 1, when $\Delta H_m>4RT_m$, f is equal to $0.2\Delta T_r$.

The values of I and U were calculated as functions of temperature as shown in Figure 2.22. The crystallization rate denoted by r (s^{-4}) was then calculated using Eq (8).

$$r = \frac{\pi}{3} I U^3 \qquad \text{Eq (8)}$$

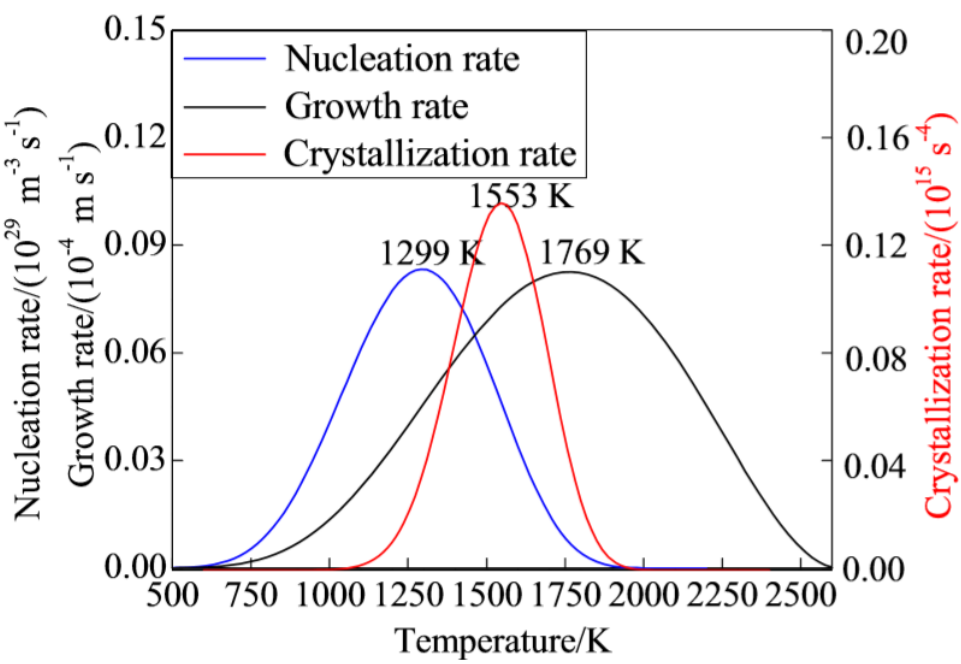

Figure 2.22: Nucleation, growth, and crystallization rates of $MgCr_2O_4$ crystals [47].

The optimum temperature for spinel crystallization was determined to be around 1553K with a suitable temperature range of 1523-1623K. To verify the results of the theoretical calculation, high temperature experiments were performed on stainless steel slags with 40.8% CaO, 27.2% SiO_2, 9% MgO, 3% FeO, 12% Al_2O_3, 5% Cr_2O_3, and 3% CaF_2. The samples were heated to 1873K and held for 30min to ensure complete melting. The slags were then cooled at a rate of 5K/min to 1423, 1473, 1523, 1573, 1623, 1673, and 1773K before water quenching.

The results of XRD and SEM-EDS analyses show that the main phases present for the samples quenched from 1773K are spinel, merwinite and dicalcium silicate (Figure 2.23). The glass phase has as high as 0.38 at.% Cr while merwinite phase contains 0.21 at% Cr. At 1673K and 1623K the Cr content in the glass phase declined to 0.3 and 0.19 at.% respectively. Further decrease in temperature to 1573K reduces all the Cr in the glass phase to an undetectable range with almost all the Cr enriched in the spinel. Melilite also precipitates at this temperature. Further reduction in temperature has no detectable change in the Cr distribution. The results of the study are in excellent agreement with the theoretical findings as spinel formation is expected to be the highest below the 1623K threshold with maximum formation at 1553K. Samples at 1773K are also expected to have the highest Cr leaching due to the lack of spinel nucleation according to the theoretical analysis.

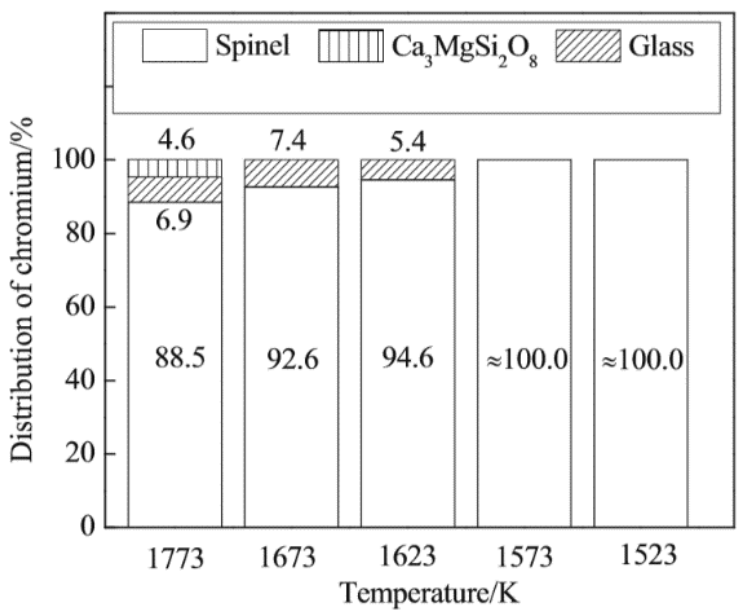

Figure 2.23: Distribution of chromium in samples at different quenching temperatures [47].

The mean diameter of spinel crystals is 6.5µm at 1773K and it slightly increases at 1623K. The most significant growth of spinel is observed when cooling from 1623K to 1523K where the mean diameter increases from 10.8 to 24.8µm. The growth rate is much lower when cooling to temperatures below 1523K. This observation is consistent with the theoretical calculations.

The research was further verified using leaching tests on the samples quenched from 1873K and 1573K [50]. The study determined that glass dicalcium silicate and merwinite are the main source of chromium release in acidic systems. These phases disappear when the samples are quenched from 1573K. Leaching tests show that Cr content in a standard acid solution with 2:1 mass ratio of sulfuric acid and nitric acid and pH of 3.2 is less than 0.01mg/L for slag quenched from 1573K. This sample has almost all of its chromium in the spinel phase. The research was able to conclude that quenching slags from 1573K can significantly reduce Cr leaching from stainless steel slag compared to those quenched from 1873K.

2.7. Effect of Oxygen Partial Pressure on Cr Release

Heat treatment can be crucial to the formation of spinel and the subsequent stabilization of Cr in slag. However, the same heat treatment regime can produce different results based on the atmosphere in which it is conducted. The oxygen partial pressure of the atmosphere is critical during the heat treatment process. While our research will not observe the effect of oxygen partial pressure, it will employ the results of the previous studies to choose a proper atmosphere for the furnace.

As shown in Figure 2.21, the effect of heat treatment under different oxygen partial pressure was examined using CaO-MgO-SiO_2-Cr_2O_3-(Al_2O_3) slags [14]. The chromium content in leachate solution is lower in case of heat treatment cycle with lower oxygen partial pressure compared to the heat treatment conducted in air. In samples soaked in the air, the magnesium spinel solid solution phase contained foreign ions such as Ca^{2+} and Si^{4+}. These ions create point defects in the spinel phase, disturbing its growth and making the phase less thermodynamically stable. In addition, chromium (III) easily oxidizes to chromium (VI) at high temperature in presence of oxygen.

Partial pressure of oxygen in CO atmosphere has a similar effect on Cr release from the ferrochromium slag in equilibrium with ferrochromium [51]. Decreasing the CO partial pressure

(increasing the oxygen partial pressure) seems to increase the Cr leachability of the slag. It is concluded that the oxygen partial pressure of the furnace atmosphere should be kept at a minimum to reduce Cr leaching.

2.8. Leaching Method

The largest environmental concern relating to FeCr slag reuse and disposal is the release of Cr from it. While most of the Cr in slag remains stabilized inside spinel crystals, a small amount might be released from the slag through prolonged exposure and leaching. Appropriate leaching tests need to be conducted on FeCr slag to determine its suitability to be reutilized as a construction material.

The AV002.1 availability test was designed to measure the maximum mobile faction of inorganic constituents that can be released into a solution from a solid matrix in the presence of a strong chelating agent such as EDTA (ethylenediamine tetra acetic acid) [52]. The test was developed in collaboration with the United States Environmental Protection Agency (USEPA) to determine the potentially extractable content of chromium under environmental conditions and to overcome the limitations of the more commonly used US based toxicity characteristic leaching procedure (TCLP). The over-broad application of the TCLP test was criticized as concerns were raised regarding its technical considerations. The AV002.1 availability test more accurately estimates leaching behaviour of wastes over several parameters including pH, liquid-solid (L/S) ratio and waste form compared to the more commonly used tests [52].

The AV002.1 test employs 50 mM EDTA in DI (de-ionized) water as a chelating agent to extract metals of interest at near-neutral pH (7.5). The test is a batch extraction process where pH remains between 7-8 after extraction, as it is used for materials that may be heterogenous in acid neutralization capacity. A L/S ratio of 100 ml extractant to 1 g sample is maintained with a contact time of 48 hours to reduce limitations of mass transfer. The slurry/solution is tumbled in an end-over-end fashion at 28 ± 2 rpm at room temperature. pH value of the leachate is measured after 48 hours. The procedure is repeated if necessary, by changing the starting pH until the end pH is close to 7.5. The final solution is filtered to remove solid residue and the solution is used for subsequent analysis.

The effectiveness of the AV002.1 availability test was compared with a more commonly used NEN 7341 availability test using concrete samples containing FeCr slag [53]. NEN 7341 is a double extraction process where the solid is leached using DI water at two different pH values of 4 and 7. The L/S ratio is maintained at 50 ml/g for both extractions and the end solutions are mixed and then filtered to obtain the final solution. Concrete samples were prepared by replacing parts of the fine aggregate with water cooled FeCr slag and parts of the coarse aggregate with air cooled FeCr slag. The composition of the two different FeCr slag are presented in Table 2.9.

Table 2.9: Major constituents (mass%) of FeCr slag determined by XRF analysis [53].

FeCr Slag	Cr_2O_3	Al_2O_3	SiO_2	MgO	CaO	Fe_2O_3
Water cooled	10.37	19.57	27.33	32.28	2.49	4.12
Air Cooled	8.32	22.84	28.87	30.32	2.96	2.85

Using Atomic Absorption Spectrometer (AAS) analysis the total Cr content of the concrete samples were measured to be 2.85-3.55 mass%. Cr(VI) concentration was also measured to be 6.5-12.8 ppm, using a UV/Vis Spectrophotometer. This showed that majority of the Cr was present as Cr(III) in the samples. The low concentrations of Cr(VI) was expected, since the slag was obtained from the highly reducing environment of a submerged arc furnace process. Samples leached using the NEN 7341 availability test had a leachate total Cr concentration of 24.7-26.8 mg/kg sample and a Cr(VI) concentration of 1.66-2.13 mg/kg sample. In comparison, the AV002.1 availability test produced a leachate total Cr concentration of 27.8-31.4 mg/kg sample and a Cr(VI) concentration of 1.88-2.58 mg/kg sample. The US EPA TCLP method, on the other hand, had a leachate total Cr concentration of 11-17.6 mg/kg sample and a Cr(VI) concentration of 0.96-1.68 mg/kg sample The AV002.1 availability test was able to extract more Cr from the concrete samples than the NEN 7241 test as well as the US EPA TCLP test. The study showed that only 0.022-0.046% of the Cr(III) was released in the solution. However significantly higher percentages of Cr(VI), i.e. 35-38% was dissolved in the solution. This is because Cr(VI) compounds are generally more soluble than the Cr(III) compounds.

Since Cr concentrations in the leachate of the AV002.1 availability test is higher than the US TCLP or the NEN 7341, we conclude that the AV002.1 is a more conservative method for examining Cr

leaching from FeCr slag. The total Cr release from the slag will be compared to the Ontario's aqueous waste leachate limit of 2.77 mg/L total Cr from TCLP test [15] to determine its environmental compatibility and subsequent reutilization.

2.9. Scope and Objective

Chromium is a highly carcinogenic element that causes significant harm if it's allowed to leach into the environment. While the importance of ferrochromium production is undeniable in meeting the demands for the stainless steel production around the world, careful precautions should be taken to prevent potential environmental damage from the production process. The slag produced during FeCr production poses a probable threat of leaching Cr from it, whether the slag is dumped in landfills or utilized elsewhere. Spinel phase formed in the slag has been proven to prevent Cr from leaching. The spinel crystals trap Cr ions in its structure and prevent its dissolution in water.

The current work is part of an extensive research conducted by NRCan (Natural Resources Canada) to investigate the properties of the ferrochromium slag as a byproduct of chromium extraction from the Ring of Fire deposits. The objective of this research is to stabilize Cr in synthetic Al_2O_3-MgO-SiO_2-CaO-FeO-Cr_2O_3 slag system through spinel formation.

The scope of this research includes the following:

1. Examining the effect of temperature on the formation of the spinel phase.
2. Investigating the effect of Al_2O_3 content on Cr leachability of the slag.
3. Examining the effect of basicity on Cr leachability of the slag.

A base composition of the synthetic slag has been provided by NRCan. The heat treatment profile will be determined based on the calculated liquidus temperature, complex pseudo-quaternary phase diagrams and studies on spinel crystallization. The Al_2O_3 and basicity of the slag will be varied in a reasonable range to observe their effect on the Cr stability in the slag. The degree of the stabilization of Cr will be determined using leaching experiments to obtain leachable Cr in the slag. Chemical analysis of the samples will be conducted to determine changes in mineralogy and structure of the slag due to changes in composition.

3. Materials and Methods

The chapter will elaborate on the methodology used to prepare, heat treat, and leach synthetic slag samples and the equipment used in each process. We will also discuss the different chemical analysis and characterization processes used for the synthetic slag and their leachates.

3.1. Materials

Slag samples were synthesized using reagent grade oxides. Pure Al_2O_3 (99%), MgO (99%+), SiO_2 (99%), Cr_2O_3 (99.6%) were obtained from Alfa Aesar and CaO (99.9%+) was obtained from Fisher Scientific. The MgO and CaO powders were calcined at 1000ºC in a muffle furnace (Figure 3.1) to decompose any possible hydroxides and carbonates in them. The SiO_2, Cr_2O_3 and Al_2O_3 were dried at 110ºC in a muffle furnace to get rid of moisture.

Figure 3.1: Muffle furnace used for calcining the reagents.

FeO was synthesized from metallic Fe (95.3% purity, 0.6% Mn, 0.012% P, 0.02% sulfide) chips from Fisher Chemical and reagent grade Fe_2O_3 (99%+) from Sigma Aldrich. Fe chips and Fe_2O_3 were mixed in a 1:1 molar ratio inside an agate mortar and pressed into an alumina crucible. The crucible was then placed inside a vertical tube furnace and heated at 1000ºC for 24 hours in argon

atmosphere to synthesize FeO. The synthesized FeO was analyzed using XRD to confirm the complete reaction between Fe metal and Fe_2O_3 and the formation of FeO. The XRD pattern of synthesized FeO is presented in Figure 3.2. The chemical composition of the synthesized samples with variations in Al_2O_3 content and basicity (CaO/SiO_2) are shown in Table 3.2 and Table 3.2 respectively.

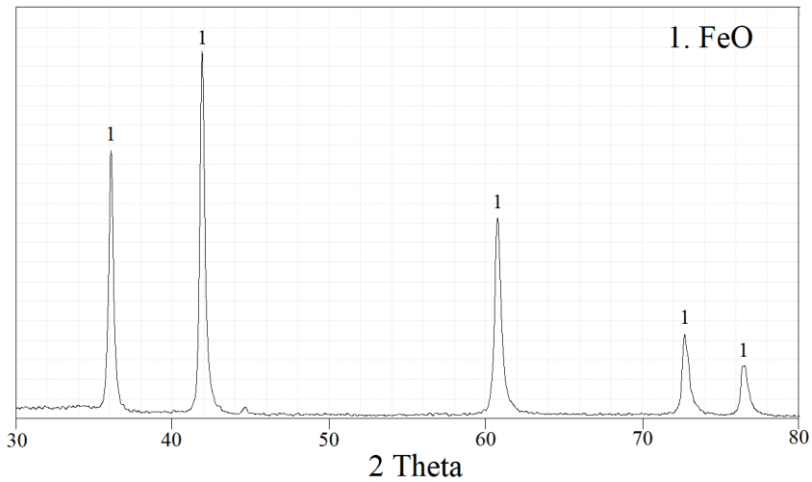

Figure 3.2: XRD pattern of synthesized FeO.

Table 3.1: Chemical composition (mass%) of synthetic slag with varying Al_2O_3 content.

Series	Basicity	Al_2O_3	MgO	SiO_2	FeO	CaO	Cr_2O_3	Total
A1	0.5	20.00	25.00	30.00	4.00	15.00	6.00	100
A2	0.5	15.00	25.00	33.33	4.00	16.67	6.00	100
A3	0.5	12.00	25.00	35.33	4.00	17.67	6.00	100
A4	0.5	9.00	25.00	37.33	4.00	18.67	6.00	100
A5	0.5	6.00	25.00	39.33	4.00	19.67	6.00	100
A6	0.5	3.00	25.00	41.33	4.00	20.67	6.00	100
A7	0.5	0.00	25.00	43.33	4.00	21.67	6.00	100

Table 3.2: Chemical composition (mass%) of synthetic slag with varying Basicity.

Series	Basicity	Al_2O_3	MgO	SiO_2	FeO	CaO	Cr_2O_3	Total
B1	0.3	20.00	25.00	34.61	4.00	10.39	6.00	100
B2	0.4	20.00	25.00	32.14	4.00	12.86	6.00	100
A1	0.5	20.00	25.00	30.00	4.00	15.00	6.00	100
B4	0.6	20.00	25.00	28.13	4.00	16.88	6.00	100
B5	0.7	20.00	25.00	26.47	4.00	18.53	6.00	100

Sample A1 was used in both series as a representative of 20% Al_2O_3 content in Table 3.2 and 0.5 basicity in Table 3.2.

3.1.1. Liquidus temperature and viscosity of the synthetic slag

Theoretical values for the liquidus temperature and viscosity of the slag compositions were calculated before synthesis and heat treatment (Table 3.4 and

Table 3.3). The liquidus temperature was confirmed to be around 1650ºC and below 1700ºC which is the maximum operating temperature for the vertical tube furnace for prolonged use. The liquidus temperature was calculated using Eq (1) and the viscosity was calculated using Eq (2) presented is sections 2.3.1 and 2.3.2 respectively.

Table 3.3: Estimated values for liquidus temperature and viscosity of slag with varying Al_2O_3 content.

Series	Al_2O_3	CaO/SiO_2	Liquidus (°C)	Viscosity(P)
A1	20	0.5	1674.18	3.8
A2	15	0.5	1654.19	3.7
A3	12	0.5	1642.58	3.6
A4	9	0.5	1631.26	3.5
A5	6	0.5	1620.22	3.3
A6	3	0.5	1609.45	3.2
A7	0	0.5	1598.93	3.0

Table 3.4: Estimated values for liquidus temperature and viscosity of slag with varying CaO/SiO_2.

Series	Al_2O_3	CaO/SiO_2	Liquidus (°C)	Viscosity(P)
B1	20	0.3	1656.40	3.2
B2	20	0.4	1665.94	3.5
A1	20	0.5	1674.18	3.8
B4	20	0.6	1681.38	4.3
B5	20	0.7	1687.72	5.0

3.2. Heat Treatment

Predetermined amounts of reagent grade oxides were measured to make different compositions of slag. The slag constituents were mixed in an agate mortar before being pressed inside an MgO crucible (15ml). The total mass of the slag for all the samples was constant and equal to 10g. The

sample loaded MgO crucible was then placed inside an Al_2O_3 crucible (50ml) and hung inside a vertical tube furnace (model# STTV-1700C-3.5-12) using 1mm dia, 99.95% pure Molybdenum (Mo) wire (Figure 3.3).

Figure 3.3: Front view of the vertical tube furnace with an image of the MgO crucible placed inside the Al_2O_3 crucible.

The furnace is fitted with an Al_2O_3 tube (90 mm inner dia x 900 mm height x 3.5 mm thickness) with two removable Al_2O_3 plugs (85 mm outer dia x 100 mm height) on both ends of the tube. The plugs have 300mm long alumina tubes in the middle to allow gas to enter and exit the furnace. The Mo wire is fed through the top plug pipe until the crucible is positioned in the middle of the tube and then fastened using a rubber cork as shown in Figure 3.4.

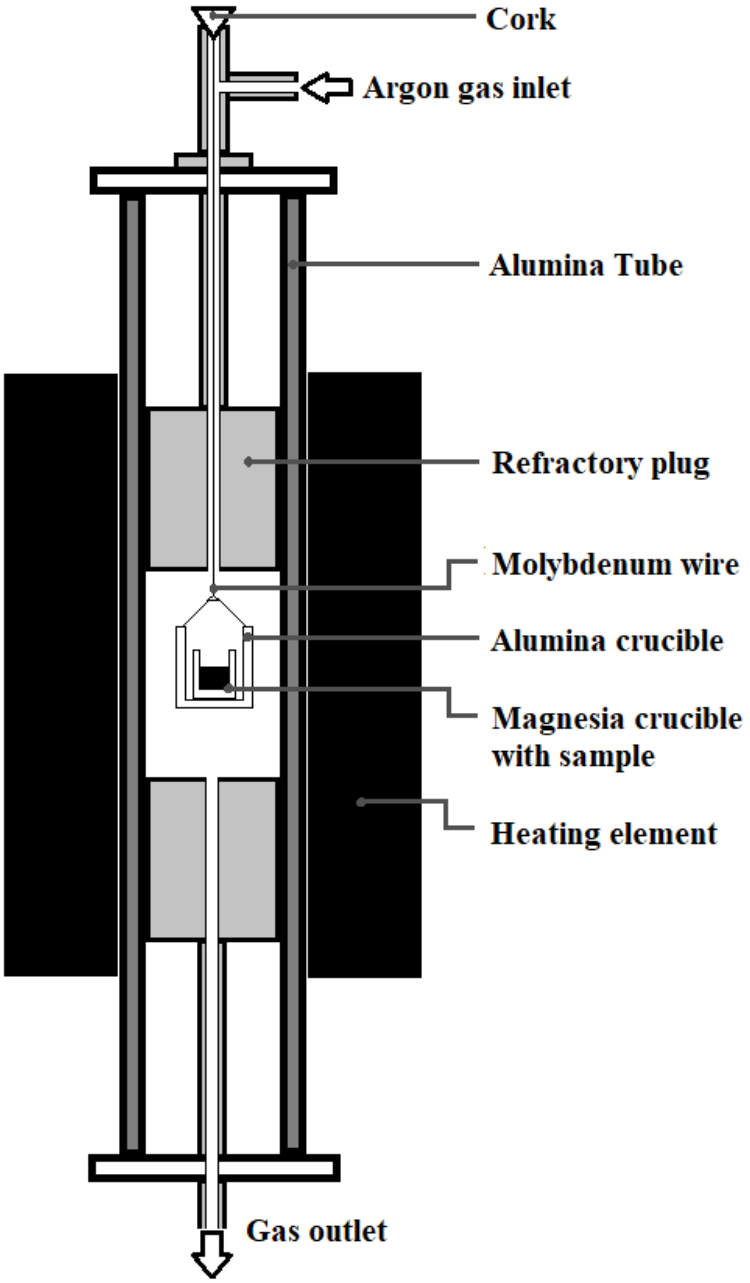

Figure 3.4: Schematic view of the vertical tube furnace with the loaded crucibles hung from a Mo wire.

The furnace is kept in an inert atmosphere with high purity (99.997%) argon gas (supplied by Praxair) at a flow rate of 4 lit/h. After placing the sample, the furnace temperature was raised to 1000ºC at 4ºC/min and then to 1650ºC at 3ºC/min where it was kept for 10 hours to melt the sample. The temperature profile of the furnace is shown in Figure 3.5. The 10 h holding time was determined through preliminary melting experiments by observing the cross sections of melted slag and confirming the absence of undissolved reagents visually. Note that the 1650ºC melting temperature was sufficient despite being lower that some of the calculated liquidus temperature of the slag samples.

Following melting, the temperature was reduced to the holding temperature (1400, 1475, 1550ºC) at 3ºC/min and held for 12 h. After the holding time, the bottom cap is removed and the sample is dropped in a bucket of cold tap water for quenching, by cutting the Mo wire.

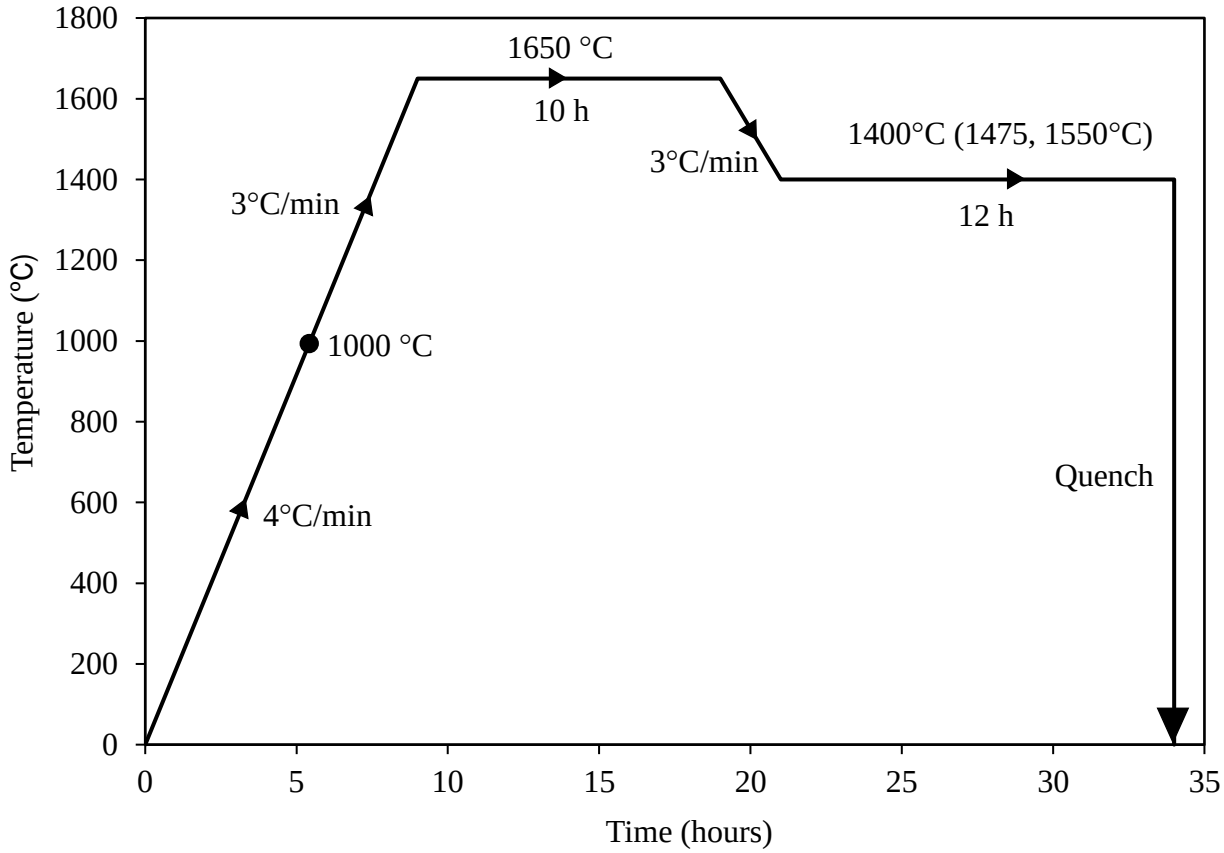

Figure 3.5: Melting and heat treatment cycle for the slag samples.

3.3. Slag Extraction and Processing

Quenched slag samples were allowed to dry in air and weighed to observe any weight loss of the samples. MgO crucibles were initially heated at 1650ºC before being used for slag synthesis to account for mass loss of the crucible during heating. The slag was fused with the crucible and could only be separated physically by using a diamond cutter (Figure 3.6). Half of the sample was extracted to be used for leaching and chemical analysis. Extracted samples were milled using a ball mill (Figure 3.7) inside a 50ml stainless steel container loaded with tungsten carbide milling balls.

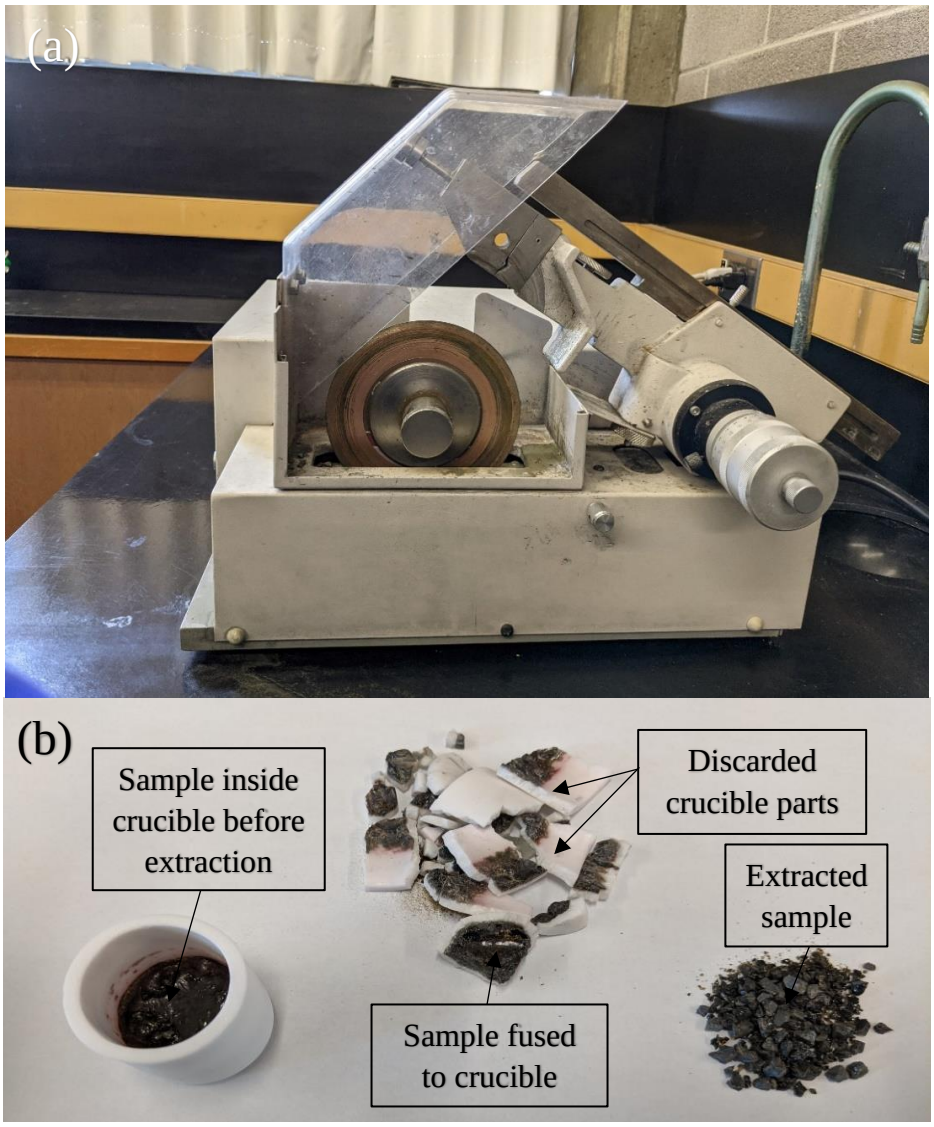

Figure 3.6: (a) The diamond cutter and (b) samples extracted using diamond cutter.

Extracted samples were milled and sieved to <106 µm for leaching and chemical analysis. Sample sized was determined based on preliminary leaching tests on larger size factions showing no detectable Cr in ICP-AES analysis.

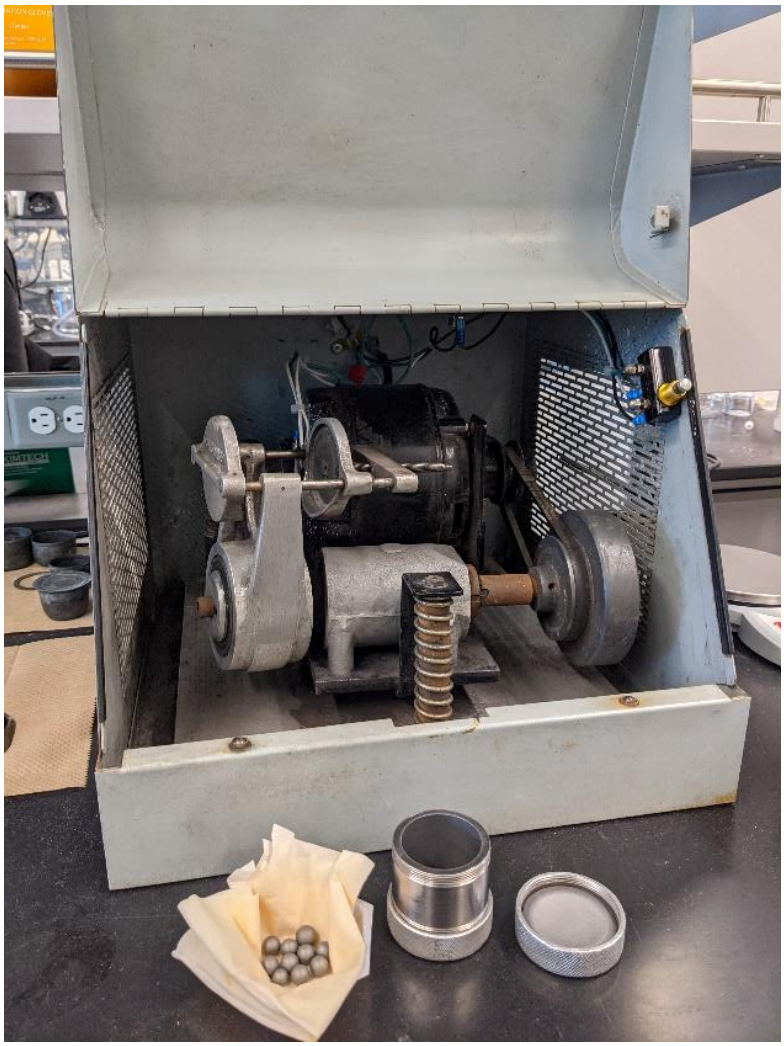

Figure 3.7: Front Image of the ball mill with container and milling balls.

3.4. Leaching Experiment

Leaching experiments were conducted on slag samples with particle size of <106 µm using AV002.1 availability test [52]. Extraction liquid of 50mM EDTA was prepared by dissolving 18.61 g of 99+% purity ethylenediaminetetraacetic acid disodium salt dihydrate salt ($C_{10}H_{14}N_2O_8Na_2.2H_2O$) from Alfa Aesar in 1L of DI water. The pH of the solution was adjusted to 7.5 before leaching by using 2N nitric acid (HNO_3) solution and 1N potassium hydroxide (KOH)

solution. 1 g of <106 µm slag with 100ml of EDTA extraction liquid were placed in 150 ml high density polypropylene (HDPP) containers. The extraction containers were tightly sealed and attached to a makeshift rotary tumbler using a clamp (Figure 3.8) and set to rotate in an end-over-end fashion for 48 h at 35 rpm using a worm geared motor. The leachate was then filtered using a Whatman no.1 filter paper to remove the solid residue. The leachate was stored for analysis with Inductively Coupled Plasma Atomic Emission Spectroscopy (ICP-AES).

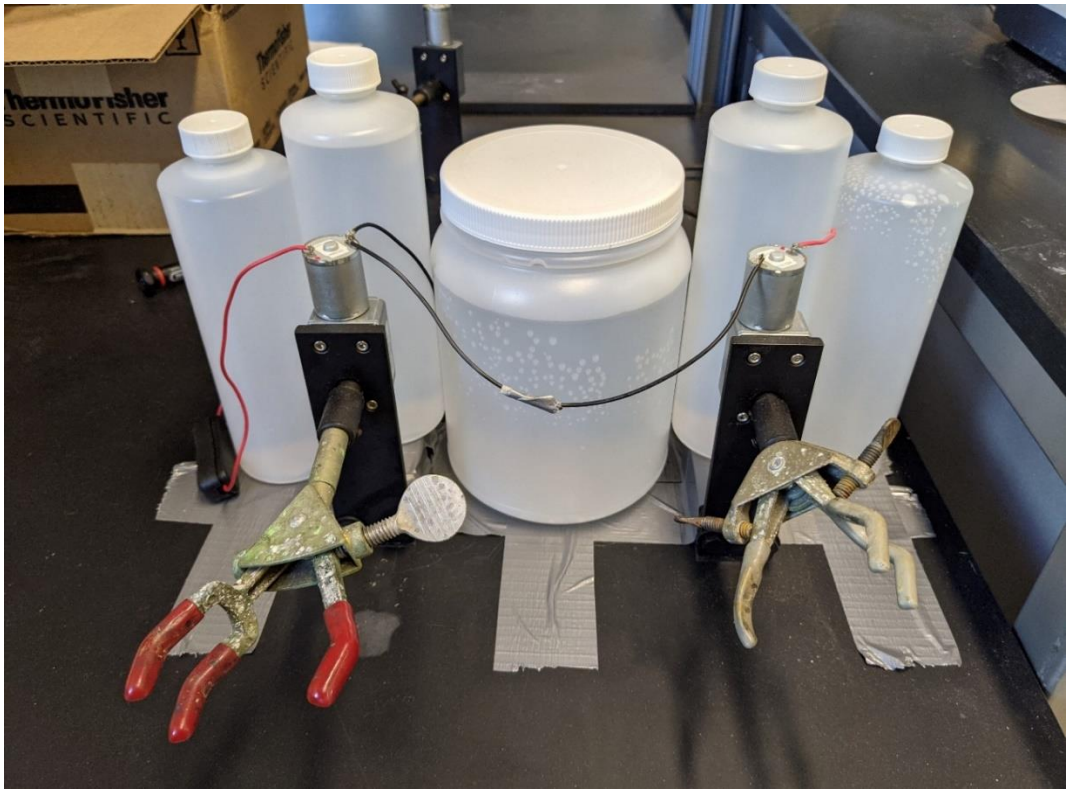

Figure 3.8: The makeshift rotary tumbler for leaching experiment.

3.5. Chemical Analysis

The slag samples were characterized using X-Ray Diffraction (XRD) and Scanning Electron Microscopy with Energy Dispersive X-Ray Spectroscopy (SEM-EDX)) before leaching. The leachate obtained from the leaching experiments were analyzed using ICP-AES.

3.5.1. X-Ray Diffraction

XRD is an analytical technique where crystals are placed in the path of an X-ray beam. The diffracted beam is then processed for intensity and diffraction angle to determine the crystal

structure of molecules. The minerology of slag samples was determined using XRD analysis of >40μ size slag using a Bruker D9 Focus Bragg-Bentano diffractometer with a CoKα radiation source operated at 35kV and 40mA. The equipment collects continuous data of diffracted X-ray with a 2θ range of 3-80° for 30 minutes per sample. The International Centre for Diffraction Database was used to determine the mineralogy of the samples using the diffractogram data.

3.5.2. Scanning Electron Microscopy

In SEM analysis, the interaction of a focused electron beam with the atoms of a sample is used to produce microscopic images of the sample. This can produce different signals using secondary electrons (SE) or back scattered electrons (BSE). Moreover, the electron beam displaces the electrons in the sample atom and the energy released from the atom can then be used for elemental analysis using EDX. For SEM-EDX analysis, slag samples were prepared using small pieces of slag. The pieces were resin mounted and then polished using 240-1200 size polishing paper and 1-6μ polishing cloth. The polished surface was coated with Palladium (Pd) for better imaging using a Denton Vacuum Desk -II sputterer. Hitachi S3000N scanning electron microscope was used for SEM-EDX analysis of the slag samples to determine the crystal size and elemental composition of different phases present in each sample.

3.5.3. Inductively Coupled Plasma Spectroscopy

Elemental compositions of aqueous samples are analyzed using ICP-AES using ionized argon gas. The argon gas flows through a 6000-10000K torch to get rapidly ionized and collides with aqueous samples to break them down to charged ions. The characteristic radiation emitted from different molecule breakdowns in the sample are detected and analyzed for intensity and wavelength. The data obtained from the samples are compared to the data obtained from solutions with known concentration (standards) to determine the elemental concentrations of the samples. For ICP-AES analysis of the leachate obtained from the slag leaching experiments, 9 standards were prepared with Cr concentration ranging from 0 to 1 ppm. Standards were prepared with a 1000 ppm Cr in 2% HNO_3 standard solution and the 50 mM EDTA extraction liquid using a 5000 μL Sartorius mechanical pipette for accuracy. Varian 725-ES ICP spectrometer was used for ICP-AES analysis of the leachates and standards.

4. Results and Discussion

The stabilization of Cr in the current slag system was achieved through variation in holding temperature and changes in chemical composition. The holding temperature that yielded the least Cr leachability of the slag was used to prepare the subsequent samples to observe the effect of chemical composition. Two sets of synthesized samples, with varying Al_2O_3 content and basicity, were analyzed using XRD to observe their mineralogy. SEM analysis was also conducted on select samples to note the changes in phase composition and grain size. Each sample underwent leaching experiments, and the Cr concentrations of the leachates were analyzed using ICP-OES to investigate the Cr stability of the slag samples.

4.1. Cr Stabilization by Heat Treatment

Slag samples with A1 composition were synthesized at dwelling temperatures of 1400ºC, 1475ºC, and 1550ºC followed by quenching. Since the phase diagram for the CaO-MgO-SiO_2-Al_2O_3-Cr_2O_3-FeO system is not available due to its complexity, a simpler pseudo-ternary CaO-MgO-SiO_2-Al_2O_3 phase diagram was used to predict phase formations in the slag. Due to the low composition of Cr_2O_3 (6%) and FeO (4%) in the slag, they were ignored to simplify the initial phase analysis. A pseudo-ternary phase diagram for the CaO-MgO-SiO_2-Al_2O_3 system with fixed 20% Al_2O_3 content was used as shown in Figure 4.1. An estimated composition range for A1 slag is marked for reference. While previous studies have estimated that a temperature range of 1250-1350ºC is ideal for spinel crystallization [47], the solidus temperature of the CaO-MgO-SiO_2-Al_2O_3 phase diagram suggests the formation of other phases such as melilite, merwinite and monticellite besides spinel [54]. Based on the phase diagram in Figure 4.1 holding temperatures 1400ºC, 1475ºC, and 1550ºC were selected to ensure that only spinel crystallizes before other phases. All the Al_2O_3 content of slag samples is expected to be consumed upon the completion of spinel crystallization.

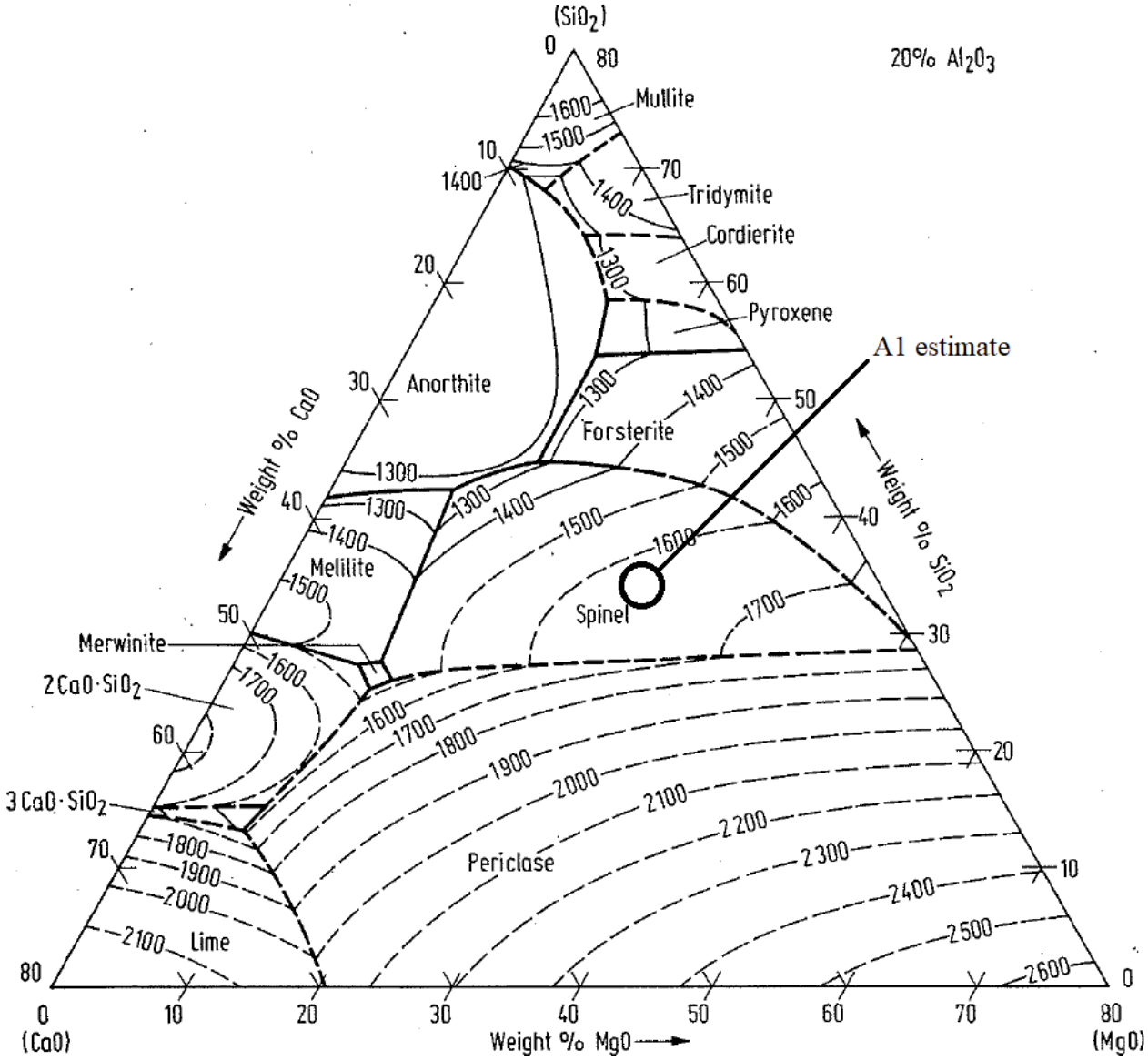

Figure 4.1: Liquidus surface in the CaO-MgO-SiO_2-Al_2O_3 system containing 20% Al_2O_3 with the approximate composition of A1 sample [54].

After the Al_2O_3 content had crystallized, the liquid slag can be essentially treated as a CaO-MgO-SiO_2 system. Incorporation of all the Al_2O_3 (20 wt% of the total slag) in the spinel, would involve removing 8 wt% MgO from the liquid slag. The estimated composition for the liquid portion of the A1 slag in the CaO-MgO-SiO_2 system, after complete spinel crystallization is shown in Figure 4.2. Based on the phase diagram we assumed that spinel crystallization will be followed by forsterite (Mg_2SiO_4) formation and subsequently monticellite ($CaMgSiO_4$) or akermanite ($Ca_2MgSi_2O_7$) formation.

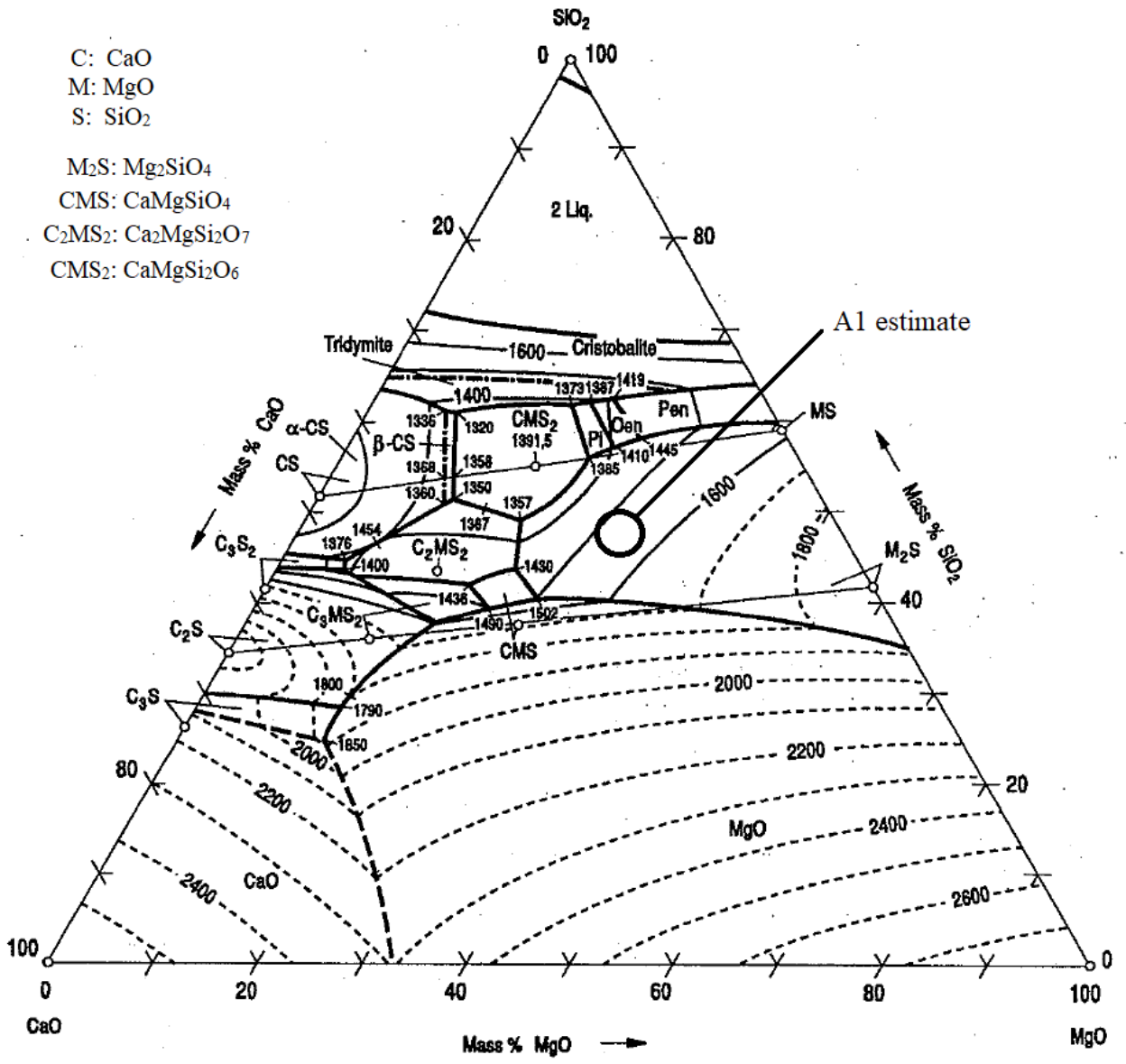

Figure 4.2: Liquidus surface in the CaO-MgO-SiO_2 system with estimate composition for A1 sample after complete spinel crystallization [54].

4.1.1. XRD Analysis

The heat-treated samples with different holding temperatures were analyzed using XRD to determine their minerology. Figure 4.3 shows that the majority phases in all three slag samples are spinel, ringwoodite and akermanite. We also observe minor phases of Cr bearing magnesiochromite complex, $(Mg,Fe)(Al,Cr)_2O_4$, and quartz. There is also a visible amorphous phase present in the slag, shown by the broad non-crystalline peak in the XRD spectrum.

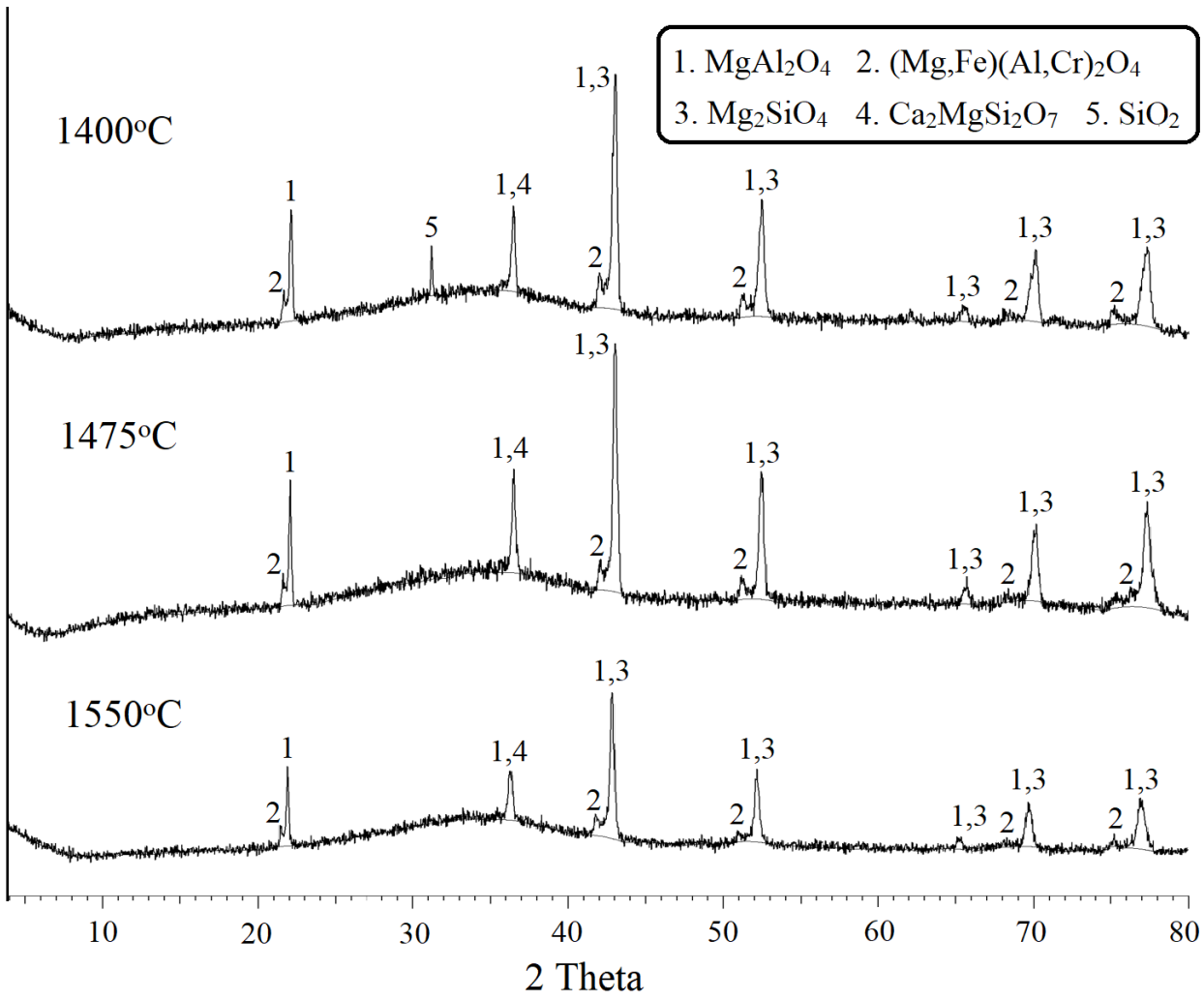

Figure 4.3: XRD analysis of the slag samples with a holding temperature of 1400°C, 1475°C and 1550°C.

The major phases are in agreement with the estimates made through phase diagram analysis of the slag. Spinel and ringwoodite (polymorph of forsterite) are expected to crystallize first, followed my akermanite formation. The Cr bearing spinel complex was not estimated from the phase diagram analysis since Cr and Fe bearing oxides were not considered for simplicity. However, the presence of a complex spinel phase is expected based on the previous studies on characterisation of FeCr slag.

Due to the overlap among the spectra of these major phases, it is difficult to quantify them using XRD analysis. A simple mass balance of the different phases as shown in Table 4.1 is used to find an approximation of the quantity of the different phases. Since spinel is the only Al bearing phase,

its wt% was calculated based on the Al_2O_3 content. Similarly, the akermanite wt% was calculated based on the CaO content. The remaining MgO content after spinel and akermanite calculation was used to determine the ringwoodite wt%. Finally, quartz wt% was determined based on the remaining SiO_2 after ringwoodite calculation. Akermanite is observed to be lower in the XRD spectra compared to the mass balance calculation. This is possibly because akermanite crystallized during the quenching process and not during the holding time. The quenching period being significantly short, it did not provide enough time for most of the akermanite phase to crystallize.

Table 4.1: Mass balance calculation (in wt%) of phases in A1 slag (FeO excluded).

Sample	Spinel	Cr.Spinel	Akermanite	Ringwoodite	Quartz
A1	27.90	7.59	36.46	17.65	6.42

There are slight differences in the XRD spectra of the slag samples held at varying temperatures. The slag held at 1550ºC has a smaller spinel peak in the spectra compared to the slags held at 1400ºC and 1475ºC. This is due to the holding temperature at 1550ºC being too high for spinel crystallization. In other words, holding temperature of 1550ºC prevents the formation of spinel during the dwelling period. High temperature would allow better growth of the spinel crystals but reduce the nucleation rate of new crystals [47]. Crystalline quartz was only present in the slag held at 1400ºC and absent in the slags held at 1475ºC and 1550ºC. Since the crystallization temperature of quartz is 870ºC, it would only crystallize during the quenching period. Since the slag held at 1400ºC possibly had more crystallized phases before quenching, it was easier for quartz to nucleate on those phases.

4.1.2. SEM Analysis

Initial SEM-EDX analysis of the samples was conducted to identify the different phases in the micrograph. Elemental mapping with BSE signal was used on sample A1 as a reference to differentiate between the phases based on their chemical composition (Figure 4.4). The majority of the Al content in the slag is expected to be inside the spinel phase along with Cr. Si and Ca are expected to be outside the spinel phase in the silicate matrix. Mg will be present in both the spinel and the matrix phase. Fe being in low concentration and possibly present in both phases can be ignored for the phase identification. Based on these assumptions the spinel phase was identified as

a polygonal crystal phase shown in the micrograph in Figure 4.4. The spinel has a rough surface while the matrix has a uniform smooth appearance.

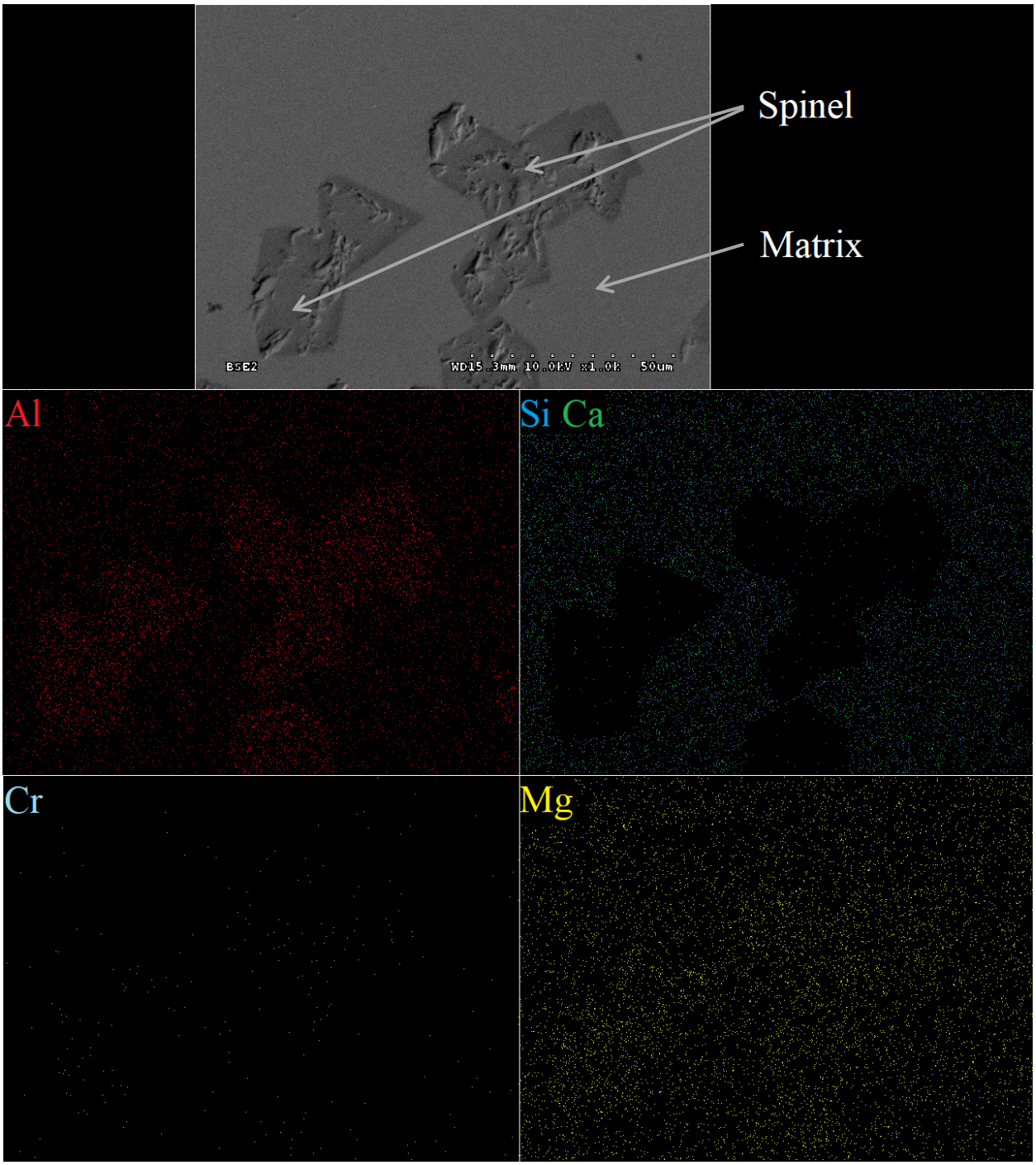

Figure 4.4: SEM micrograph (1000X) and elemental mapping of A1 Slag.

SEM micrographs of A1 slag held at 1400, 1475 and 1550°C are presented in Figure 4.7, Figure 4.6, and Figure 4.7 respectively, to observe the changes in spinel crystals due to the variation in holding temperature. The area of each spinel crystal in the micrograph were measured using ImageJ software by manually tracing the crystal perimeters. The term A_{80} was used to define the apparent cross-sectional area under which 80% of spinel crystals would fall under.

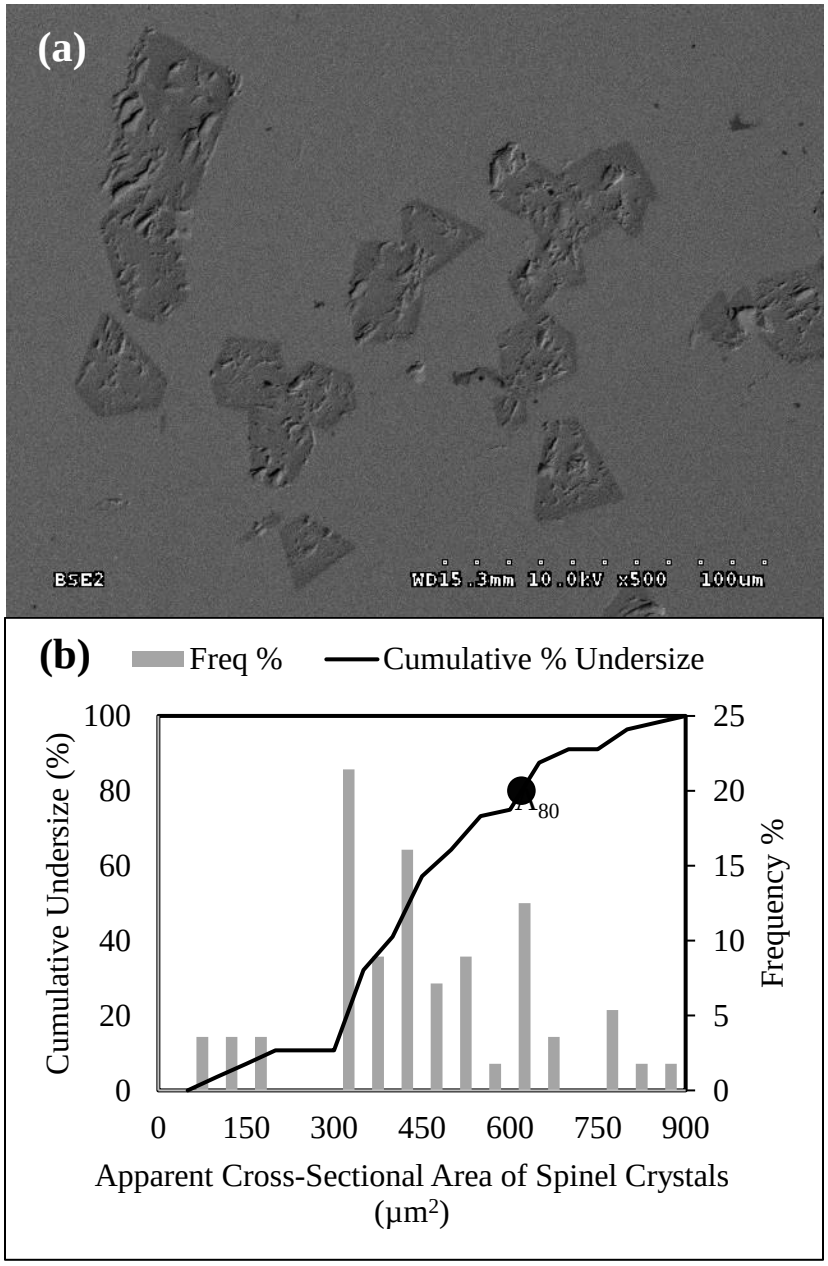

Figure 4.5: (a) SEM micrograph (500X) and (b) crystal size distribution of A1 slag held at 1400°C measured using ImageJ.

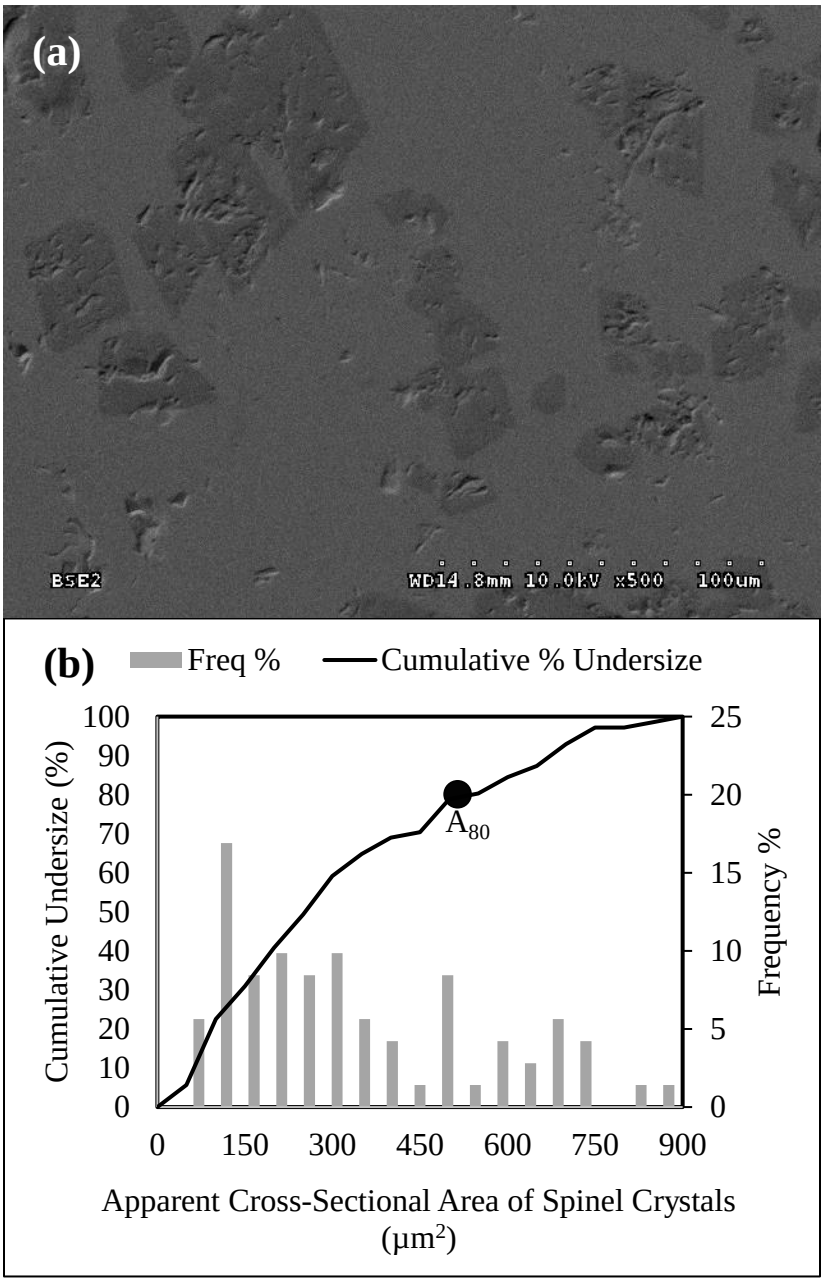

Figure 4.6: (a) SEM micrograph (500X) and (b) crystal size distribution of A1 slag held at 1475°C measured using ImageJ.

The number of particles measured for spinel size analysis in each sample is in the range of 56-92 based on all the observable crystals in two separate SEM micrographs for each sample. The slag held at 1550ºC was observed to have smaller spinel crystals present with a A_{80} of 241 μm^2, compared to the slag held at 1400ºC with a A_{80} of 620 μm^2. Considering the previous findings [47], these smaller spinel crystals possibly nucleated during the quenching phase since spinel

growth is optimum at 1500ºC. In addition, samples at 1400ºC had more time for spinel growth as it cooled down from 1650ºC.

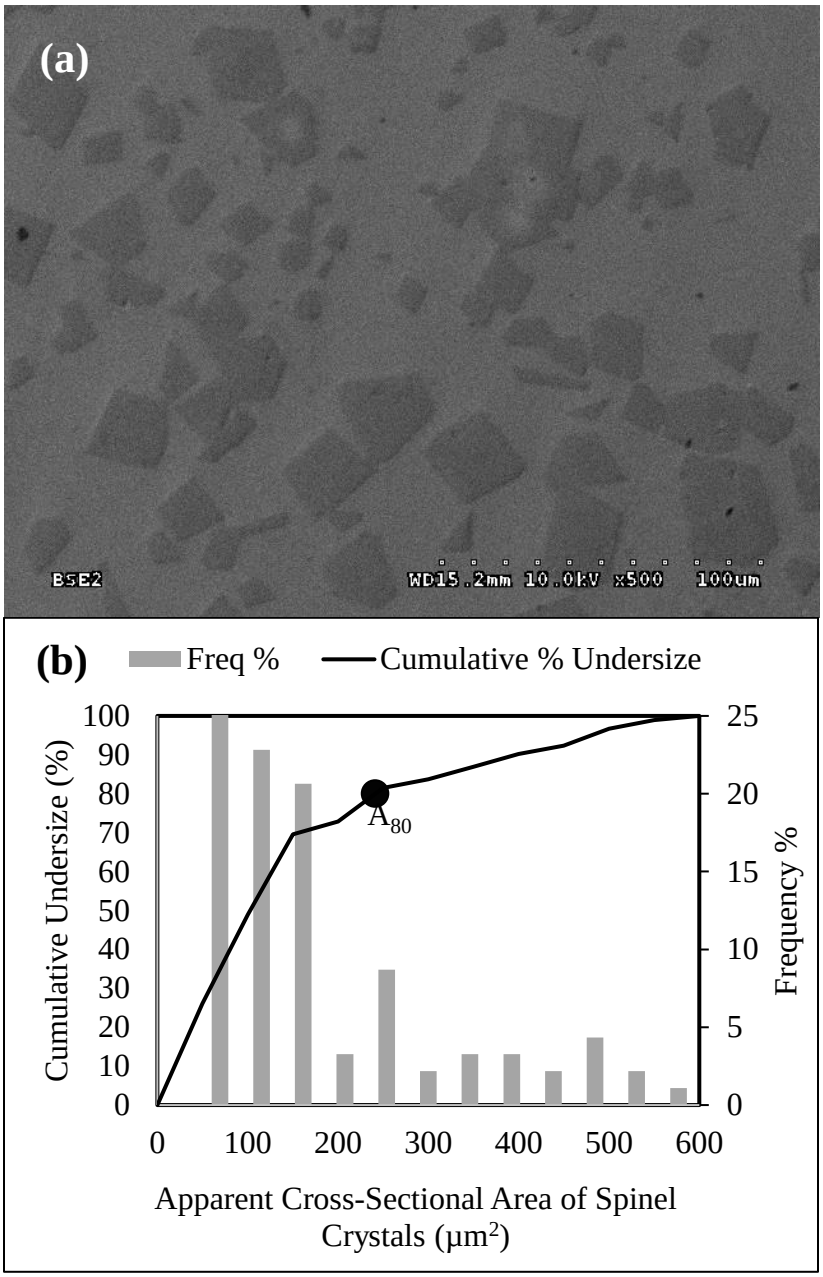

Figure 4.7: (a) SEM micrograph (500X) and (b) crystal size distribution of A1 slag held at 1550°C measured using ImageJ.

The crystals in the sample quenched from 1550ºC also appear to show less roughness compared to the spinel crystals formed at 1400ºC. The thermal shock applied during quenching to already crystalized spinel crystals are the possible reason for the rough surface, whereas the spinel

crystallized during quenching did not undergo such drastic thermal change. Slag held at 1475ºC appears to have a combination of spinel crystallized before and during quenching with a A_{80} of 515 µm^2. The slag has both large and small spinel crystals, with the larger crystals showing a rougher surface.

To better understand the Cr partition in the slag, SEM-EDX analysis of samples held at 1400, 1475 and 1550ºC were conducted. Lack of detectable Cr in the matrix phase indicate that most of the Cr is present in the spinel phase. The elemental composition range of the spinel crystals in the samples were determined using area analysis on 5-7 spinel crystals on each sample (Table 4.2). For samples held at 1400ºC and 1475ºC the composition range of the spinel crystals is mostly similar, except the Si and Ca concentration range being wider for the sample held at 1475ºC. The sample held at 1550ºC however, has a much wider range of compositions. Some spinel crystals have a higher Cr content (~24 wt%) than those held at lower temperatures (<20%). This would indicate higher Cr partition in the spinel phase of the 1550ºC sample, but XRD analysis of the sample also indicates a relatively lower total spinel content. Si and Ca inclusions in the spinel crystals are also significantly higher in some spinel crystals at 1550ºC, which would create a more unstable spinel structure [5]. Further clarification on Cr stabilization due to differences in holding temperature, are obtained through leaching experiments.

Table 4.2: The range of the elemental composition (wt%) of 5-7 spinel crystals in slag samples with holding temperatures of 1400, 1475 and 1550ºC.

Temperature	Mg	Al	Si	Ca	Cr	Fe
1400°C	11.61-11.98	9.45-14.17	3.21-7.55	1.30-4.43	10.25-19.68	2.34-2.94
1475°C	11.37-12.20	10.87-15.15	2.86-8.08	1.81-5.22	10.28-18.27	1.89-2.33
1550°C	11.48-13.27	8.87-18.93	2.25-16.9	0.99-10.32	8.25-23.79	1.28-2.16

4.1.3. ICP Analysis of Leachate

Slag samples with the particle size of <106 µm were leached using AV002.1 availability test [52] and the Cr concentration of the leachate was determined using ICP using two aliquots for each leachate and the average of triplicates for each aliquot. The maximum difference in the Cr concentration obtained from the two aliquots of the samples is 0.01 ppm. The Cr concentration of

the leachate for slags with different holding temperature are shown in Figure 4.8. There is a notable increase in Cr concentration of the leachate for samples held at higher temperatures. Slag held at 1550ºC showed visibly lower spinel content for Al bearing spinel in the XRD analysis. At higher holding temperature, spinel would nucleate at a lower rate (no nucleation around 1600ºC) and only precipitate from the liquid slag during quenching. The spinel formed during quenching would not be allowed the same time to absorb Cr into its structure as the spinel formed before quenching [41]. Slag sample held at 1550ºC had a significantly higher Cr concentration in the leachate (0.28 ppm) than sample held at 1400ºC (0.18 ppm). Samples held at 1475ºC had a leachate Cr concentration in between the other two (0.20 ppm) but closer to the sample held at 1400ºC. We can observe from the XRD results that samples held at 1400ºC and 1475ºC had similar spinel content despite the difference in holding temperature. For the samples held at 1475ºC the samples possibly had lower spinel content before quenching with the rest of the spinel crystallizing during quenching, as observed from the SEM images.

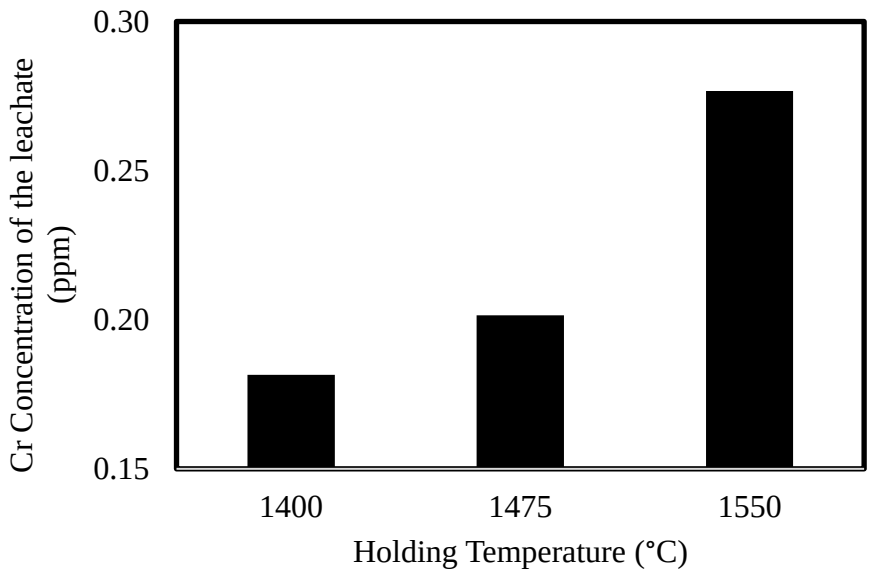

Figure 4.8: Cr concentration of the leachate obtained using AV002.1 availability test vs. holding temperature of slag.

4.2. Influence of Al_2O_3 Content on Cr Stability

Slag samples A1-A7 were prepared with Al_2O_3 content varying from 0-20%, to study the effect of Al_2O_3 content on the Cr leachability of FeCr slag. Considering the advantage of lower holding temperatures for mitigating Cr release, 1400ºC was selected as the holding temperature for all the

samples in this series of experiments. The phases present in sample A1 are discussed in section 4.1.1. The results of the aforementioned phase analysis will be used to explain the mineralogy of slags A2-A7.

4.2.1. XRD and SEM Analysis

XRD analysis of Slag A1 shows the presence of spinel, ringwoodite, and akermanite along with minor amounts of quartz and Cr bearing spinel. A comparative study of the XRD spectrum for all the varying alumina content series of slag shown in Figure 4.9 was used to determine the changes in minerology with Al_2O_3 content.

There is a noticeable drop in spinel content of the slag with the decrease in Al_2O_3 content, notably slag A7 with 0% Al_2O_3 showing no spinel phase. The drop in spinel, although expected, was also supposed to be accompanied with and increase in ringwoodite and akermanite. This is because the decrease in Al_2O_3 content was compensated by an increase in CaO and SiO_2 content in the slag. According to the mass balance for slags A1-A7 shown in Table 4.3, the slag samples should have a small increase in ringwoodite (~10%), a moderate increase in akermanite (~16%), and a large decrease in spinel (~28%), as the Al_2O_3 content decreased from 0 to 20%.

Since the spinel and ringwoodite XRD peaks superimpose there should be a net decrease in the peaks according to the mass balance which can be confirmed in the XRD analysis. However, the akermanite peaks do not show any noticeable increase with Al_2O_3 reduction as the mass balance suggests. This is possibly due to the crystallization of akermanite during the quenching phase and not the holding period of the heat treatment cycle. In addition, the volume of the crystallized phases in the slag before quenching is smaller for samples with lower Al_2O_3 content. Hence, there are less regions for nucleation of new akermanite crystals during quenching. This would also explain the decrease in quartz phase in the slag on Al_2O_3 reduction, despite the mass balance showing higher free SiO_2. Quartz having the lowest crystallization temperature of all the phases would have the shortest time to crystallize during quenching.

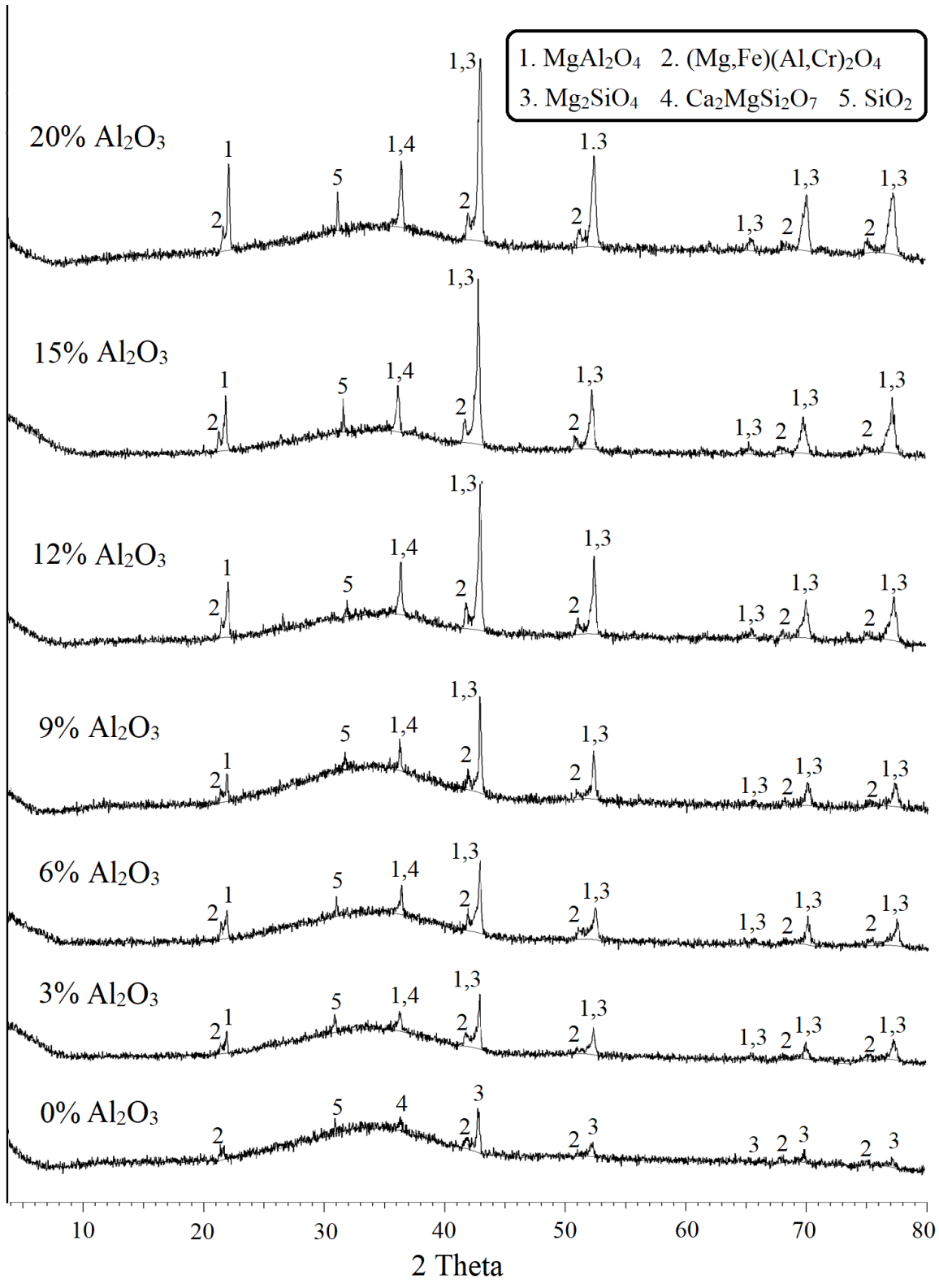

Figure 4.9: XRD analysis of slag samples with varying Al_2O_3 content.

Table 4.3: Mass balance calculation (in wt%) of phases in varying Al_2O_3 slag (FeO excluded)

Sample	Al_2O_3	Spinel	Cr.Spinel	Akermanite	Ringwoodite	Quartz
A1	20.00	27.90	7.59	36.46	17.65	6.42
A2	15.00	20.93	7.59	40.52	20.05	6.94
A3	12.00	16.74	7.59	42.95	21.50	7.25
A4	9.00	12.56	7.59	45.38	22.94	7.57
A5	6.00	8.37	7.59	47.81	24.38	7.88
A6	3.00	4.19	7.59	50.25	25.82	8.20
A7	0.00	0.00	7.59	52.68	27.26	8.51

EDX analysis of samples A1, A4 and A7 were conducted to clarify the Cr partition in the slag. Since EDX is semi quantitative in nature, only samples with large differences in chemical composition were selected to avoid confusions caused by overlapping of data. No detectable Cr is observed in the silicate matrix, indicating that almost all of the Cr is in the spinel phase. EDX area analysis was performed for samples A1, A4 and A7 on 5-7 spinel crystals on each sample. Analysis of the spinel crystals confirm a high Cr content with variations in Al content (Table 4.4). Sample A1 with the highest Al_2O_3 content (20%) has more Al% in the spinel crystals than Sample A4 with 9%. The Cr content in the spinel crystals is also lower in Sample A1 compared to samples A4 and A7 with lower Al_2O_3 contents (9% and 0% respectively).

Table 4.4: SEM-EDX area analysis of spinel crystals in sample A1, A4 and A7 in wt%.

Slag	Mg	Al	Si	Ca	Cr	Fe
A1	11.61-11.98	9.45-14.17	3.21-7.55	1.30-4.43	10.25-19.68	2.34-2.94
A4	11.56-12.72	6.21-10.49	1.35-6.65	0.87-5.29	16.03-34.86	2.34-3.14
A7	11.71-13.34	0	1.48-9.04	0.00-4.64	16.63-35.85	0-4.04

4.2.2. ICP Analysis of the Leachate

The Cr concentration of the leachate obtained from slag samples A1-A7 with particle size <106 µm using two aliquots of each leachate and average of triplicates for each aliquot are shown in

Figure 4.10. The maximum difference in the Cr concentration of the leachate obtained from the two aliquots of the samples is 0.01 ppm. The Cr concentration increases from 0.10 to 0.18 ppm as the Al_2O_3 content increased from 0% to 20%.

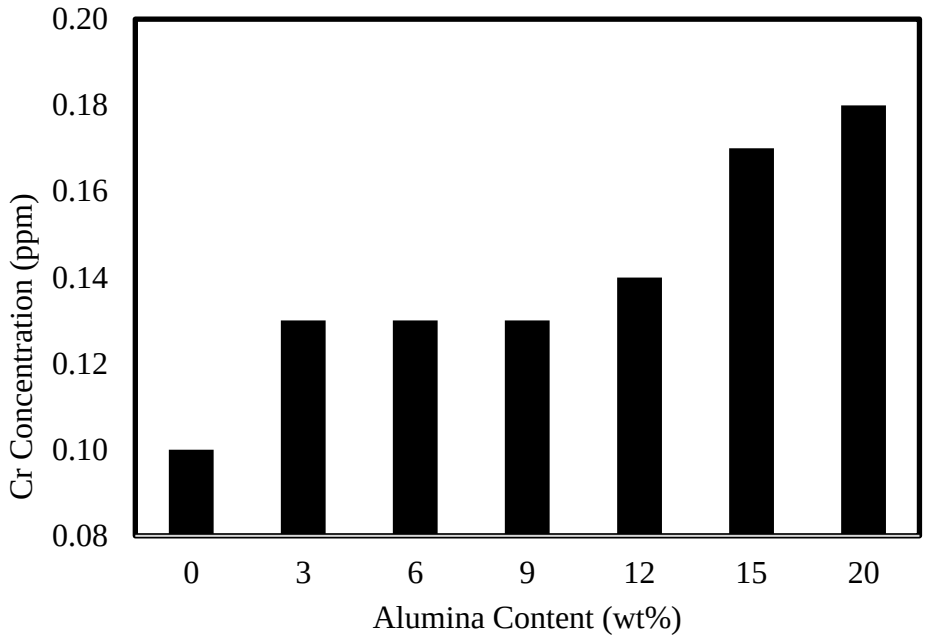

Figure 4.10: Cr concentration of leachate vs. Al_2O_3 content of slag using AV002.1 availability test.

The increase in Al_2O_3 content of the slag promotes Cr leaching out of it. It is proposed that Al^{3+} ions replace the Cr^{3+} ions in the stable spinel phase that resists Cr dissolution in water. The Cr present in silicate phases (akermanite, ringwoodite, quartz) of the matrix would not be able to completely resist water dissolution and thus leach out of the slag.

The results of the current study are in agreement with the literature claims on Al_2O_3 destabilizing the Cr present in spinel [14]. However, it does not clarify the claims in the previous research regarding the benefits of Al_2O_3 in stabilizing Cr by removing water-soluble periclase (MgO) [40]. It should be noted that periclase or free MgO was not detected in our samples since the MgO that was left after spinel crystallization was consumed in the formation of silicates. Further verification

on the stabilizing effect of Al_2O_3 on Cr stabilization can be achieved in future research with samples with free MgO. This can be done by using slags with higher MgO content or less SiO_2 to bond with MgO.

4.3. Influence of the Slag Basicity on Cr Release

We synthesized slag samples B1-B5 with basicity ranging from 0.3 to 0.7 to determine its effect on Cr leachability of FeCr slag. The effect of basicity on Cr leaching has been widely observed to be detrimental on Cr stability in slag. Since the concentration of Cr in the leachate has been low in all previous samples of the current experiment, it was necessary to determine if changes in basicity would have any noticeable effect on the Cr release.

4.3.1. XRD and SEM Analysis

A comparative XRD spectrum of samples B1-B5 is shown in Figure 4.11. The spectra of samples show peaks for spinel, ringwoodite, akermanite and Cr bearing spinel with similar intensities. Quartz peaks can be observed in slag with 0.3, 0.4 and 0.5 basicity and are absent in the other slags with higher basicity. The mass balance of phases in slag B1-B5 shown in Table 4.5 is used to better understand the XRD spectra. Mass balance indicates that increase in basicity from 0.3 to 0.7 would result in small decrease in ringwoodite phase (~5%), moderate decrease in quartz phase (~15%) and a large increase in akermanite phase (~20%). The spinel phase remains unchanged as the amount of Al_2O_3 in all five slag samples is kept constant. The calculated increase in akermanite is not readily observed in the XRD spectra since the decrease might be too small to be noted, especially since it shares peaks with spinel. The reason for relatively constant akermanite peak intensity in all slag samples might be the dominance of the crystallisation of akermanite during the quenching phase rather than the holding time.

Despite the difference in CaO and SiO_2 content of the slag, the amount of akermanite crystallized in each slag sample remains the same due to the short time for nucleation and growth of new crystals during quenching. Quartz crystallized only in samples B1, B2 and A1 (basicity ≤0.5) since samples with higher basicity have lower SiO_2 content and thus lower free SiO_2 according to the mass balance. The amount of crystallized quartz in B1, B2 and A1 slag is similar despite the difference in SiO_2 content because, much like akermanite, quartz crystallizes only during the quenching phase.

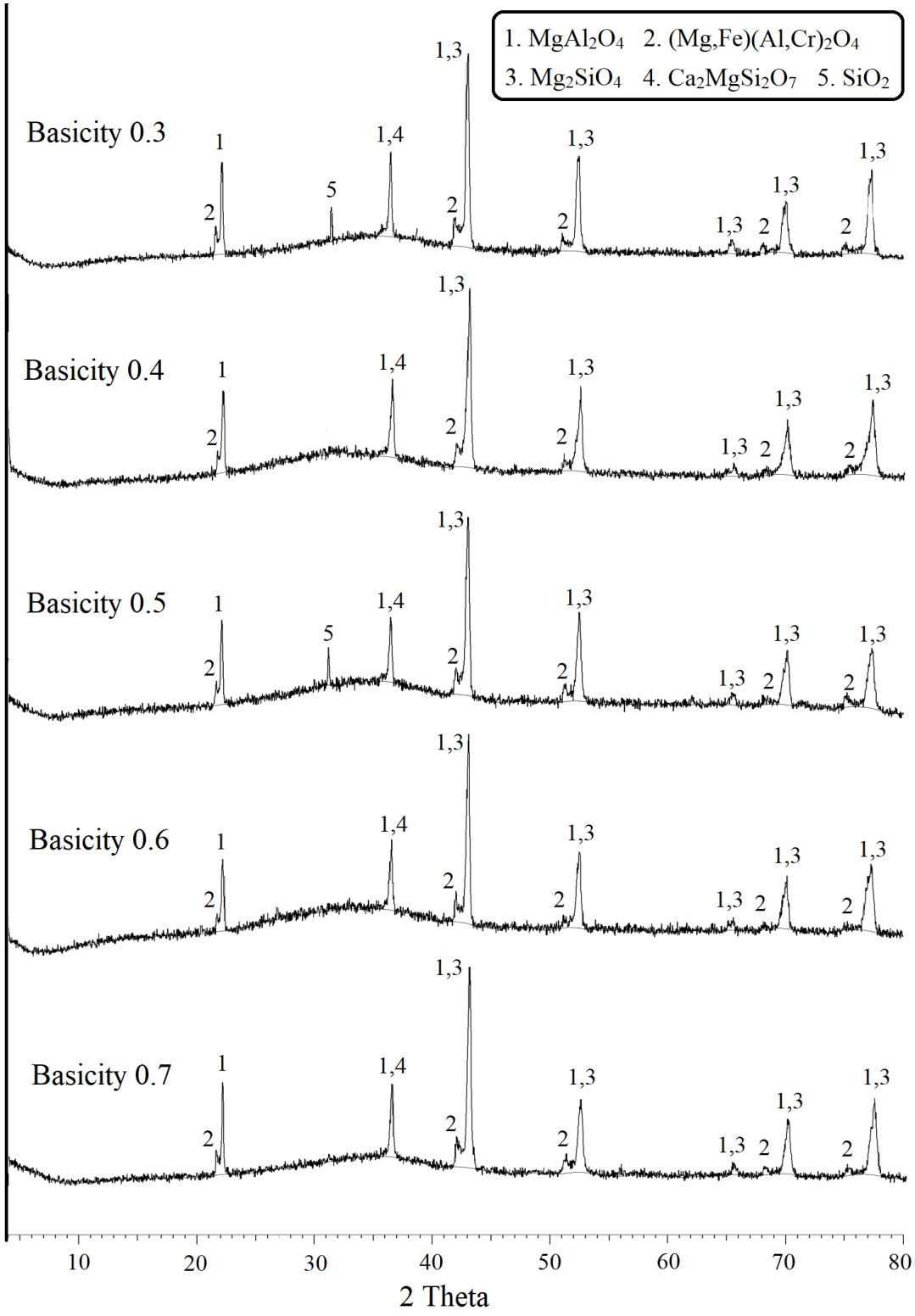

Figure 4.11: XRD analysis of the slag samples with varying basicity.

Table 4.5: Mass balance calculation (in wt%) of phases in slags with varying basicity (FeO excluded).

Sample	Basicity	Spinel	Cr.Spinel	Akermanite	Ringwoodite	Quartz
B1	0.3	27.90	7.59	25.26	20.54	14.74
B2	0.4	27.90	7.59	31.26	18.99	10.28
A1	0.5	27.90	7.59	36.46	17.65	6.42
B4	0.6	27.90	7.59	41.02	16.48	3.04
B5	0.7	27.90	7.59	45.04	15.44	0.05

Samples B1, A1 and B5 were analyzed using EDX to observe elemental partition in the different phases. Similar to the A series experiments, only samples with large difference in chemical composition (0.2 Basicity) were used to avoid the misinterpretations that might be caused by the semi-quantitative nature of EDX analysis. The matrix phase of the samples contains no detectable Cr. The spinel crystals in the samples, however, show a noticeable difference in Cr content (Table 4.6). Analysis of samples B1, A1 and B5 were performed via EDX area analysis of 5-7 spinel crystal on each sample.

Table 4.6: SEM-EDX area analysis of spinel crystals in sample B1, A1 and B5 in wt%.

Slag	Mg	Al	Si	Ca	Cr	Fe
B1	10.28-12.47	6.22-10.65	1.12-2.82	0.00-0.52	17.84-33.79	2.56-3.74
A1	11.61-11.98	9.45-14.17	3.21-7.55	1.30-4.43	10.25-19.68	2.34-2.94
B5	11.37-11.87	9.47-14.16	3.68-10.65	1.78-6.32	7.02-23.97	2.57-3.09

The spinel phase in sample B1 with the lowest basicity (0.3) has a higher Cr content than sample B5 with the highest (0.7) basicity. The Ca and Si content of sample B1 is higher than the other samples and could possibly lead to higher Cr leachability due to the destabilizing effect of Ca and Si ions on the spinel structure [14]. Ca and Si can create point defects in the spinel crystal which can lead to Cr partitioning out of it.

4.3.2. ICP Analysis of the Leachate

Similar to the previous samples, ICP analysis was conducted on the leachates obtained from slag samples B1-B5 with particle size <106 µm using two aliquots of the leachate and average of triplicates for each aliquot, to determine their Cr concentration (Figure 4.12). The maximum difference in the Cr concentration of the leachate obtained from the two aliquots of the samples is 0.01 pm. A noticeable Cr concentration difference in the leachates is observed by increasing basicity. The leachate of slag B1 with basicity of 0.3 has 0.15 ppm Cr. The Cr concentration increases to 0.25 ppm for the leachate of sample B5 with the basicity of 0.7. Cr concentrations in the third decimal values are below the lower limit (0.01 ppm) of the instrument and were thus ignored for the analysis. The increase in basicity has a noticeable increase in Cr leaching. Increase in basicity was achieved by an increase in CaO content and a decrease in SiO_2 content of the slag. As the CaO content of the slag increases it also increases the probability of the formation of water-soluble $CaCr_2O_4$ and $CaCrO_4$ [6]. Silicate phases, while not as effective as spinel in reducing Cr dissolution in water, are more Cr stable than $CaCr_2O_4$ and $CaCrO_4$ phases since they themselves do not dissolve in water [6][14]. The decrease in SiO_2 content in addition to the increase in CaO content result in higher Cr dissolution as the basicity increases.

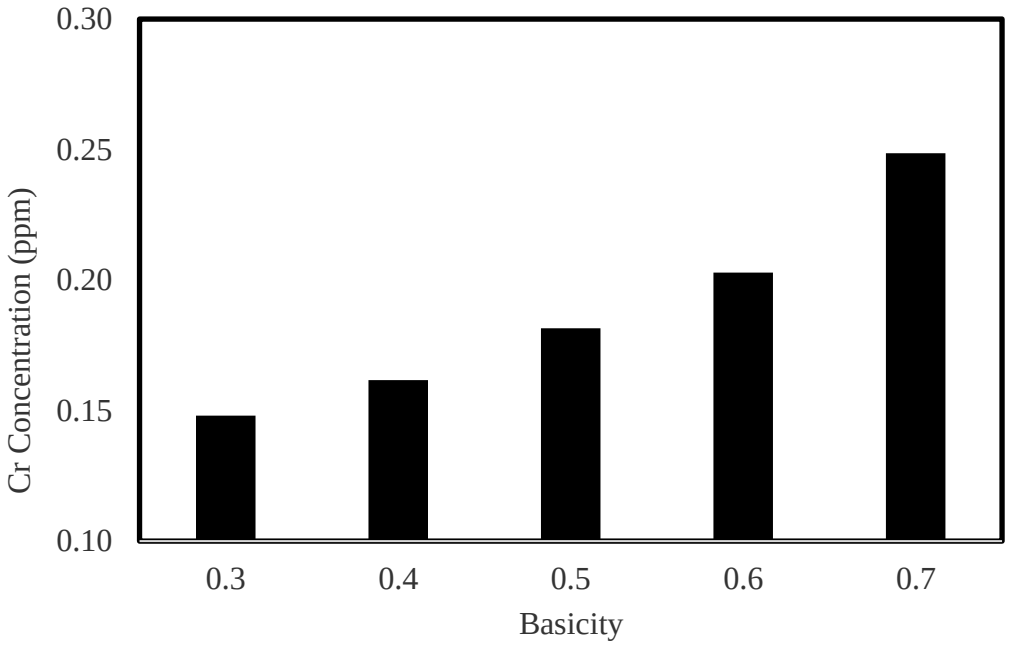

Figure 4.12: Cr concentration of the leachate vs. basicity of the slag using AV002.1 availability test.

4.4. XRF Analysis

Changes in Al_2O_3 content and basicity show meaningful differences in Cr leachability, however, the leached Cr content is below 0.3 ppm in all cases despite significant composition changes. To verify that the samples contain similar Cr content before and after synthesis, we used XRF (X-Ray Fluorescence) analysis on the A1 sample. The elemental concentration (in ppm) based on the average of three separate runs of the slag was used to calculate the oxide composition shown in (Table 4.7).

Table 4.7: Sample A1 composition based on XRF analysis.

MgO	Al_2O_3	SiO_2	CaO	Cr_2O_3	FeO	Total
40	22	17	8	8	5	100

The analysis confirms the presence of Cr_2O_3 in the sample with a content close to the one used for synthesis. There is a noticeable difference in for the percentage of some oxides. MgO content of the sample is significantly higher than the initial percentage. This is due to the use of an MgO crucibles for slag synthesis. The high MgO content in the samples is associated with the contamination of the sample by the crucible. Moreover, SiO_2 and CaO percentages of the slag are lower than the initial amount. This is possibly due to higher amount of MgO, which dilutes the concentration of SiO_2 and CaO in the slag.

4.5. Repeatability of the Experiments

Due to the time-consuming nature of the high temperature experiments (~40 hours per sample), it is not conventional to repeat all the experiment. Sample A1 was prepared twice and analyzed to confirm the repeatability of the experiments. Samples were synthesized using the same amount of reagents and identical procedures and were analyzed for leaching behaviour using ICP-AES.

ICP results of Cr content of leachate obtained from both sets for sample A1 were the same up to the 2nd decimal point (0.18 ppm).

5. Conclusion

Leaching experiments on slag samples at holding temperatures of 1400, 1475 and 1550°C reveal that the highest Cr stabilization occurs at 1400°C. The Cr concentrations of the leachate for the slag sample held at 1550ºC was 0.28 ppm, significantly higher than the sample held at 1400ºC (0.18 ppm). The slag held at 1475ºC had a leachate Cr concentration of 0.20 ppm, relatively close to the value obtained for the sample held at 1400ºC. XRD and SEM analysis show high spinel crystallization at 1400°C and 1475°C with larger spinel size at 1400°C. The slag held at 1550ºC was observed to have smaller spinel crystals with A_{80} of 241 μm^2, compared to the slag held at 1400ºC with A_{80} of 620 μm^2. The sample held at 1475ºC has a combination of spinel crystals that formed before and during quenching with A_{80} of 515 μm^2.

Al_2O_3 content of slag samples are observed to increase Cr leachability in slag, with the highest Al_2O_3 content (20%) slag releasing 0.18 ppm Cr in the leachate. XRD spectrum of slag samples have visibly higher Al spinel peaks as the Al_2O_3 content increases, while the Cr spinel peaks remain relatively unchanged. This indicates that, despite the observable increase in total spinel content, Al is destabilizing the Cr trapped in spinel. SEM-EDX analysis of spinel crystals indicate higher Cr content in spinel at lower Al_2O_3 content.

Increase in slag basicity in samples with a fixed Al_2O_3 and MgO content show further destabilization of Cr during leaching experiments. The Cr concentration of the leachates are as high as 0.25 ppm for the slag samples with the basicity of 0.7. The Cr concentration of the leachate drops to 0.15 ppm when the basicity is lowered to 0.3. XRD analysis of samples show no distinct change in spinel content with changes in basicity. SEM-EDX analysis show higher Ca content in spinel crystals of slags with higher basicity.

The Cr content of the leachate of all the slag samples examined in this work are below the Canadian and Ontario criteria of maximum 2.77 mg/L of Cr in waste leachate using TCLP test [15]. The Cr content of the leachates are also lower than the non-potable ground water limit of 0.81 ppm total Cr but higher than Ontario's total Cr content standard limit of 0.05 ppm for drinking water [55].

6. Future Work

The Cr release from the samples examined in this work were below 0.3 ppm in all the leachates. Small differences in the Cr content of the leachate were observed despite significant variation in chemical composition and heat treatment. The high stability of Cr in samples is associated with high MgO content of the slag (25 wt%) and is possibly influenced by the use of MgO crucibles during synthesis. Decreasing the MgO content of the slag may clarify the effect of Al_2O_3 content and basicity on Cr release from the slag.

XRF analysis of samples revealed higher MgO content than intended during synthesis. The MgO crucible used for synthesis is the likely source of the higher MgO content. In the future, the MgO contamination can be avoided by replacing the MgO crucible with an inert replacement. SiO_2 and CaO content for slag samples were also lower than intended for synthesis. The loss of these oxides might have occurred during milling or due to reaction of the oxides with the MgO crucible during synthesis. The changes in SiO_2 and CaO content can be investigated by analysing non-milled samples synthesized in an inert crucible, possibly with a more accurate quantitative analysis such as acid digestion/salt fusion followed by ICP-OES.

References

[1] D. Yu, D. Paktunc (2018), *Direct Production of Ferrochrome by Segregation Reduction of Chromite in the Presence of Calcium Chloride*, Metals 2018, Vol 8, pp. 69.

[2] N. Sahu, A. Biswas, G.U. Kapure (2016), *A Short Review on Utilization of Ferrochromium Slag*, Mineral Processing and Extractive Metallurgy Review, Vol. 37, Issue 4, pp. 211-219.

[3] D. Yu, D. Paktunc (2018), *Kinetics and Mechanisms of the Carbothermic Reduction of Chromite in the Presence of Nickel*, Journal of Thermal Analysis and Calorimetry, Vol. 132, pp. 143–154.

[4] P. Richard(2015), *Overview of the Global Chrome Market*, Presentation, INDINOX Stainless Steel Conference, Ahmedabad.

[5] G.J. Albertsson, F. Engström, L. Teng (2014), *Effect of the Heat Treatment on the Chromium Partition in Cr-Containing Industrial and Synthetic Slags*, Steel Research Int., Vol. 85, Issue 10, pp. 1418-1431.

[6] H. Cabrera, A. R. Serrano, B. Zeifert, A. H. Ramirez, M. H. Lopez, A. C. Ramirez (2012), *Effect of MgO and CaO/SiO2 on the Immobilization of Chromium in Synthetic Slags*, Journal of Material Cycles and Waste Management, Vol. 14, pp. 317–324.

[7] J. Guertin, J.A. Jacobs, C.P. Avakian (2004), *Chromium(VI) Handbook*, CRC Press, USA, pp. 216-225, 511.

[8] R.J. Bartlett (1991), *Chromium Cycling in Soils and Water: Links, Gaps, and Methods*, Environmental Health Perspectives, Vol. 92, pp. 17-24.

[9] I. Hininger, R. Benaraba, M. Osman, H. Faure, A.M. Roussel, R.A. Anderson (2007), *Safety of Trivalent Chromium Complexes: No Evidence for DNA Damage in Human HaCaT Keratinocytes*, Free Radical Biology and Medicine, Vol. 42, Issue 12, pp. 1759-1765.

[10] World Health Organization International Agency for Research on Cancer (1990), IARC *Monographs on the Evaluation of Carcinogenic Risks to Humans: Chromium, Nickel and Welding*, Lyon France, Vol. 49, pp. 1-648.

[11] Y. Ishikawa, K. Nakagawa, Y. Satoh, T. Kitagawa, H. Sugano, T. Hirano, E. Tsuchiya (1994), "*Hot Spots" of Chromium Accumulation at Bifurcations of Chromate Workers' Bronchi*, Cancer Research, Vol. 54, Issue 9, pp. 2342-2346.

[12] L.M. Beaver, E.J. Stemmy, S.L. Constant, A. Schwartz, L.G. Little, J.P. Gigley, G. Chun, K.D. Sugden, S.M. Ceryak, S.R. Patierno (2009), *Lung Injury, Inflammation and Akt Signaling Following Inhalation of Particulate Hexavalent Chromium*, Toxicology and Applied Pharmacology, Vol. 235, Issue 1, pp. 47-56.

[13] F. Engström (2010), *Mineralogical Influence on Leaching Behaviour of Steelmaking Slags*, Doctoral Thesis, Luleå University of Technology, Sweden, ISBN 978-91-7439-197-8.

[14] G.J. Albertsson (2013), *Abatement of Chromium Emissions from Steelmaking Slags - Cr Stabilization by Phase Separation*, Doctoral Thesis, Royal Institute of Technology, ISBN 978-91-7501-666-5.

[15] *Ontario Environmental Protection Act R.R.O 1990*, Regulation 347, General Waste Management, pp. 65-145.

[16] R. Stregmann, K. -U. Heyer, R. Cossu (2005), *Leachate Treatment*, proceedings for Sardinia 2005, Tenth International Waste Management and Landfill Symposium, pp. 3.

[17] *Potential Toxic Effects of Chromium, Chromite Mining and Ferrochrome Production: A Literature Review* (May 2012), MiningWatch Canada.

[18] J.P. Beukes, S.P. du Preez, P.G. van Zyl, D. Paktunc, T. Fabritius, M. Päätalo, M. Cramer (2017), *Review of Cr(VI) Environmental Practices in the Chromite Mining and Smelting Industry - Relevance to Development of the Ring of Fire, Canada*, Journal of Cleaner Production, Vol. 165, pp. 874-889.

[19] Y.R. Murthy, S.K. Tripathy, C.R. Kumar (2011), *Chrome Ore Beneficiation Challenges and Opportunities - a Review*, Mining Engineering, Vol. 24, Issue 5, pp. 375-380.

[20] J. Chong (2014), *Resource Development in Canada: A Case Study on the Ring of Fire*, Library of Parliament, Ottowa, Publication No. 2014-17-E.

[21] M.F. Gazulla, A. Barba, M.P. Gomez, M. Orduna (2007), *Chemical Characterization of Chromites by XRF Spectrometry*, Vol. 37, pp. 237-243.

[22] A. Kim, A. Akberdin, R. Sultangaziyev (2020), *Ways to Improve Texture Technology Reflective Chromite Ore of Kazakhstan*, Metalurgija, Vol. 59, Issue 4, pp. 496-498.

[23] S.D. Iyer, E.V.S.S.K. Babu, P.G. Mislankar, A.R. Gujar, N.V. Ambre, V.J. Loveson (2010), *Occurrence and Emplacement of Chromite Ores in Sindhudurg District, Maharashtra, India,* Acta Geologica Sinica, Vol. 84, Issue 3, pp. 515-527.

[24] J.P. Beukes, R.N. Guest (2001), *Technical Note: Cr(VI) Generation During Milling*. Minerals Engineering, Vol 14, Issue 4, pp. 423-426.

[25] R.I. Glastonbury, W.V.D. Merwe1, J.P. Beukes, P.G.V. Zyl1, G. Lachmann1, C.J.H. Steenkamp, N.F. Dawson, H.M. Stewart (2010), *Cr(VI) Generation During Sample Preparation of Solid Samples – A Chromite Ore Case Study*, Water SA, Vol. 36, Issue 1, ISSN 1816-7950.

[26] D.Yu, D. Paktunc (2018), *Direct Production of Ferrochrome by Segregation Reduction of Chromite in the Presence of Calcium Chloride*, Metals, Vol 8, pp. 69.

[27] O. Sariev, S. Kim, YE. Zhumagaliev, B. Kelamanov, M. Sultanov, N. Nurgali (2020), *Viscosity and Crystallization Temperature of Ferroalloy Slags from Kazakhstan Ore*, Metalurgija, Vol. 59, Issue 4, pp. 525-528.

[28] M.E. Fleet (1986), *X-ray Diffraction and Spectroscopic Studies on the Structure of Silicate Glasses, in Short Course on Silicate Melts,* edited by C.M. Scarfe, Mineralogical Soc. Ottawa, Canada, pp. 1-35.

[29] J. Dong, D. Zhang, L. Gan (2019), *An Empirical Formula for Accurate Calculation of Liquidus Temperature of Blast Furnace Slags in SiO_2–Al_2O_3–CaO–MgO System*. Ironmaking & Steelmaking, Vol. 46, Issue 1, pp. 71-74.

[30] K.C. Mills, L. Yuan, R.T. Jones (2011), *Estimating the Physical Properties of Slags.* The Southern African Institute of Mining and Metallurgy, Vol. 111, Issue 10, pp. 649-658.

[31] P.V. Riboud, Y. Roux, L.D. Lucas, H. Gaye (1981), *Improvements of Continuous Casting Powders*, Fachber Huttenprax Metallweiterverarb, Vol. 19, Issue 10, pp. 859–869.

[32] Urbain, G (1987), *Viscosity Estimation of Slags*, Steel Research, Vol. 58, pp. 111–116.

[33] T. Iida, H. Sakai, Y. Kita, K. Shigeno (2000), *An Equation for Accurate Prediction of the Viscosities of Blast Furnace Type Slags from Chemical Composition*, ISIJ International, Vol. 40, pp. S110-S114.

[34] F.-Z. Ji, S. Du, S. Seetharaman (1997), *Experimental Studies of the Viscosities in the CaO-Fe_nO-SiO_2 Slags*, Metallurgical and Materials Transactions B, Vol. 28, Issue 5, pp. 827-834.

[35] V. Arredondo-Torres, A. Romero-Serrano, B. Zeifert, J. Cruz-Rivera, P. Flores-Sánchez, A. Cruz-Ramírez (2006), *Stabilization of $MgCr_2O_4$ spinel in slags of the SiO_2–CaO–MgO–Cr_2O_3 system*, Revista de Metalurgia, Vol. 42, Issue 6, pp. 417–424.

[36] E. Garcia-Ramos, A. Homero-Berranc, B. Zeifert, P. Flores-Sanchez, M. Hallen-Lepez, E.G. Palaclos (2008), *Immobilization of Chromium in Slags Using MgO and Al_2O_3*, Steel Res Int, Vol. 79, Issue 5, pp. 332–338.

[37] G.A. Brooks, M.M. Hasan, M.A. Rhamdhani (2019), *Slag Basicity: What Does It Mean?*, In: Jiang T. et al. (eds) 10th International Symposium on High-Temperature Metallurgical Processing. The Minerals, Metals & Materials Series. Springer, Cham, pp. 297-308.

[38] *Mexican Official Norms*. NOM-053-ECOL (1993). http://www.semarnat.gob.mx.

[39] L.H. Cao, C.J. Liu, Q. Zhao, M.F. Jiang (2017), *Effect of Al_2O_3 Modification on Enrichment Behavior of Chromium in Stainless Steel Slag*, J. Iron Steel Res. Int., Vol. 24, pp. 258–265.

[40] Q. Zeng, J.L. Li, Q.Q. Mou, H.G. Zhu, Z.L. Xue (2019), *Effect of FeO on Spinel Crystallization and Chromium Stability in Stainless Steel-Making Slag*, The Minerals, Metals & Materials Society, JOM, Vol. 71, Issue 7, pp. 2331-2337.

[41] M. Kuhn, D. Mudersbach, J.M. Baena Liberato, V. De Angelis, D. Capodilupo, U. de Fries (2006), *Chrome Immobilisation in EAF Slags from High-Alloy Steelmaking: Development of a Slag Treatment Process*, Technical Steel Research, ISBN 92-79-02077-3, ISSN 1018-5593.

[42] M. Tossavainen, F. Engstrom, Q. Yang, N. Menad, M. Lidstrom Larsson, B. Björkman (2007), *Characteristics of Steel Slag Under Different Cooling Conditions*, Waste Management, Vol. 27, pp. 1335-1344.

[43] CEN, 2002b. Final draft prEN 12457-3. *Characterization of waste-leaching-compliance test of leaching of granular waste material and sludges – Part 3: two-stage batch test at a liquid to solid ration of 2 l/kg and 8 l/kg for materials with high solid content and with particle size below 4 mm (with or without particle reduction).*

[44] CEN, 2002a. Final draft prEN 12457-2. *Characterization of waste-leaching-compliance test of leaching of granular waste material and sludges – Part 2: one-stage batch test at a liquid to solid ration of 10 l/kg for materials with particle size below 4 mm (with or without particle reduction).*

[45] M. Loncnar, M. Zupan, P. Bukovec, A. Jakli (2009), *The Effect of Water Cooling on the Leaching Behaviour of EAF slag from Stainless Steel Production*, Materiali in tehnologije / Materials and technology, Vol. 43, Issue 6, pp. 315-321.

[46] F. Engström, D. Adolfsson, Q. Yang, C. Samuelsson, B. Björkman (2010), *Crystallization Behaviour of Some Steelmaking Slags*, Steel Research Int., Vol 81, Issue 5, pp. 362-371.

[47] L.H. Cao, C.J. Liu, Q. Zhao, M.F. Jiang (2018), *Growth Behavior of Spinel in Stainless Steel Slag During Cooling Process*, Metall. Res. Technol., Vol. 115, pp. 114–121.

[48] D.R. Uhlmann (1972), *A Kinetic Treatment of Glass Formation*, Journal of Non-Crystalline Solids, Vol. 7, Issue 4, pp. 337-348.

[49] D. Turnbull (1950), *Formation of Crystal Nuclei in Liquid Metals*, Journal of Applied Physics, Vol. 21, Issue 10, pp. 1022-1028.

[50] Q. Zhao, C.J. Liu, L.H. Cao, X. Zheng, M.F. Jiang (2018), *Stability of Chromium in Stainless Steel Slag During Cooling*, Minerals, Vol. 8, pp. 445.

[51] X. Pan, R.H. Eric (2004), *Chromium Distribution Between Slag and Non-Carbon Saturated Metal Phases Under Changing Partial Pressure of Carbon Monoxide*, The Journal of The South African Institute of Mining and Metallurgy, Vol. 10, pp. 583-587.

[52] D.S. Kosson, H.A. van der Sloot, F. Sanchez, A.C. Garrabrants (2002), *An Integrated Framework for Evaluating Leaching in Waste Management and Utilization of Secondary Materials*, Environmental Engineering Science, Vol. 19, Issue 3, pp. 159-204.

[53] C.R. Panda, K.K. Mishra, K.C. Panda, B.D. Nayak, B.B. Nayak (2013), *Environmental and Technical Assessment of Ferrochrome Slag as Concrete Aggregate Material*, Construction and Building Materials, Vol. 49, pp. 262‑271.

[54] Slag Atlas, 2nd ed., edited by Verein Deutscher Eisenhuttenleute, Verlag Stahleisen GmbH, Düsseldorf, (1995), pp.134-156.

[55] *Soil, Ground Water and Sediment Standards for use under Part XV.1 of the Environmental Protection Act* (Apr 15, 2011), Ontario Ministry of Environment, Canada.